Supporting information for

Steric and Electronic Influences on Cu-Cu Short Contacts in β-Thioketiminato Tri-Copper(I) Clusters

Venkata Sai Sashankh Penki,[a] Yu-Ting Chu,[b] Hsing-Yin Chen,[a] Sri Sudewi,[c] Chien-Hung Li,[a] Genin Gary Huang*[a] and Sodio C.N. Hsu*[a,d]

[a.] *Department of Medicinal and Applied Chemistry, Kaohsiung Medical University, Kaohsiung 80708, Taiwan.*
[b.] *International PhD Program for Science, National Sun Yat-sen University, Kaohsiung 80424, Taiwan*
[c.] *Department of pharmacy, Faculty of Mathematic and Natural science, Universitas Sam Ratulangi, Manado 95115, Indonesia*
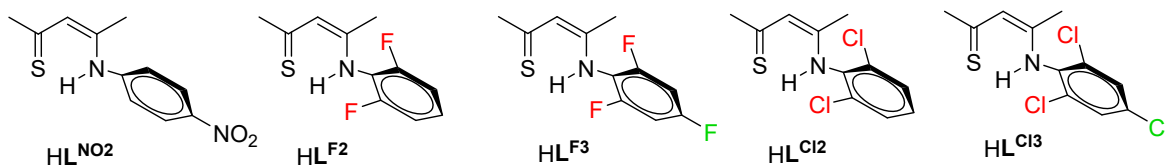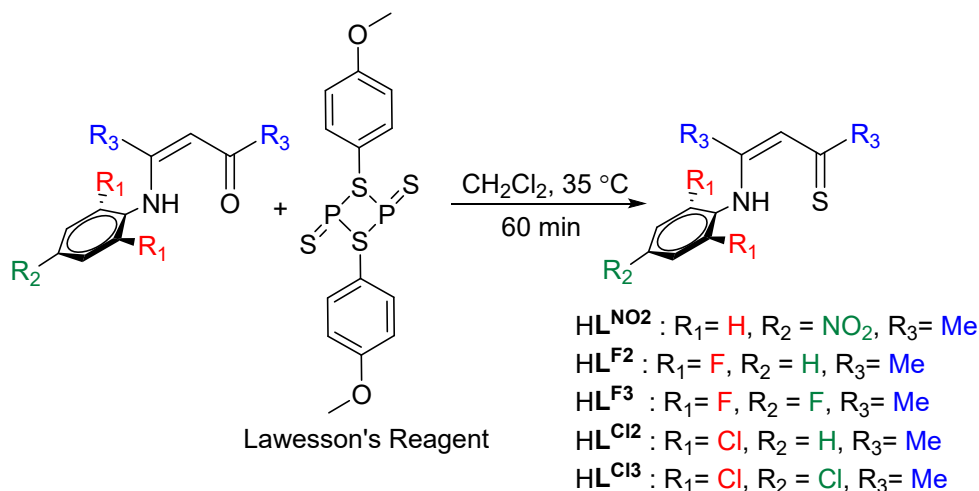[d.] *Department of Medical Research, Kaohsiung Medical University Hospital, Kaohsiung 80708, Taiwan*

Table of Contents

Experimental

Ligand Synthesis:

HL^{NO2}. The procedure of ligand synthesis is similar to previously reported HL_1 or HL_2 ligands.[1] The reaction of (Z)-4-((4-nitrophenyl)amino)pent-3-ene-2-one (5.00 g, 22.70 mmol), and Lawesson's reagent (4.58 g, 11.35 mmol) were dissolved in dichloromethane (50 ml approx.) and heated at 35 °C for 60 min. The volatiles were removed under vacuum to give a reddish-orange oil purified by column chromatography ethyl acetate/hexane 1:10 ratio. The oily product solidified into bright reddish-orange solid and stored at -7 °C (4.45 g, 85 % yield). ^{1}H NMR (CDCl$_3$, 400 MHz, 298K, δ): 15.63 (bs, 1H, NH), 8.27 (d, 2H, J = 8.0 Hz, *meta*-ArH), 7.34 (d, 2H, J = 8.0 Hz, *ortho*-ArH), 6.33 (s, 1H, backbone-CH), 2.65 (s, 3H, backbone-CH$_3$), 2.24 (s, 3H, backbone-CH$_3$), ^{13}C{^{1}H} NMR (C$_6$D$_6$, 100 MHz, 298K, δ): 209.10, 165.28, 145.62, 133.13, 128.98, 124.00, 112.45, 39.15, 29.02, 25.09, 22.48, 20.39. Anal. Calcd. for C$_{11}$H$_{12}$N$_2$O$_2$S: C, 55.92; H, 5.12; N, 11.26. found C, 55.98; H, 4.71; N, 10.97.

HL^{F2}. Following the same procedure with HL^{NO2}, The reaction of (Z)-4-((2,6-difluorophenyl)amino)pent-3-en-2-one (5 g, 23.67 mmol) and Lawesson's reagent (4.78 g, 11.83 mmol) in dichloromethane gave purified by column chromatography ethyl acetate/hexane 1:10

ratio. Solvent is removed by vacuum to give bright-orange oil slowly solidified into yellow orange solid and stored at -7 °C. (4.66 g, 87 % yield). ^{1}H NMR (CDCl$_3$, 400 MHz, 298K, δ): 14.98 (bs, 1H, NH), 7.29 (tt, $^3J_{HH}$ = 8.5 Hz, $^4J_{HF}$ = 6.5 Hz, 1H, *para*-ArH), 7.01 (t, $^3J_{HH}$ = 8.5 Hz, $^3J_{HF}$ = 6.5 Hz, 1H, *meta*-ArH), 6.36 (s, 1H, backbone-CH), 2.63 (s, 3H, backbone-C*H*$_3$), 2.00 (s, 3H, backbone-C*H*$_3$). ^{13}C{^{1}H} NMR (CDCl$_3$, 100 MHz, 298K, δ): 212.28, 164.91, 158.88, 158.86, 156.88, 128.87 (t, $^3J_{CF}$ = 9Hz), 115.29, 114.04, 112.19 (m, $^2J_{CF}$ = 18 Hz), 111.04, 110.99, 110.92, 110.86, 39.43, 21.02, 21.00. ^{19}F NMR (CDCl$_3$, 376 MHz, 298K, δ): -117.51 (t, $^3J_{HF}$ = 6.5 Hz, 2F, *ortho*-ArF). ^{19}F{^{1}H}(CDCl$_3$, 471 MHz, 298K, δ): -117.51 (d, $^4J_{FF}$ = 3.3 Hz, 2F, *ortho*-ArF). Anal. Calcd. for C$_{11}$H$_{11}$F$_2$NS: N, 6.16; C, 58.13; H, 4.88. found N, 5.78; C, 58.33; H, 4.50.

HL^{F3}. Following the same procedure with HL^{NO2}, The reaction of (Z)-4-((2,4,6-trifluorophenyl)amino)pent-3-en-2-one (5 g, 20.38 mmol) and Lawesson's reagent (4.11 g, 10.19 mmol) in dichloromethane gave purified by column chromatography ethyl acetate/hexane 1:10 ratio. Solvent is removed by vacuum to give bright-orange oil slowly solidified into deep yellow solid and stored at -7 °C. (4.66 g, 87 % yield).^{1}H NMR (CDCl$_3$, 400 MHz, 298K, δ): 14.86 (bs, 1H, NH), 6.81 (m, $^4J_{HH}$ = 8.4, $^3J_{HF}$ = 7.5, $^5J_{HF}$ = 1.2 Hz, 2H, *meta*-ArH), 6.36 (s, 1H, backbone-CH), 2.64 (s, 3H, backbone-C*H*$_3$), 1.98 (s, 3H, backbone-C*H*$_3$). ^{13}C{^{1}H} NMR (CDCl$_3$, 100 MHz, 298K, δ): 213.23, 164.77, 162.60 (tt, $^1J_{CF}$ = 250 Hz, $^3J_{CF}$ = 15 Hz), 158.20 (dd, $^1J_{CF}$ = 250 Hz, $^3J_{CF}$ = 15 Hz), 114.05, 101.17 (td, $^2J_{CF}$ = 27 Hz, $^4J_{CF}$ = 3 Hz), 39.54, 20.98. ^{19}F NMR (CDCl$_3$, 376 MHz, 298K, δ): -106.67 (tt, $^3J_{HF}$ = 7.5 Hz, $^4J_{FF}$ = 5.6 Hz, $^5J_{HF}$ = 1.2 Hz, 2F, *para*-ArF), -114.06 (t, $^3J_{HF}$ = 7.5 Hz, $^4J_{FF}$ = 5.6 Hz, 2F, *ortho*-ArF). ^{19}F{^{1}H}(CDCl$_3$, 471 MHz, 298K, δ): -106.65 (s, br, 1F, *para*-ArF), -114.12 (dd, $^4J_{FF}$ = 6.1, 2F, *ortho*-ArF). Anal. Calcd. for C$_{11}$H$_{10}$F$_3$NS: N, 5.71; C, 53.87; H, 4.11. found N, 5.54; C, 54.08; H, 3.86.

HL^{Cl2}. Following the same procedure with HL^{NO2}, The reaction of (Z)-4-((2,6-dichlorophenyl)amino)pent-3-en-2-one (5 g, 19.21 mmol) and Lawesson's reagent (3.88 g, 9.68 mmol) in dichloromethane gave purified by column chromatography ethyl acetate/hexane 1:10 ratio. Solvent is removed by vacuum to give orange oil slowly solidified into yellow brown solid at -7 °C. (4.66 g, 87 % yield).^{1}H NMR (CDCl$_3$, 400 MHz, 298K, δ): 15.23 (bs, 1H, NH), 7.43 (d, *J* = 8.0 Hz, 2H, *meta*-ArH), 7.24 (d, *J* = 8.5 Hz, 1H, *para*-ArH), 6.37 (s, 1H backbone-CH), 2.66 (s, 3H, backbone-C*H*$_3$), 1.90 (s, 3H, backbone-C*H*$_3$). ^{13}C{^{1}H} NMR (CDCl$_3$, 100 MHz, 298K, δ):

212.21, 164.84, 134.15, 129.47, 128.81, 113.38, 39.44, 21.06. Anal. Calcd. for $C_{11}H_{11}Cl_2NS$: N, 5.38; C, 50.78; H, 4.06. found N, 5.39; C, 51.05; H, 3.88.

HL^{Cl3}. Following the same procedure with **HL^{NO2}**, The reaction of (Z)-4-((2,4,6-trichlorophenyl)amino)pent-3-en-2-one (5 g, 16.97 mmol) and Lawesson's reagent (3.42 g, 8.48 mmol) in dichloromethane gave purified by column chromatography ethyl acetate/hexane 1:10 ratio. Solvent is removed by vacuum to give orange oil slowly solidified into greenish brown solid at -7 °C. (4.66 g, 87 % yield). ^1H NMR (CDCl$_3$, 400 MHz, 298K, δ): 15.14 (bs, 1H, NH), 7.44 (s, 2H, *meta*-ArH), 6.35 (s, 1H, backbone-CH), 2.64 (s, 3H, backbone-C*H*$_3$), 1.88 (s, 3H, backbone-C*H*$_3$). $^{13}C\{^1H\}$ NMR (CDCl$_3$, 100 MHz, 298K, δ): 213.08, 164.32, 134.67, 134.39, 132.68, 128.75, 113.39, 39.45, 20.99. Anal. Calcd. for $C_{11}H_{10}Cl_3NS$: N, 4.75; C, 44.84; H, 3.42. found N, 4.83; C, 44.83; H, 3.09.
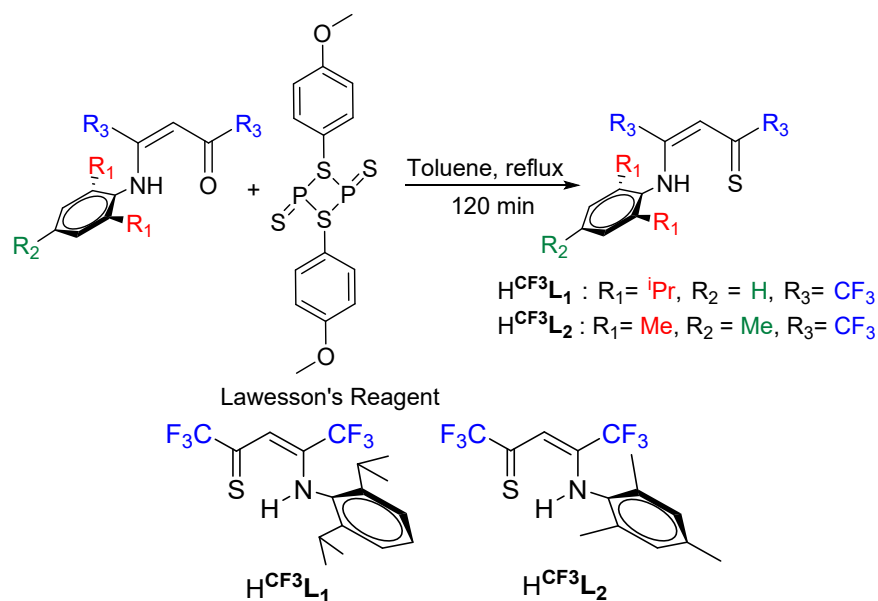
H^{CF3}L_1. The procedure of ligand synthesis is modified to previously reported **HL_1** or **HL_2** ligands.[1] The reaction of (Z)-4-((2,6-diisopropylphenyl)amino)-1,1,1,5,5,5-hexafluoropent-3-en-2-one (3.00 g, 8.16 mmol), and Lawesson's reagent (1.65 g, 4.08 mmol) were made suspension in toluene (50~60 ml approx.) and refluxed for 120 min. After cooling to room temperature, the solvent is removed under vacuum to give a reddish-brown residue that was purified by column chromatography ethyl acetate/hexane 1:10 ratio. Solvent is removed by vacuum to give deep reddish-brown oil. (2.45 g, 85 % yield). ^1H NMR (CDCl$_3$, 400 MHz, 298K, δ): 15.22 (bs, 1H,

NH), 7.39 (t, 1H, J = 8.0 Hz, *para*-ArH), 7.23 (d, 2H, J = 8.0 Hz, *meta*-ArH), 7.13 (s, 1H, backbone-CH), 2.85 (septet, 2H, J = 8 Hz, ArCH(CH$_3$)$_2$), 1.26 (d, 6H, ArCH(CH_3)$_2$), 1.12 (s, 6H, ArCH(CH_3)$_2$), ^{13}C{^{1}H} NMR (100 MHz, CDCl$_3$) δ 181.85 (q, $^2J_{CF}$ = 35Hz), 155.20 (q, $^2J_{CF}$ = 32Hz), 155.04, 146.55, 131.08, 129.91, 123.74, 120.36, 117.58, 87.30, 29.03, 25.35, 21.80. ^{19}F NMR (CDCl$_3$, 376 MHz, 298 K, δ): -66.30 (s, 3F, backbone CF$_3$), -68.41 (s, 3F, backbone CF$_3$). Anal. Calcd. for C$_{17}$H$_{19}$F$_6$NS: N, 3.65; C, 53.26; H, 5.00. found N, 3.80; C, 53.15; H, 4.84.

$H^{CF3}L_2$. Following the same procedure with $H^{CF3}L_1$, The reaction of (Z)-4-((2,4,6-trimethylphenyl)amino) 1,1,1,5,5,5-hexafluoropent-3-en-2-one (3 g, 16.97 mmol) and Lawesson's reagent (3.42 g, 8.48 mmol) in toluene reflux for 120 min. After cooling to room temperature, the crude compound purified by column chromatography ethyl acetate/hexane 1:10 ratio. Solvent is removed by vacuum to give deep brown colored oil. (2.66 g, 87 % yield). ^{1}H NMR (CDCl$_3$, 400 MHz, 298K, δ): 14.99 (bs, 1H, NH), 7.12 (s, 2H, backbone-CH), 6.95 (s, 1H, *meta*-ArH), 2.31 (s, 3H, para-ArCH_3), 2.17 (s, 6H, *ortho*-ArCH_3). ^{13}C{^{1}H} NMR (CDCl$_3$, 100 MHz, 298K, δ): 195.98 (q, $^2J_{CF}$ = 34Hz), 154.14 (q, $^2J_{CF}$ = 31Hz), 153.99, 139.14, 135.03, 131.14, 129.23, 120.97, 118.13, 105.03, 21.14, 18.24. ^{19}F NMR (CDCl$_3$, 376 MHz, 298 K, δ): -67.09 (s, 3F, backbone CF$_3$), -68.37 (s, 3F, backbone CF$_3$). Anal. Calcd. for C$_{14}$H$_{13}$F$_6$NS: N, 4.11; C, 49.27; H, 3.84. found N, 4.15; C, 49.09; H, 3.79.

Synthesis and Characterization of 2,4,6-Trimethylphenyl Isocyanide Copper(I) Adducts.

To the desired [**L**Cu^I]$_3$ complex (typically 0.1 g, 75~115 mmol) in *n*-hexane (2 ml) was added three equivalents of 2,4,6-trimethylphenyl isocyanide (225 ~ 345 mmol) dissolved in *n*-hexane (2 ml). The resulting mixture was stirred for 60 minutes under an N$_2$ atmosphere. The solvent removed under vacuum to obtain either bright yellow or pale red colored residue or precipitate as mono **L**Cu^{I}CNR adducts. These adducts are characterized by ^{1}H, ^{13}C and ^{19}F NMR techniques, respectively and FTIR methods.

$L^{NO2}Cu(2,4,6-CNC_6H_2Me_3)$. Obtained as velvet red colored solid. Yield: 95.2%. ^{1}H NMR (CDCl$_3$, 400 MHz, 298K, δ): 8.20 (d, J = 8.0 Hz, 2H, *meta*-ArH), 7.13 (d, J = 8.0 Hz, 2H, *ortho*-ArH), 6.83 (s, 2H, ArH(C≡N)), 6.35 (s, 1H, backbone-CH), 2.51 (s, 3H, backbone-CH$_3$), 2.25 (s, 3H, backbone-CH$_3$), 2.07 (s, 6H, *ortho*-ArCH$_3$(C≡N)), 1.94 (s, 3H, *para*-ArCH$_3$(C≡N)). ^{13}C{^{1}H}

4

NMR (CDCl$_3$, 100 MHz, 298K, δ): 174.97, 167.44, 159.90, 144.06, 140.09, 134.91, 128.84, 125.05, 122.88, 118.49, 35.65, 25.41, 21.38, 18.49.

L^{F2}Cu(2,4,6-CNC$_6$H$_2$Me$_3$). Obtained as bright yellow colored solid. Yield: 96.7% ^{1}H NMR (CDCl$_3$, 400 MHz, 298K, δ): 7.03~6.96 (m, 1H, *para*-ArH), 6.90 (t, J = 8 Hz, 2H, *meta*-ArH), 6.84 (s, 2H, ArH(C≡N)), 6.40 (s, 1H, backbone-CH), 2.51 (s, 3H, backbone-CH$_3$), 2.26 (s, 3H, backbone-CH$_3$), 2.12 (s, 6H, *ortho*-ArCH$_3$(C≡N)), 1.96 (s, 3H, *para*-ArCH$_3$(C≡N)). ^{13}C{^{1}H} NMR (CDCl$_3$, 100 MHz, 298K, δ): 175.12, 170.91, 156.02, 153.57, 139.70, 135.03, 128.70, 124.06 (t, $^3J_{CF}$ = 9 Hz), 118.62, 111.68 (m, $^2J_{CF}$ = 18 Hz), 35.81, 25.04, 21.38, 18.57. ^{19}F NMR (CDCl$_3$, 376 MHz, 298K, δ): -121.00 (t, J = 7.5 Hz, 2F, *ortho*-ArF) Anal. Calcd for C$_{21}$H$_{21}$CuF$_2$N$_2$S: C, 57.18; H, 4.87; N, 6.44. Found: C, 56.89; H, 4.66; N, 6.26.

L^{F3}Cu(2,4,6-CNC$_6$H$_2$Me$_3$). Obtained as bright yellow colored solid. Yield: 95.5% ^{1}H NMR (CDCl$_3$, 400 MHz, 298K, δ): 6.86 (s, 2H, ArH(C≡N)), 6.70 (t, J = 8 Hz, 2H, *meta*-ArH), 6.39 (s, 1H, backbone-CH), 2.51 (s, 3H, backbone-CH$_3$), 2.27 (s, 3H, backbone-CH$_3$), 2.16 (s, 6H, *ortho*-ArCH$_3$(C≡N)), 1.96 (s, 3H, *para*-ArCH$_3$(C≡N)). ^{13}C{^{1}H} NMR (CDCl$_3$, 100 MHz, 298K, δ): 176.09, 171.41, 154.52 ($^1J_{CF}$ = 246 Hz), 139.84, 134.96, 118.59, 100.40 (t, $^2J_{CF}$ = 26 Hz), 35.87, 25.01, 21.40, 18.54. ^{19}F NMR (CDCl$_3$, 376 MHz, 298K, δ): -115.01 (t, J = 7.5 Hz, 2F, *para*-ArF), -117.90 (d, J = 7.5 Hz, 2F, *ortho*-ArF). Anal. Calcd for C$_{21}$H$_{20}$CuF$_3$N$_2$S: C, 55.60; H, 4.40; N, 6.18. Found: C, 55.25; H, 4.24; N, 5.93.

L^{Cl2}Cu(2,4,6-CNC$_6$H$_2$Me$_3$). Obtained as bright lemon yellow colored solid. Yield: 96.2% ^{1}H NMR (CDCl$_3$, 400 MHz, 298K, δ): 7.31 (d, J = 8 Hz, 1H, *meta*-ArH), 6.94 (t, J = 8 Hz, 2H, *para*-ArH), 6.84 (s, 2H, ArH(C≡N)), 6.38 (s, 1H, backbone-CH), 2.53 (s, 3H, backbone-CH$_3$), 2.25 (s, 3H, backbone-CH$_3$), 2.12 (s, 6H, *ortho*-ArCH$_3$(C≡N)), 1.86 (s, 3H, *para*-ArCH$_3$(C≡N)). ^{13}C{^{1}H} NMR (CDCl$_3$, 100 MHz, 298K, δ): 175.42, 169.39, 147.94, 139.71, 135.08, 128.70, 128.35, 128.07, 124.60, 118.02, 35.83, 24.71, 21.38, 18.59. Anal. Calcd for C$_{21}$H$_{21}$CuCl$_2$N$_2$S: C, 53.90; H, 4.52; N, 5.99. Found: C, 53.77; H, 4.32; N, 5.82.

L^{Cl3}Cu(2,4,6-CNC$_6$H$_2$Me$_3$). Obtained as golden yellow colored solid. Yield: 96.2% ^{1}H NMR (CDCl$_3$, 400 MHz, 298K, δ): 7.19 (s, 2H, *meta*-ArH), 6.80 (s, 2H, ArH(C≡N)), 6.31 (s, 1H, backbone-CH), 2.46 (s, 3H, backbone-CH$_3$), 2.20 (s, 3H, backbone-CH$_3$), 2.10 (s, 6H, *ortho*-ArCH$_3$(C≡N)), 1.79 (s, 3H, *para*-ArCH$_3$(C≡N)). ^{13}C{^{1}H} NMR (CDCl$_3$, 100 MHz, 298K, δ): 176.67, 169.55, 146.81, 139.92, 135.10, 128.97, 128.79, 128.62, 128.25, 117.96, 117.92, 35.90,

24.76, 21.40, 18.55. Anal. Calcd for $C_{21}H_{20}CuCl_3N_2S$: C, 50.21; H, 4.01; N, 5.58. Found: C, 49.92; H, 3.81; N, 5.42.

$^{CF3}L_1Cu(2,4,6\text{-}CNC_6H_2Me_3)$. Obtained as pale red colored powdered solid. Yield: 97.2 % Single crystals suitable for X-ray diffraction were grown from saturated solution of *n*-hexane at -20 °C under N_2 atmosphere. ^1H NMR (CDCl$_3$, 400 MHz, 298K, δ): 7.16 (s, 1H, backbone-CH), 7.12 (m, *J* = 8.0 Hz, 2H, ArH), 6.84 (s, 2H, ArH(C≡N)), 2.80 (septet, *J* = 8 Hz, 2H, ArC*H*(CH$_3$)$_2$), 2.26 (s, 3H, *para*-ArCH$_3$(C≡N)), 2.04 (s, 6H, *ortho*-ArCH$_3$(C≡N)), 1.20 (s, 6H, ArCH(C*H$_3$*)$_2$), 1.18 (s, 6H, ArCH(C*H$_3$*)$_2$). ^{13}C{^{1}H} NMR (CDCl$_3$, 100 MHz, 298K, δ): 164.01 (q, $^2J_{CF}$ = 24 Hz), 154.95 (q, $^2J_{CF}$ = 26 Hz), 146.21, 140.52, 137.39, 135.47, 128.86, 125.69, 123.36, 110.36, 28.51, 25.09, 22.87, 21.41, 18.54. ^{19}F NMR (376 MHz, CDCl$_3$) δ -63.37 (s, 3F, backbone CF$_3$), -66.52 (s, 3F, backbone CF$_3$). Anal. Calcd. for $C_{27}H_{29}CuF_6N_2S$: C, 54.86; H, 4.95; N, 4.74. found C, 54.77; H, 4.48; N, 4.71.

$^{CF3}L_2Cu(2,4,6\text{-}CNC_6H_2Me_3)$. Obtained as pale red colored powdered solid. Yield: 97.5 % Single crystals suitable for X-ray diffraction were grown from saturated solution of *n*-hexane at -20 °C under N_2 atmosphere. ^1H NMR (CDCl$_3$, 400 MHz, 298K, δ): 7.15 (s, 3H, backbone-CH), 6.87 (s, 2H, ArH), 6.82 (s, 2H, ArH(C≡N)), 2.27 (s, 3H, *para*-ArCH$_3$), 2.21 (s, 3H, *para*-ArCH$_3$(C≡N)), 2.12 (s, 3H, *ortho*-ArCH$_3$), 2.09 (s, 3H, *ortho*-ArCH$_3$(C≡N)), ^{13}C{^{1}H} NMR (CDCl$_3$, 100 MHz, 298K, δ): 163.94 (q, $^2J_{CF}$ = 38 Hz), 155.58 (q, $^2J_{CF}$ = 27 Hz), 146.64, 140.44, 135.36, 134.05, 128.72, 128.62, 126.94, 124.26, 121.50, 110.10, 21.41, 20.81, 18.82, 18.38. ^{19}F NMR (376 MHz, CDCl$_3$) δ -65.90 (s, 3F, backbone CF$_3$), -65.91 (s, 3F, backbone CF$_3$). Anal. Calcd. for $C_{24}H_{23}CuF_6N_2S$: C, 52.50; H, 4.22; N, 5.10. found C, 52.67; H, 4.03; N, 5.04.

NMR spectra
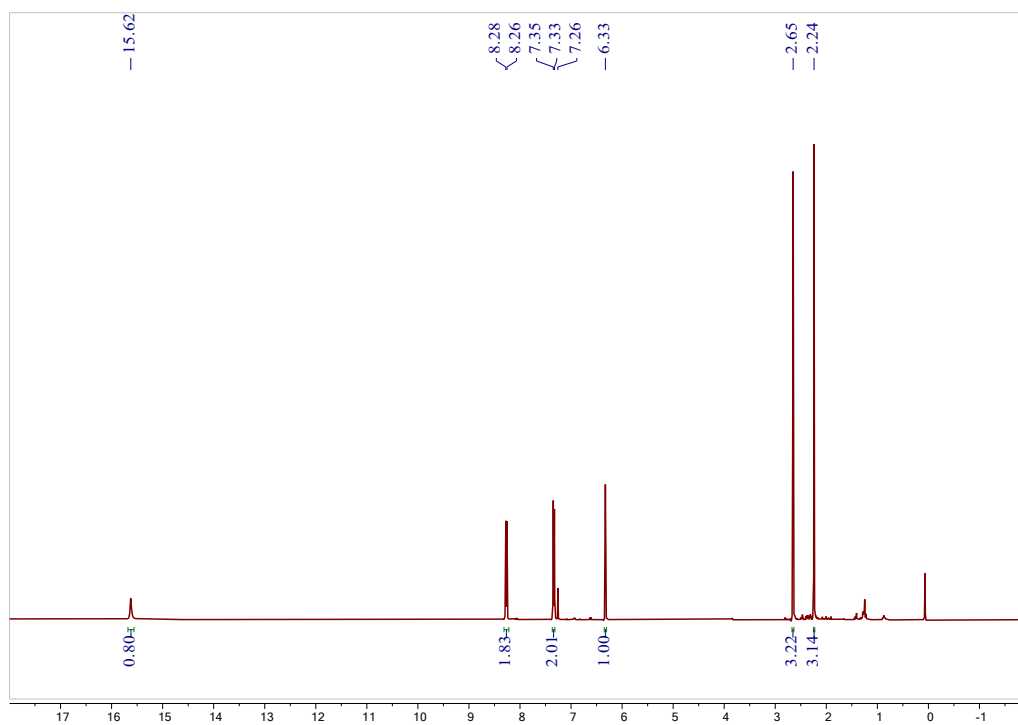
Figure S1. ^{1}H NMR spectrum of **HL^NO2** in CDCl$_3$ (400 MHz, 298 K).
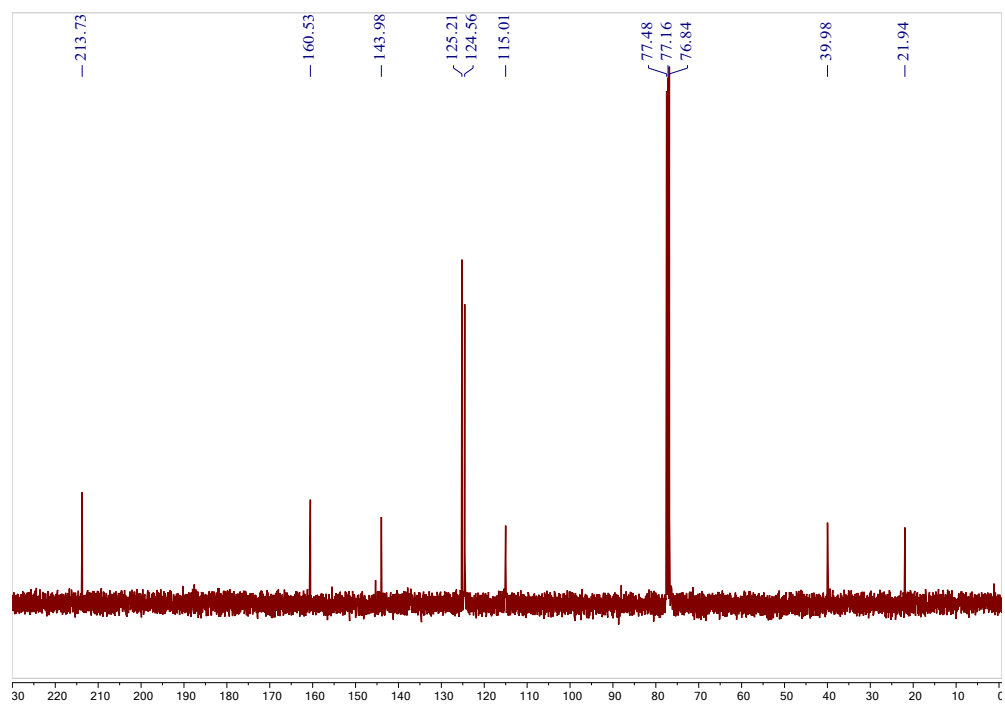
Figure S2. ^{13}C{^{1}H} NMR spectrum of **HL^NO2** in CDCl$_3$ (400 MHz, 298 K).
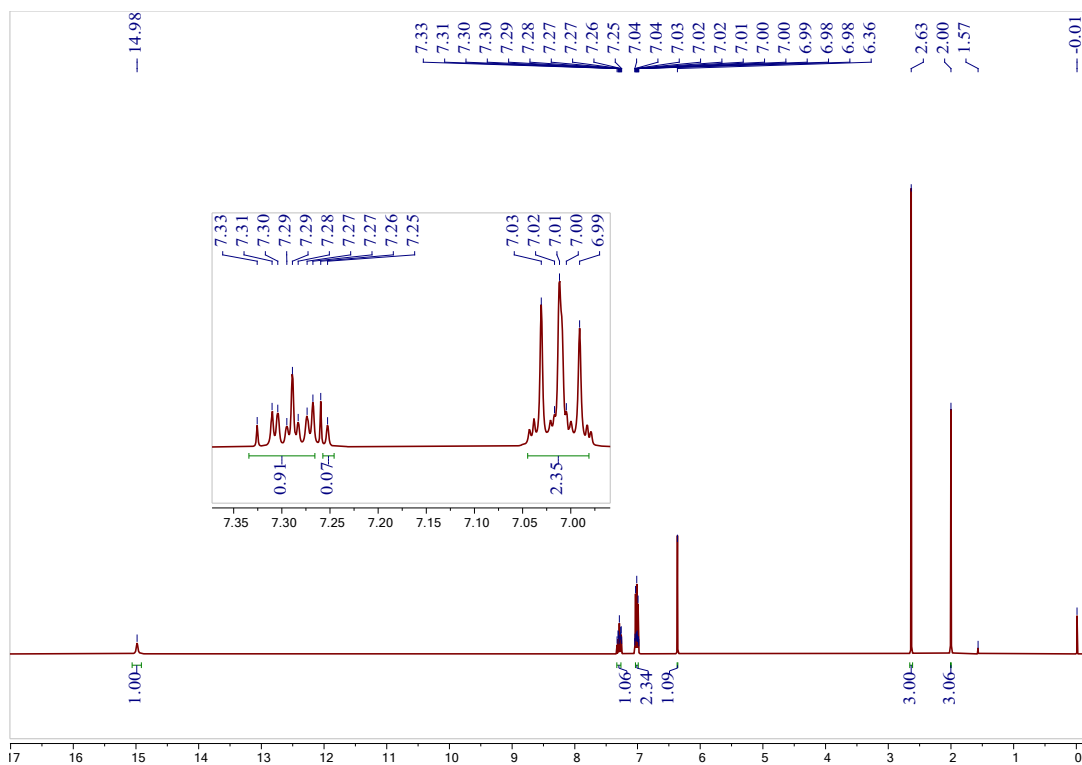
Figure S3. ^{1}H NMR spectrum of H**L**^{F2} in CDCl$_3$ (400 MHz, 298 K).
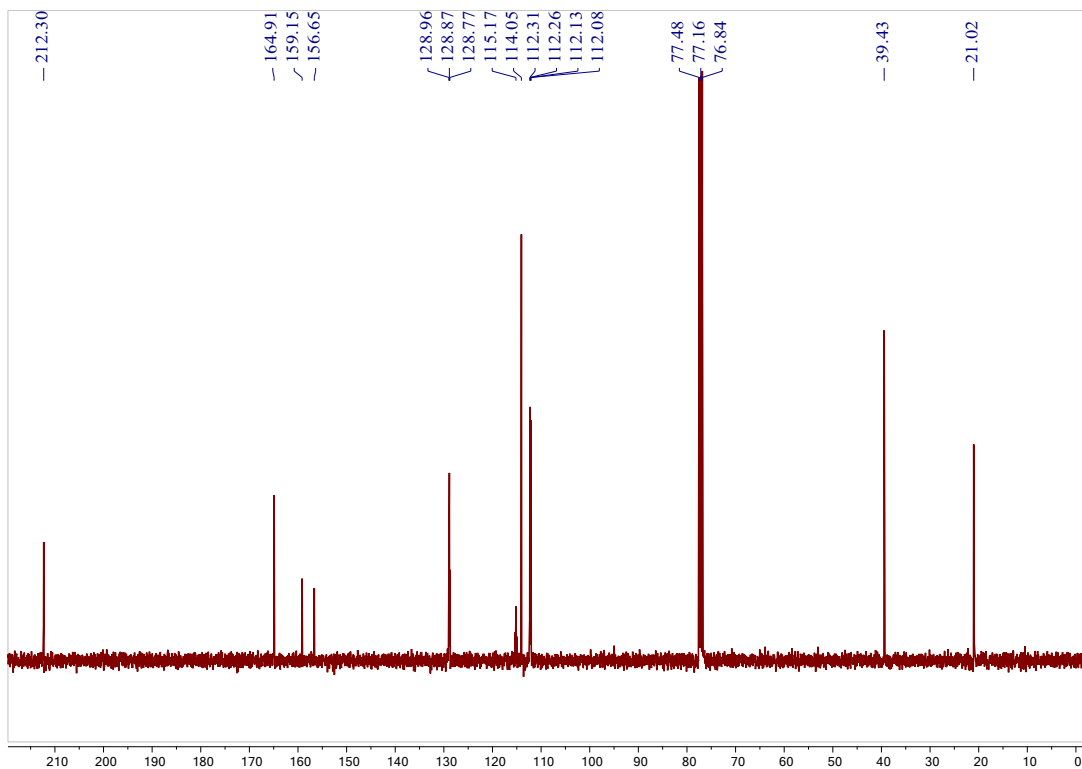
Figure S4. ^{13}C{^{1}H} NMR spectrum of HL^{NF2} in CDCl$_3$ (100 MHz, 298 K).
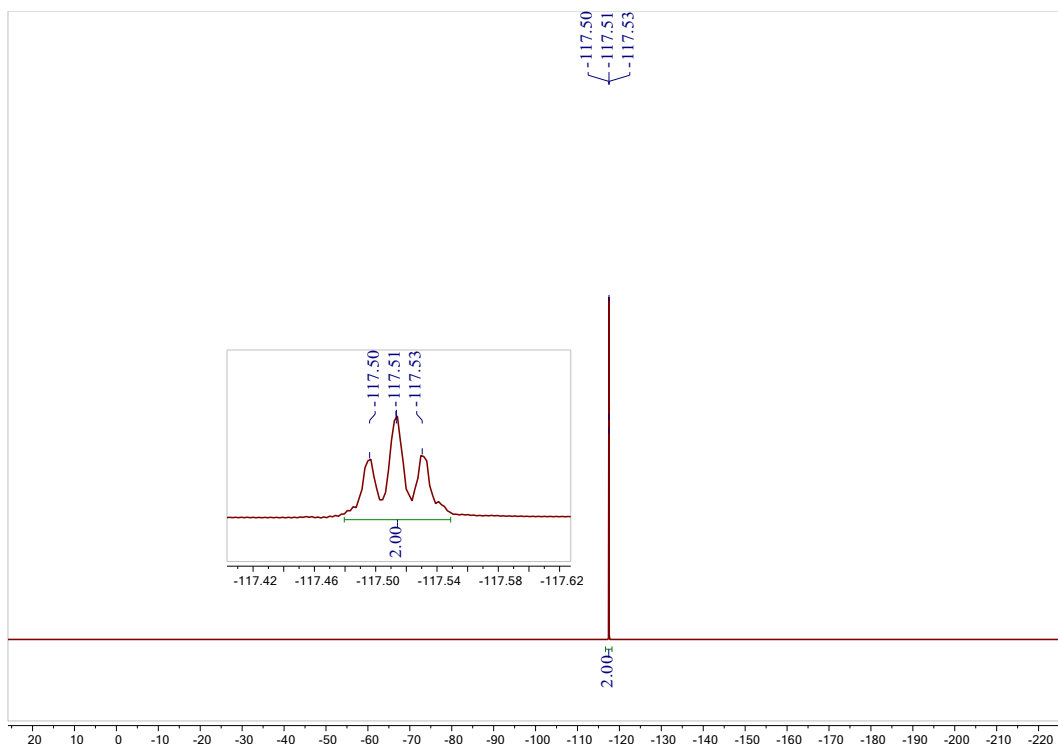
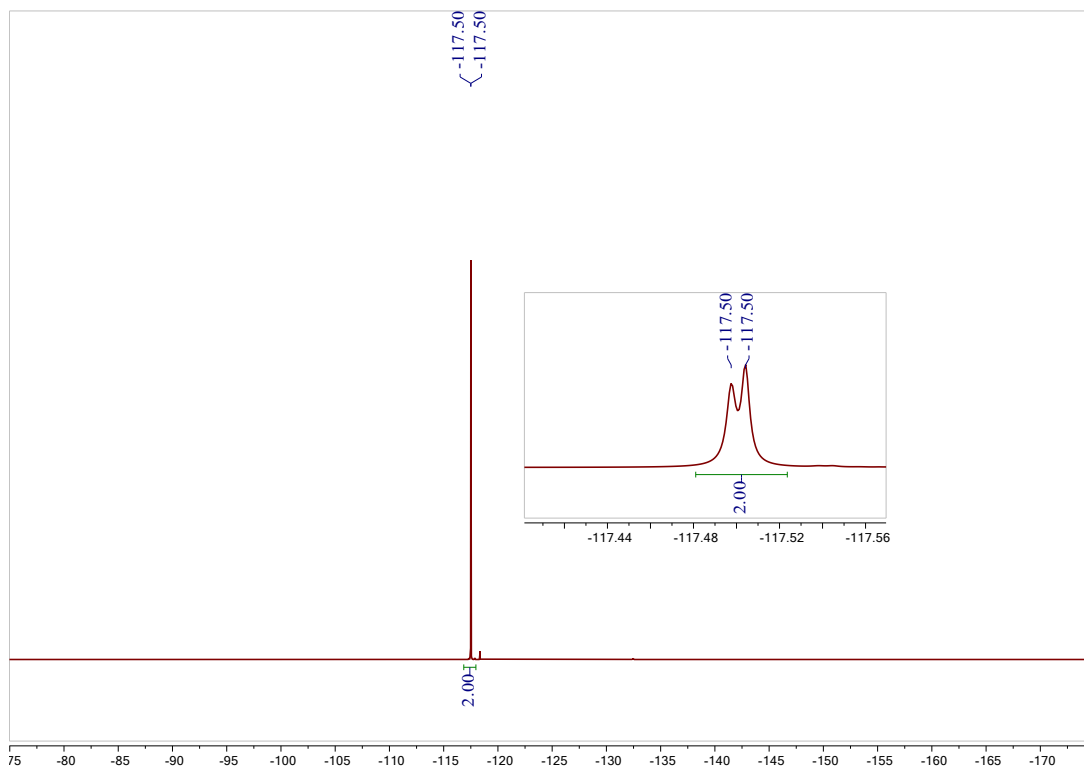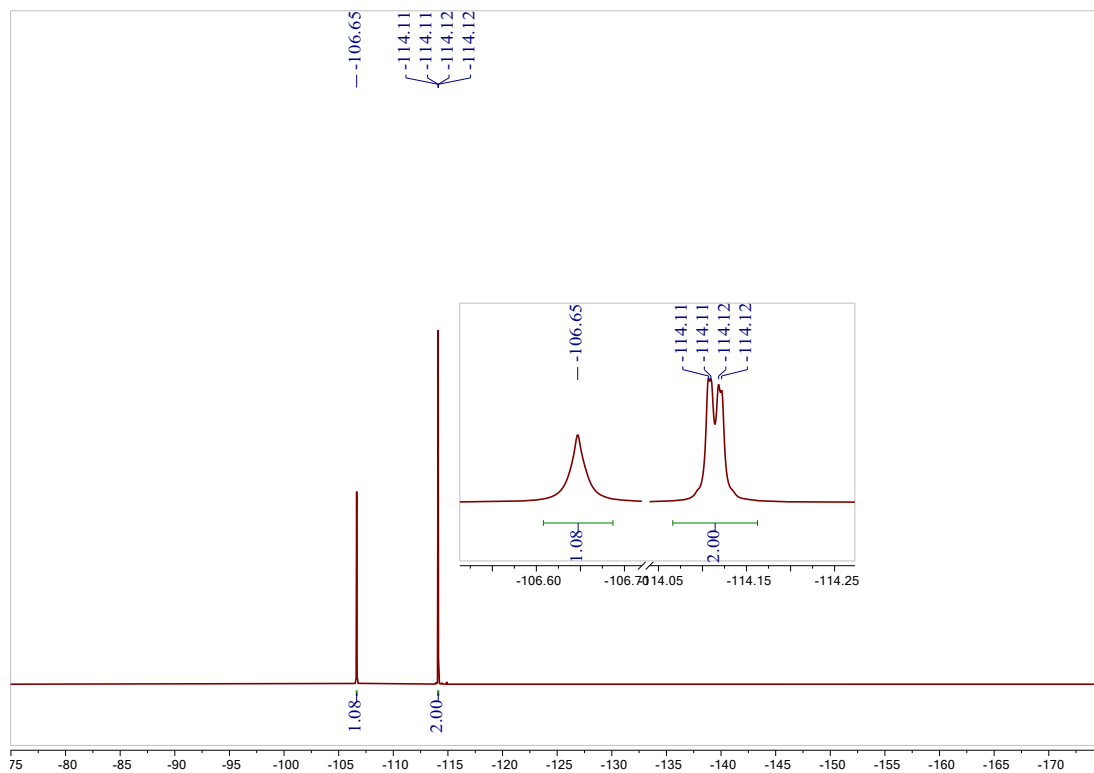**Figure S5.** ^{19}F NMR spectrum of HL^{F2} in CDCl$_3$ (376 MHz, 298 K).

Figure S6. $^{19}F\{^1H\}$ NMR spectrum of HL^{F2} in CDCl$_3$ (471 MHz, 298 K).
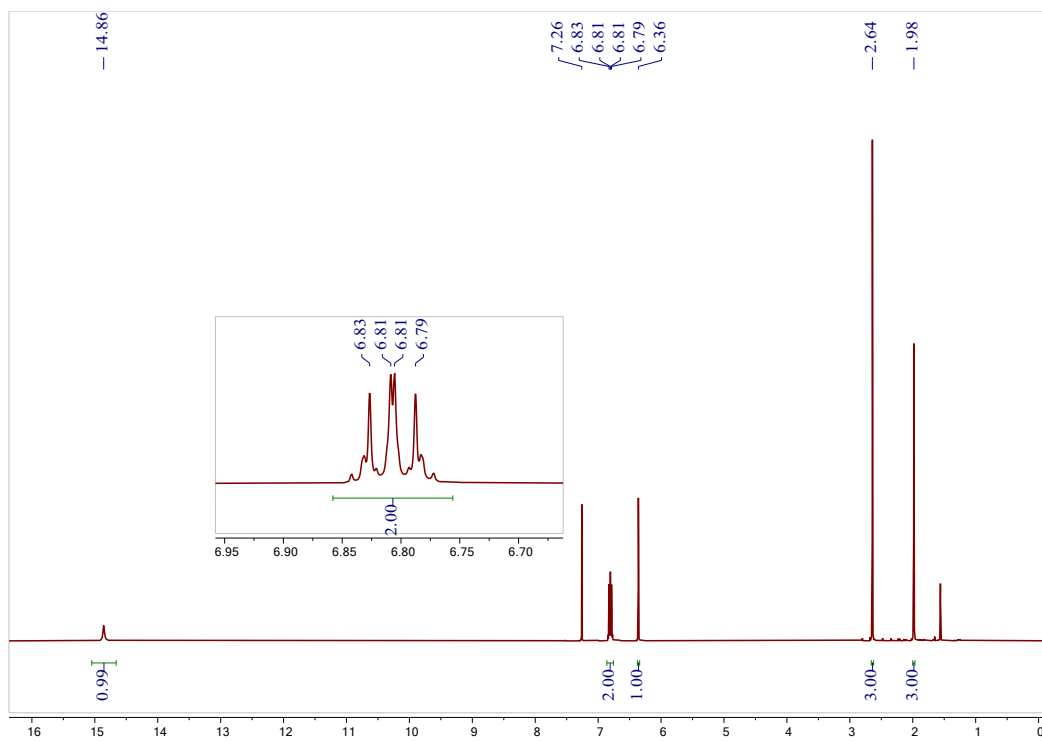
Figure S7. ^{1}H NMR spectrum of H**L**$^{\text{F3}}$ in CDCl$_3$ (400 MHz, 298 K).
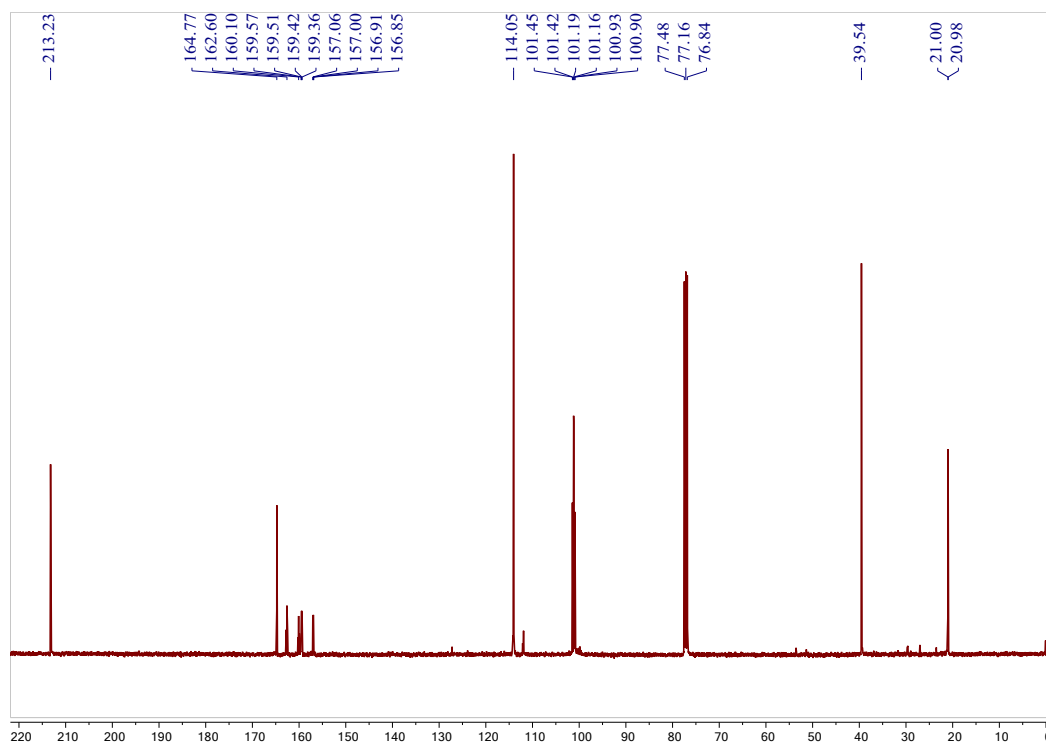
Figure S8. ^{13}C{^{1}H} NMR spectrum of H**L**$^{\text{F3}}$ in CDCl$_3$ (100 MHz, 298 K).

10
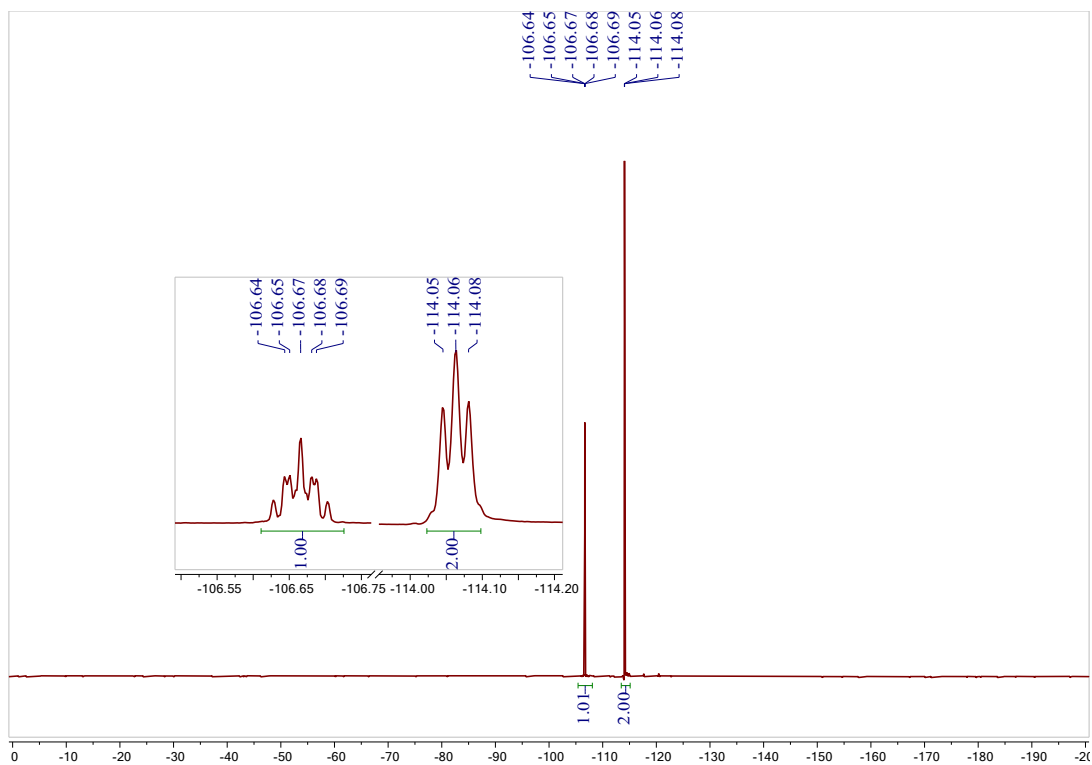
Figure S9. ^{19}F NMR spectrum of H**L^{F3}** in CDCl$_3$ (376 MHz, 298 K).

Figure S10. $^{19}F\{^1H\}$ NMR spectrum of H**L^{F3}** in CDCl$_3$ (471 MHz, 298 K).
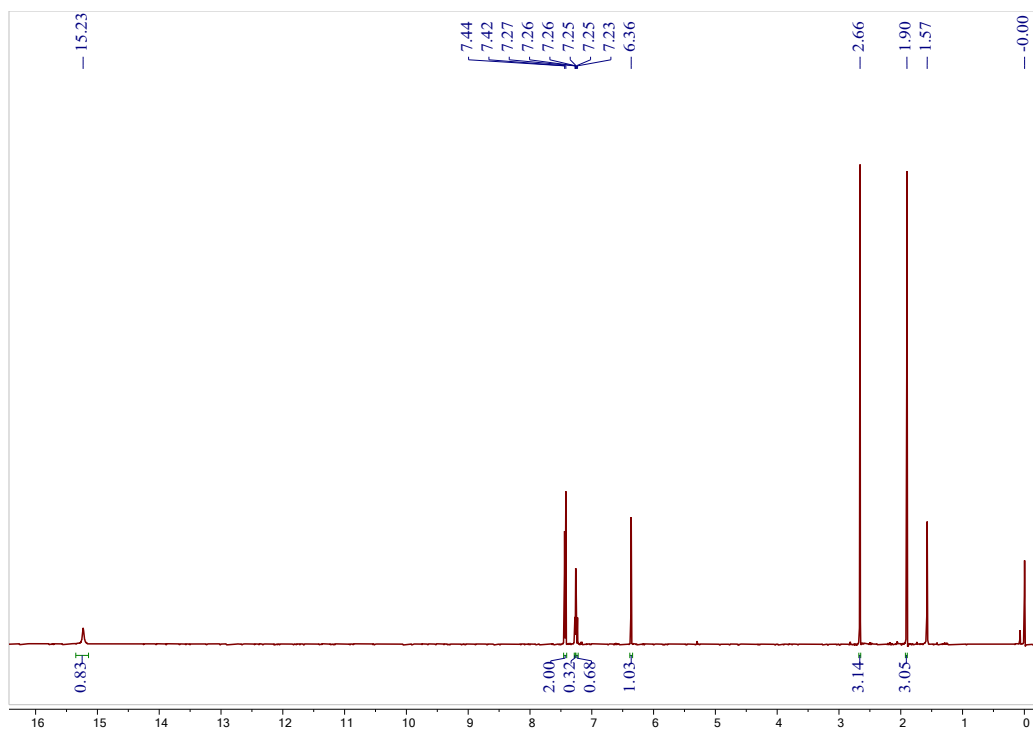
Figure S11. ^{1}H NMR spectrum of H**L**^{Cl2} in CDCl$_3$ (400 MHz, 298 K).
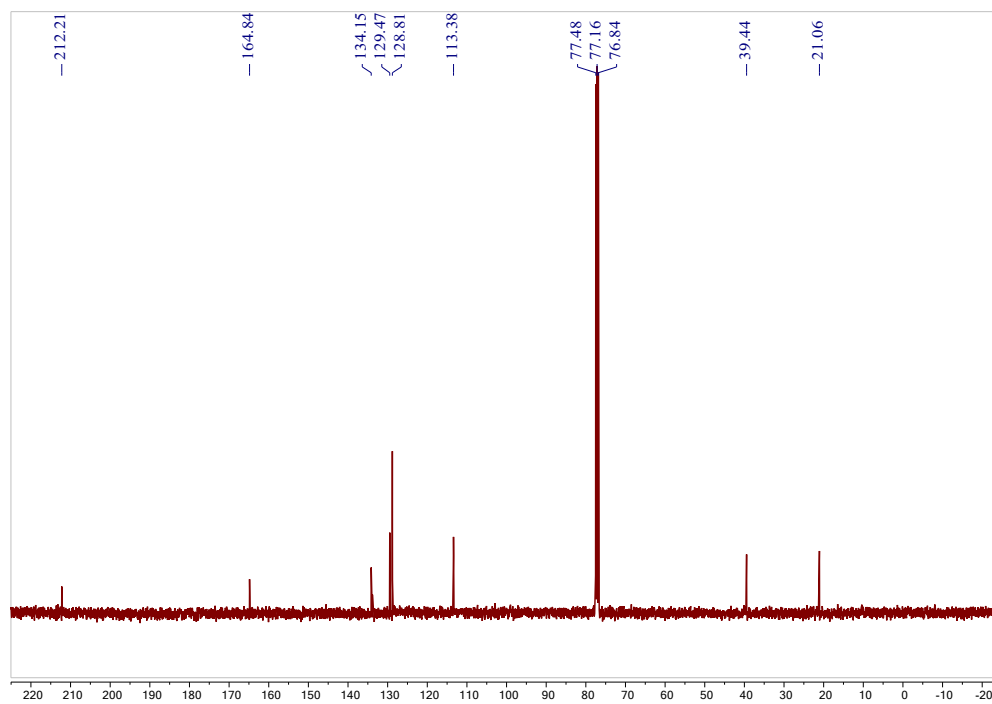
Figure S12. ^{13}C{^{1}H} NMR spectrum of H**L**^{Cl2} in CDCl$_3$ (100 MHz, 298 K).
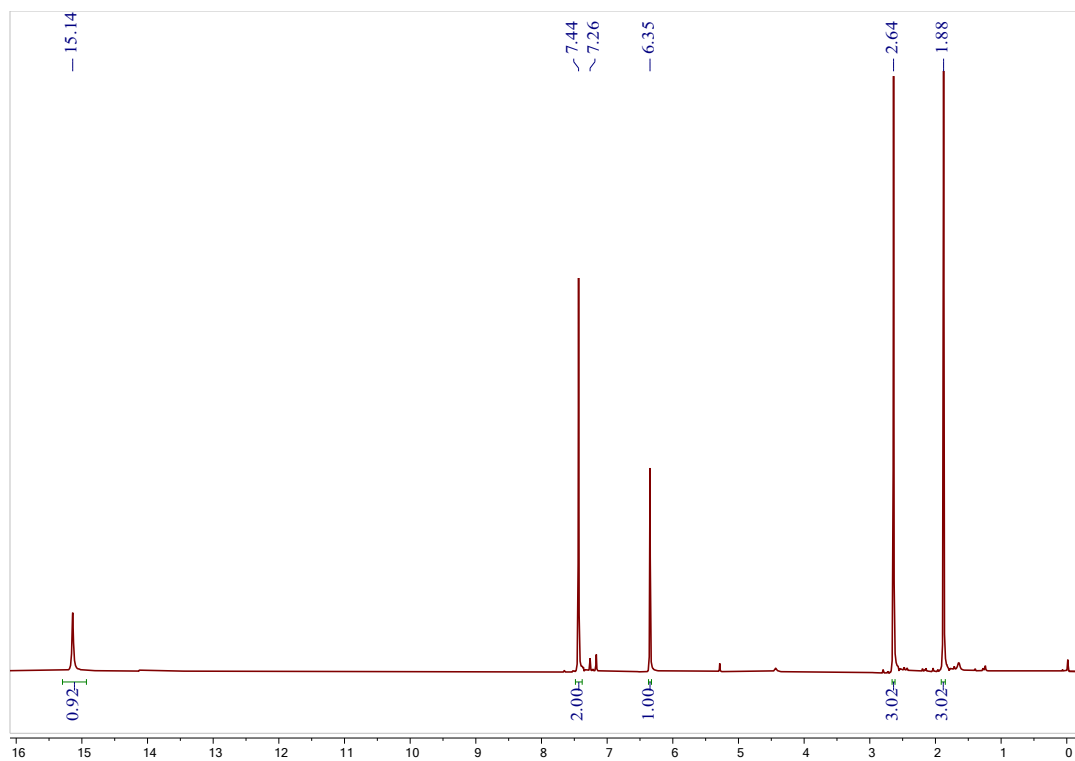
Figure S13. ^{1}H NMR spectrum of **HL^{Cl3}** in CDCl$_3$ (400 MHz, 298 K).
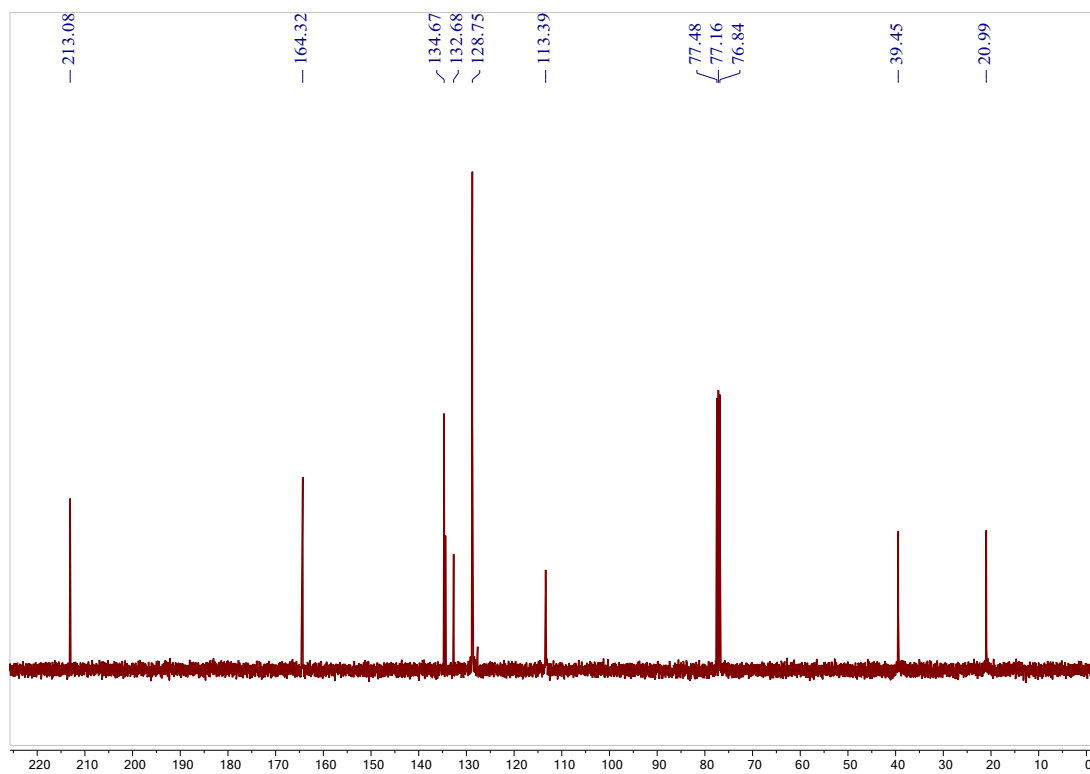
Figure S14. ^{13}C{^{1}H} NMR spectrum of **HL^{Cl3}** in CDCl$_3$ (100 MHz, 298 K).

13
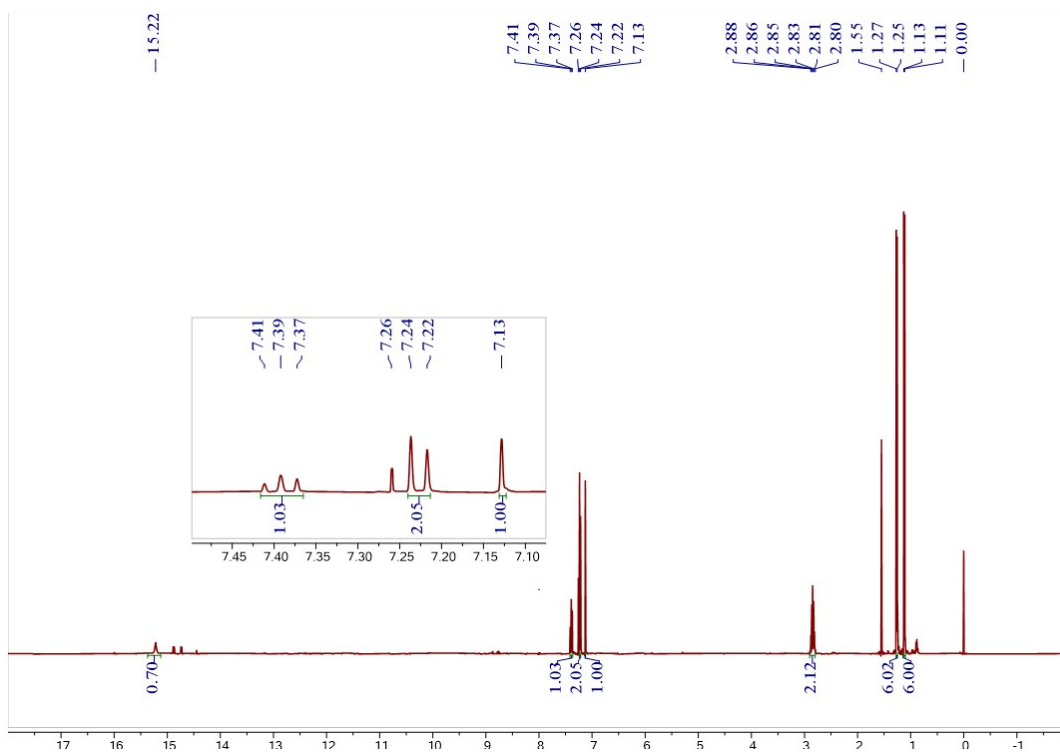
Figure S15. ^{1}H NMR spectrum of H$^{\text{CF3}}$**L$_1$** in CDCl$_3$ (400 MHz, 298 K).
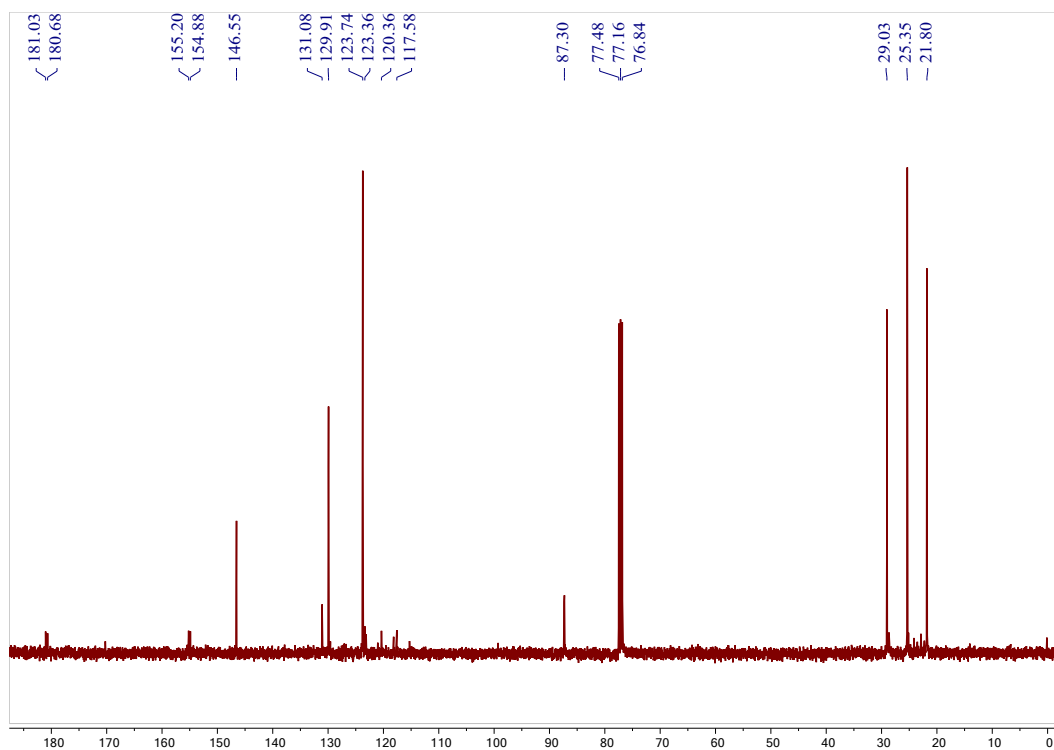
Figure S16. ^{13}C{^{1}H} NMR spectrum of H$^{\text{CF3}}$**L$_1$** in CDCl$_3$ (100 MHz, 298 K).
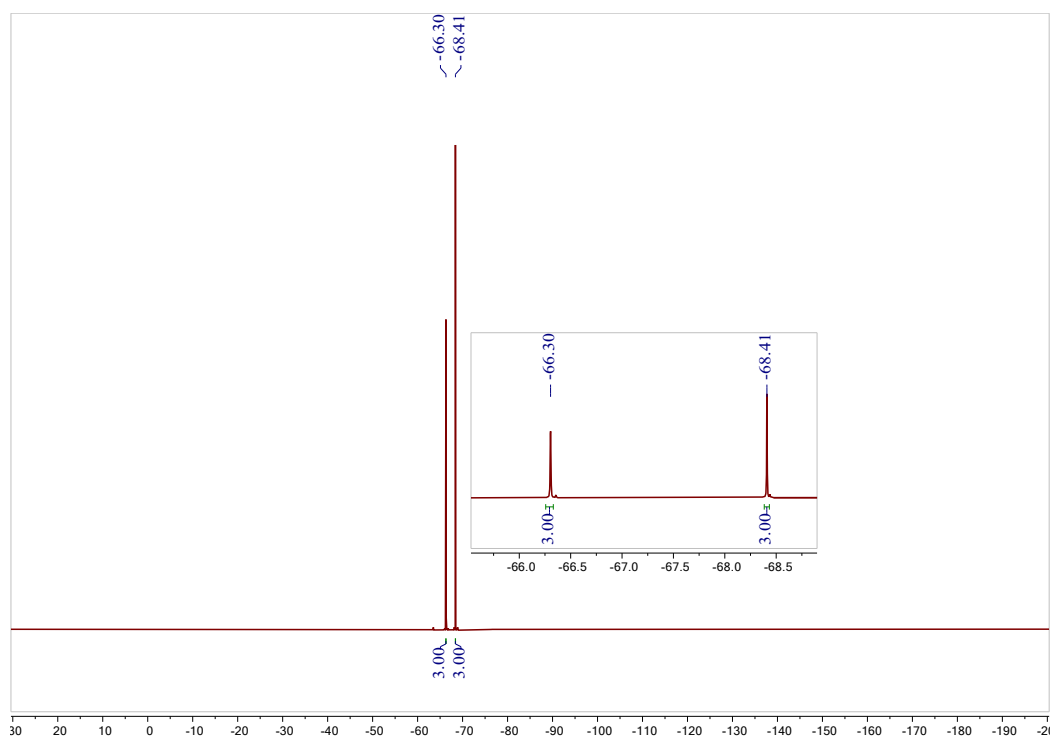
Figure S17. ^{19}F NMR spectrum of H^{CF3}L$_1$ in CDCl$_3$ (376 MHz, 298 K).
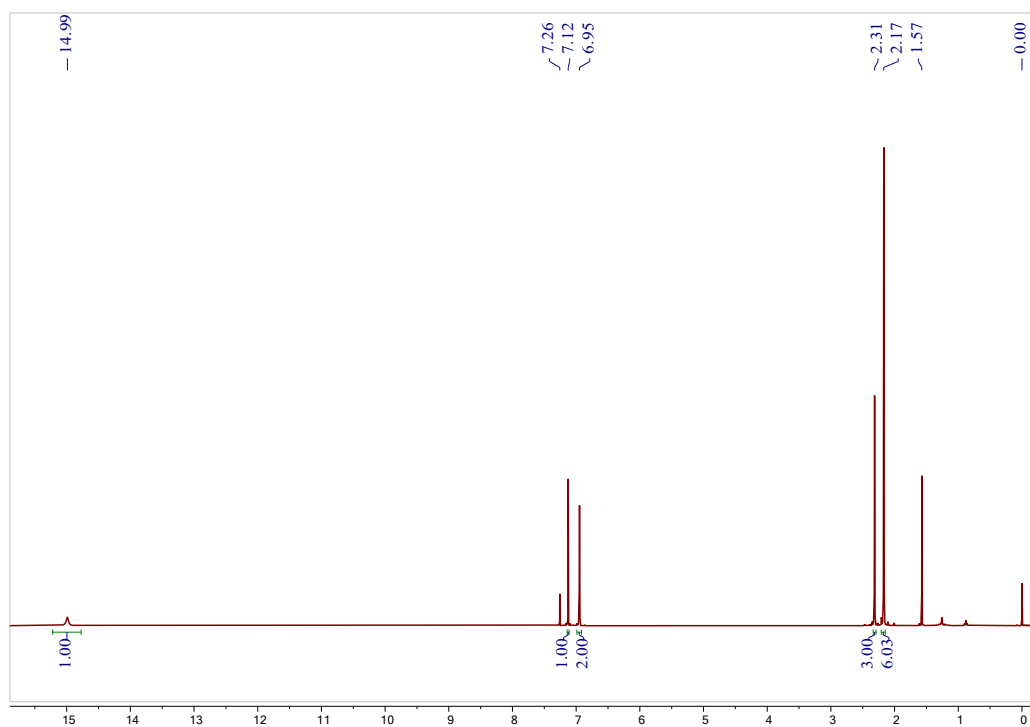
Figure S18. ^{1}H NMR spectrum of H^{CF3}L$_2$ in CDCl$_3$ (400 MHz, 298 K).

15
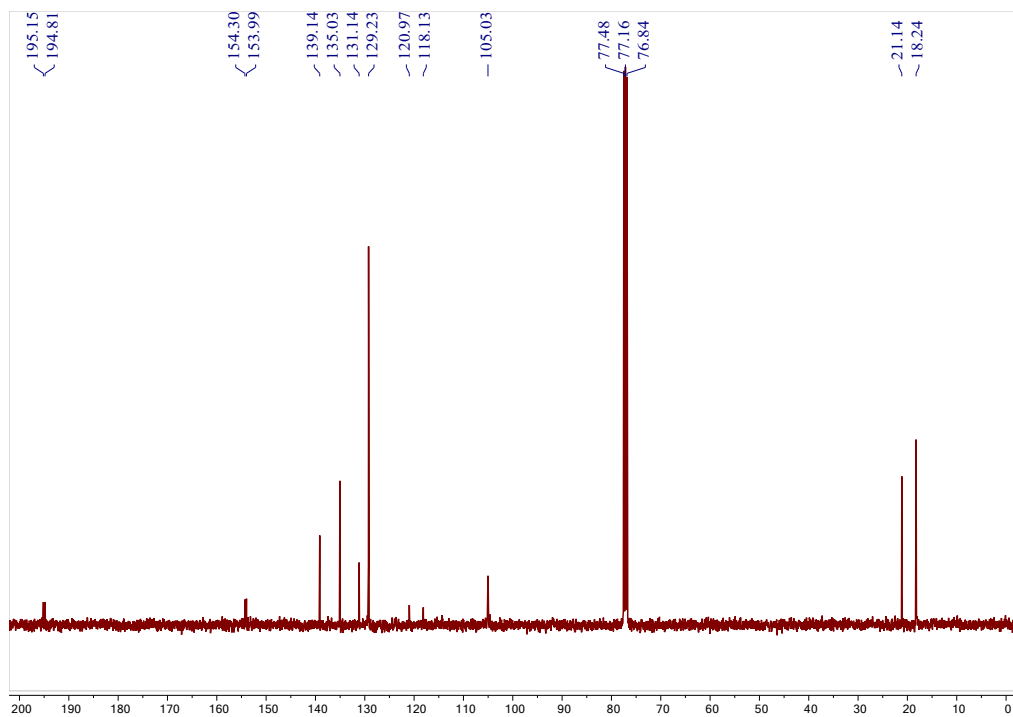
Figure S19. $^{13}C\{^1H\}$ NMR spectrum of $H^{CF3}L_2$ in $CDCl_3$ (100 MHz, 298 K).
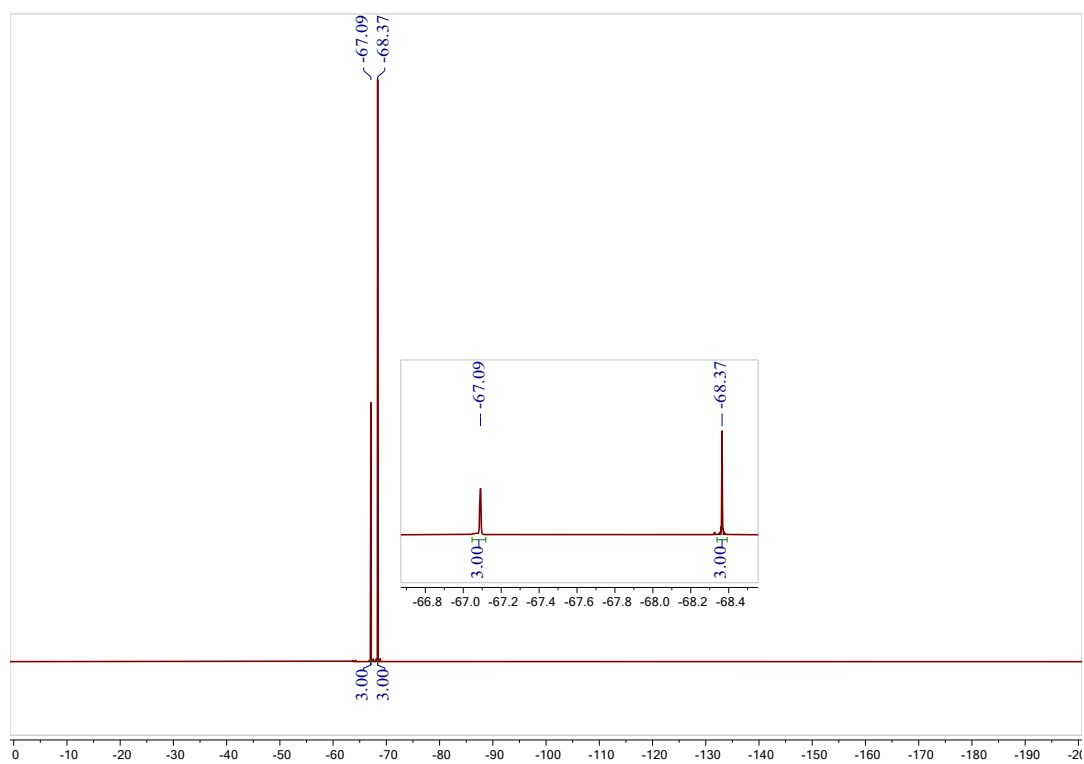
Figure S20. ^{19}F NMR spectrum of $H^{CF3}L_2$ in $CDCl_3$ (376 MHz, 298 K).
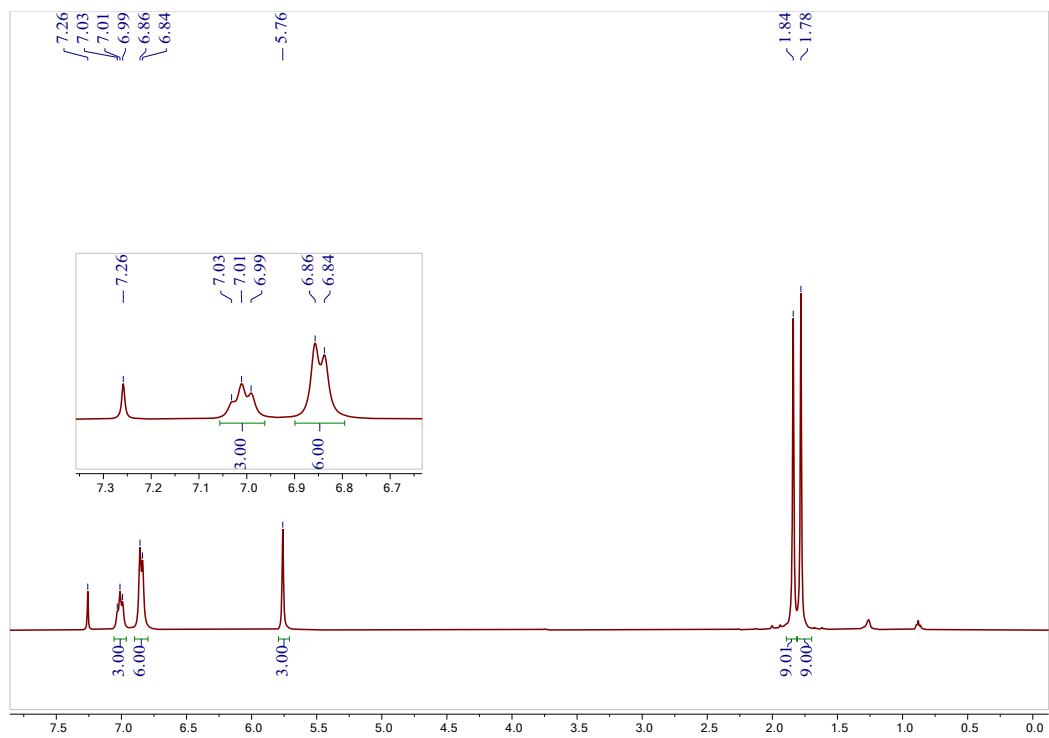
Figure S21. ^1H NMR spectrum of $[\mathbf{L^{F2}Cu}]_3$ in $CDCl_3$ (400 MHz, 298 K).
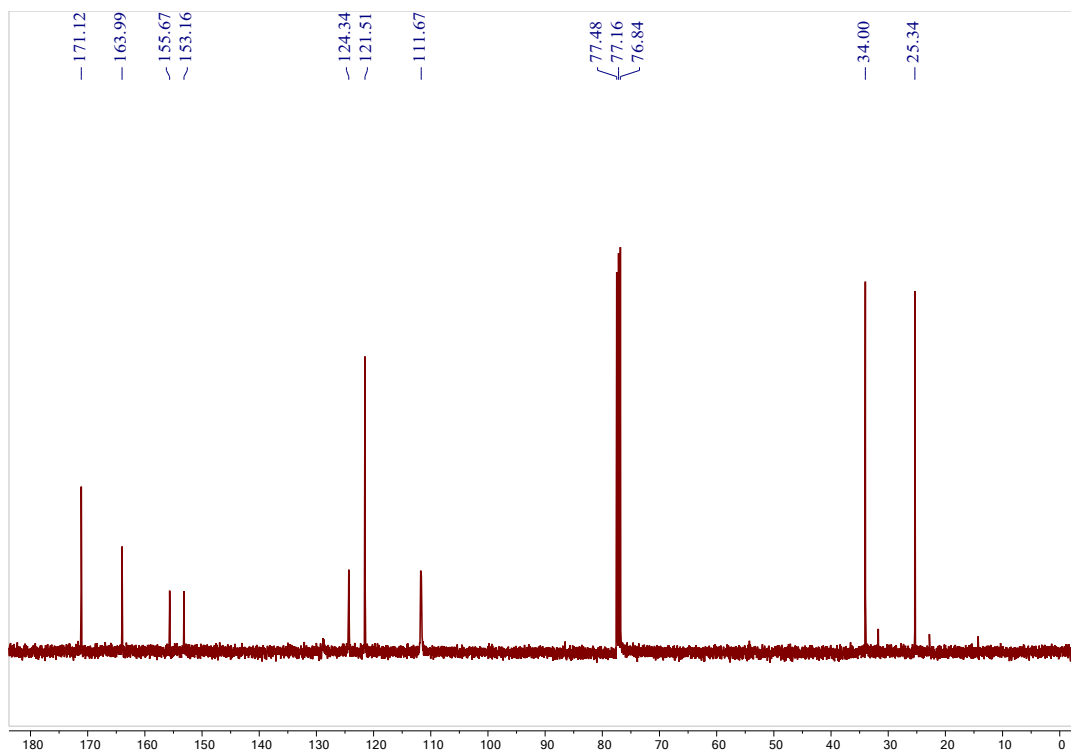
Figure S22. $^{13}C\{^1H\}$ NMR spectrum of $[\mathbf{L^{F2}Cu}]_3$ in $CDCl_3$ (100 MHz, 298 K).
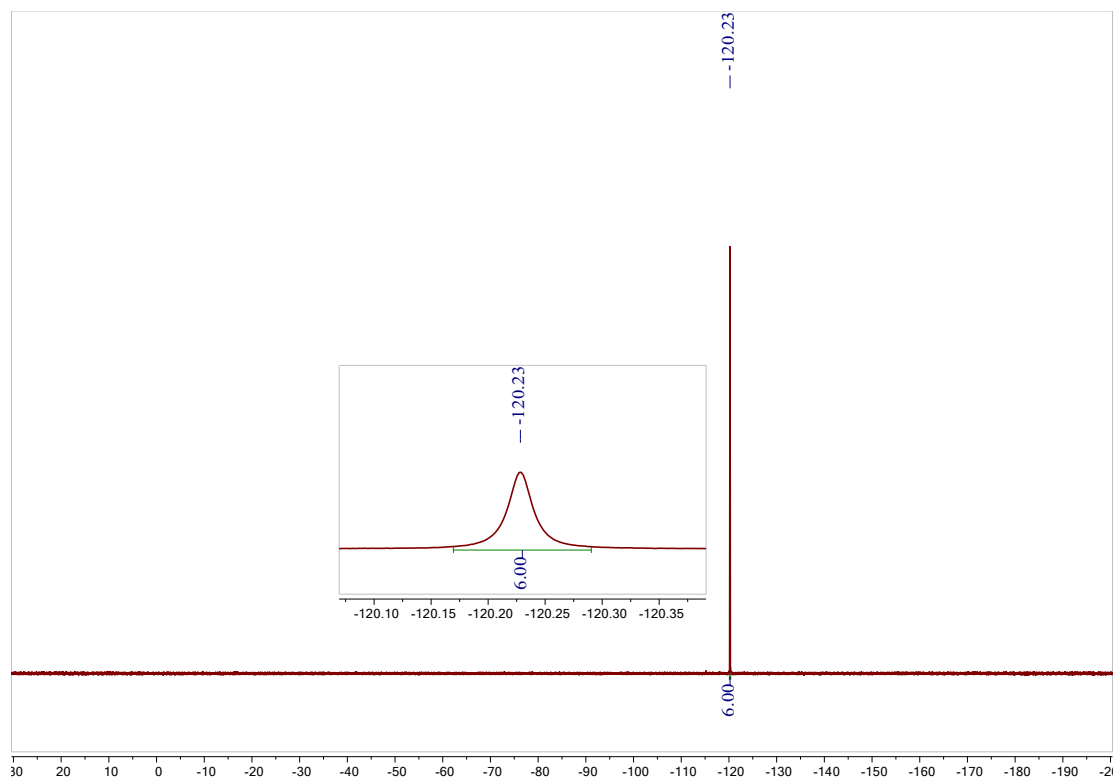
Figure S23. ^{19}F NMR spectrum of [**L^{F2}Cu**]$_3$ in CDCl$_3$ (376 MHz, 298 K).
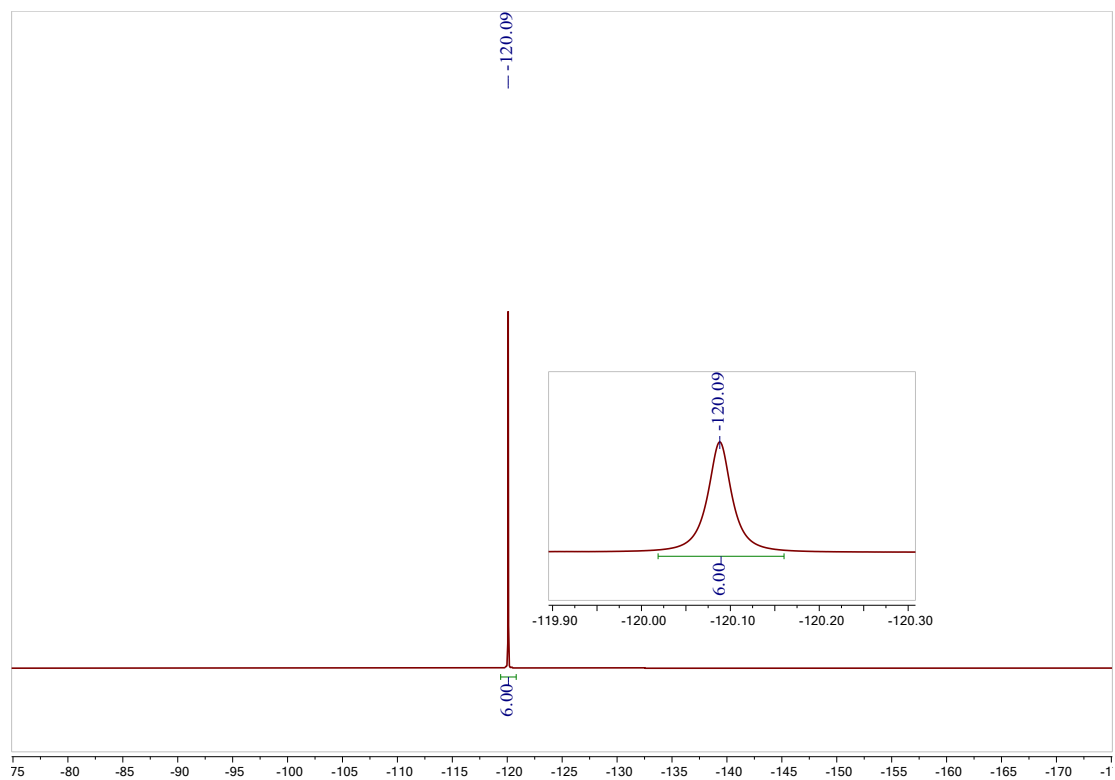
Figure S24. ^{19}F{^{1}H} NMR spectrum of [**L^{F2}Cu**]$_3$ in CDCl$_3$ (471 MHz, 298 K).

18
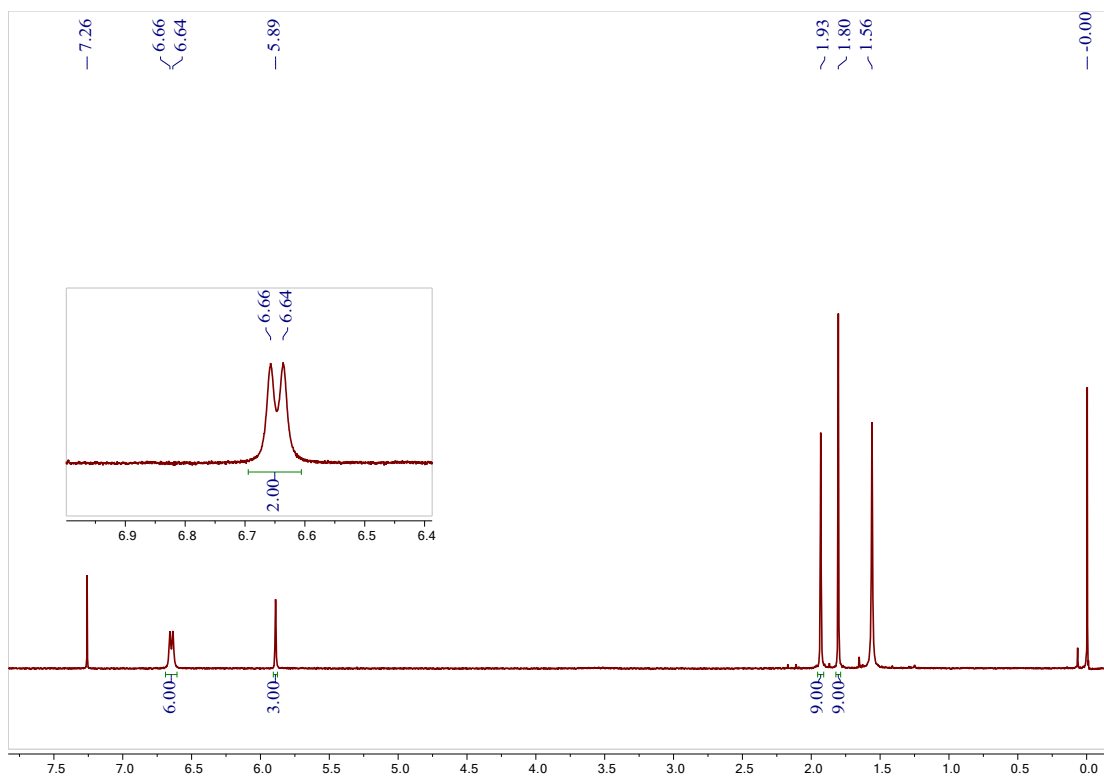
Figure S25. ^{1}H NMR spectrum of [**L**^{F3}**Cu**]$_3$ in CDCl$_3$ (400 MHz, 298 K).
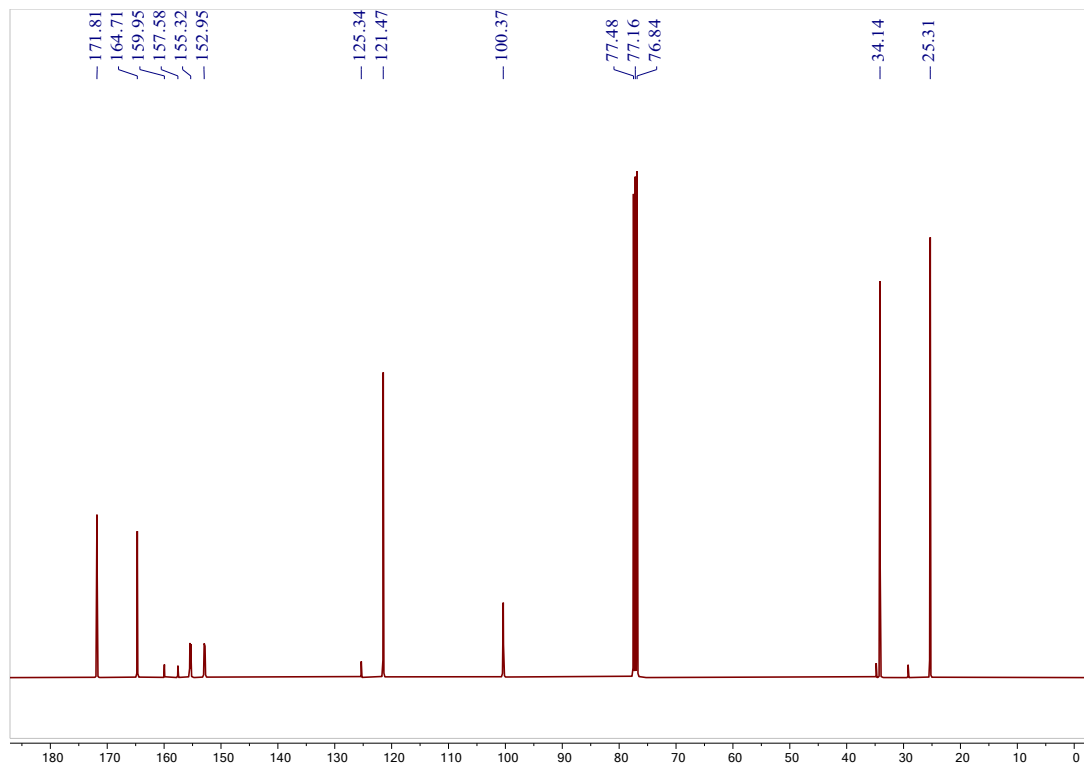
Figure S26. ^{13}C{^{1}H} NMR spectrum of [**L**^{F3}**Cu**]$_3$ in CDCl$_3$ (100 MHz, 298 K).
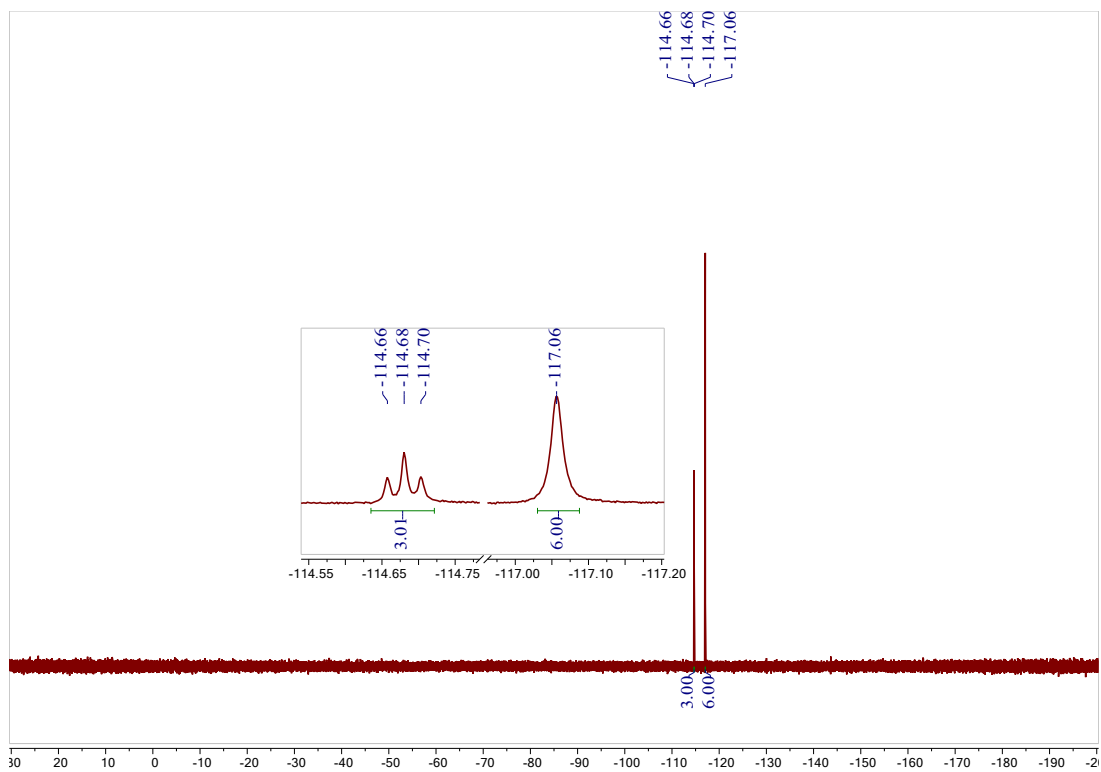
Figure S27. ^{19}F NMR spectrum of $[\mathbf{L^{F3}Cu}]_3$ in CDCl$_3$ (376 MHz, 298 K).
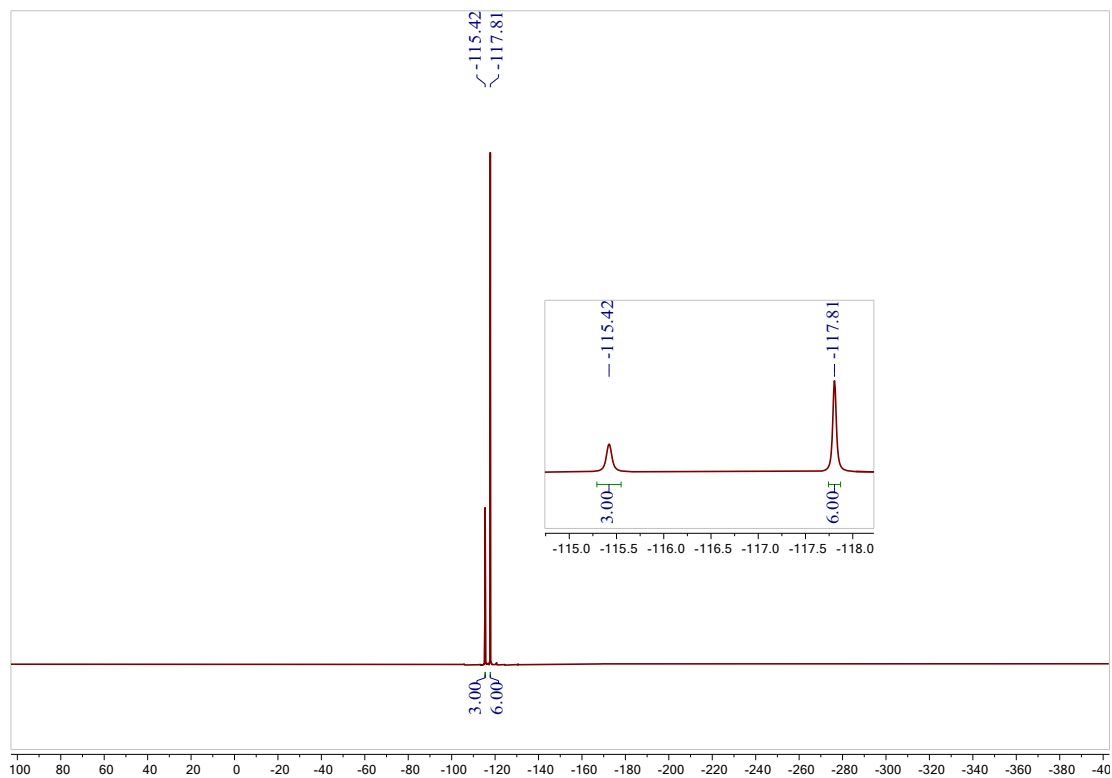
Figure S28. $^{19}F\{^1H\}$ NMR spectrum of $[\mathbf{L^{F3}Cu}]_3$ in CDCl$_3$ (471 MHz, 298 K).
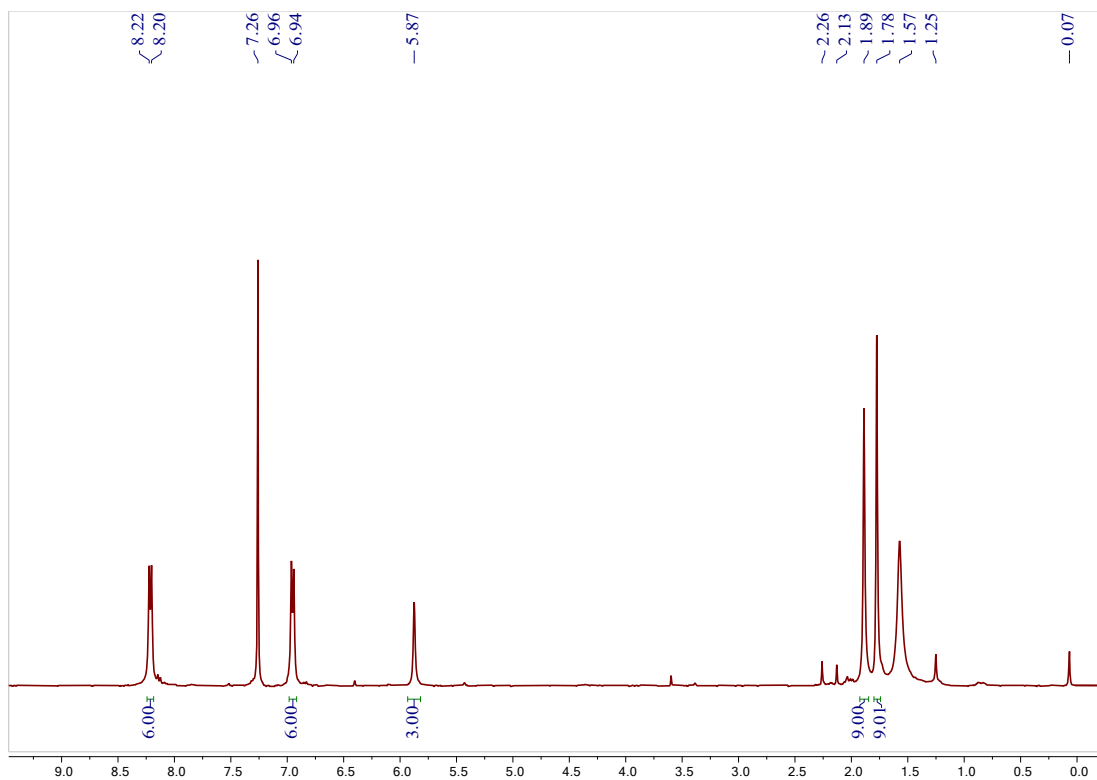
Figure S29. ^{1}H NMR spectrum of [$\mathbf{L^{NO2}}$Cu]$_3$ in CDCl$_3$ (400 MHz, 298 K).
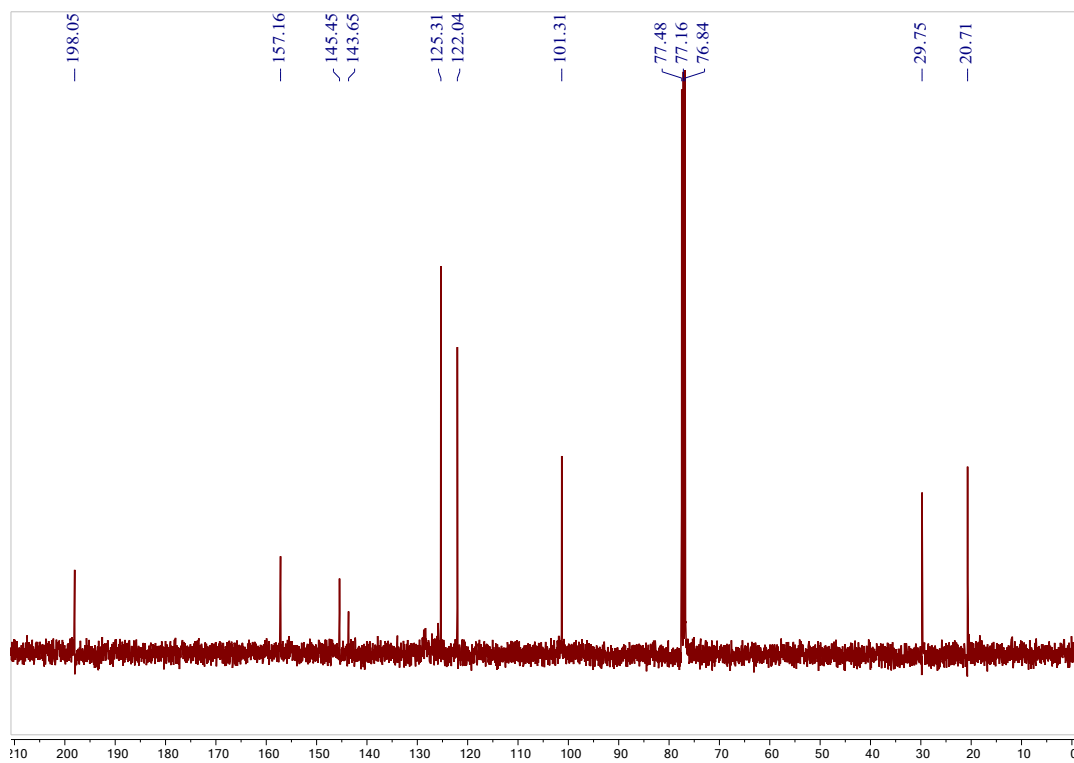
Figure S30. ^{13}C{^{1}H} NMR spectrum of [$\mathbf{L^{NO2}}$Cu]$_3$ in CDCl$_3$ (100 MHz, 298 K).

21
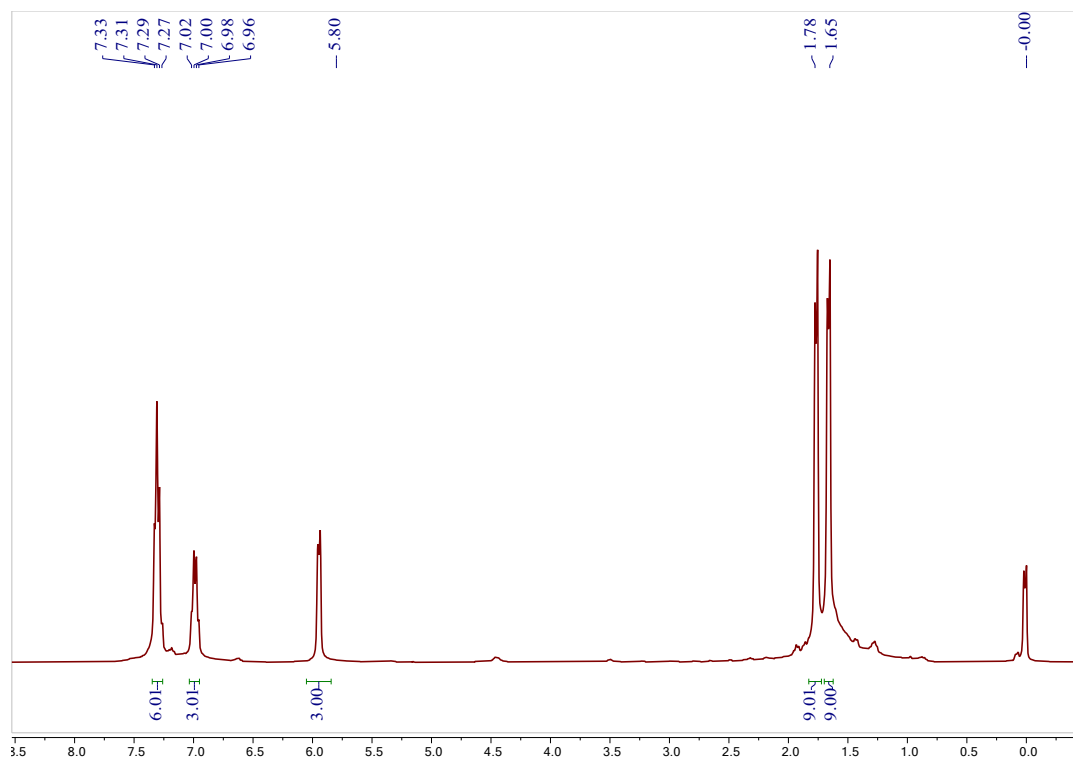
Figure S31. ^{1}H NMR spectrum of [**L**^{Cl2}Cu]$_3$ in CDCl$_3$ (400 MHz, 298 K).
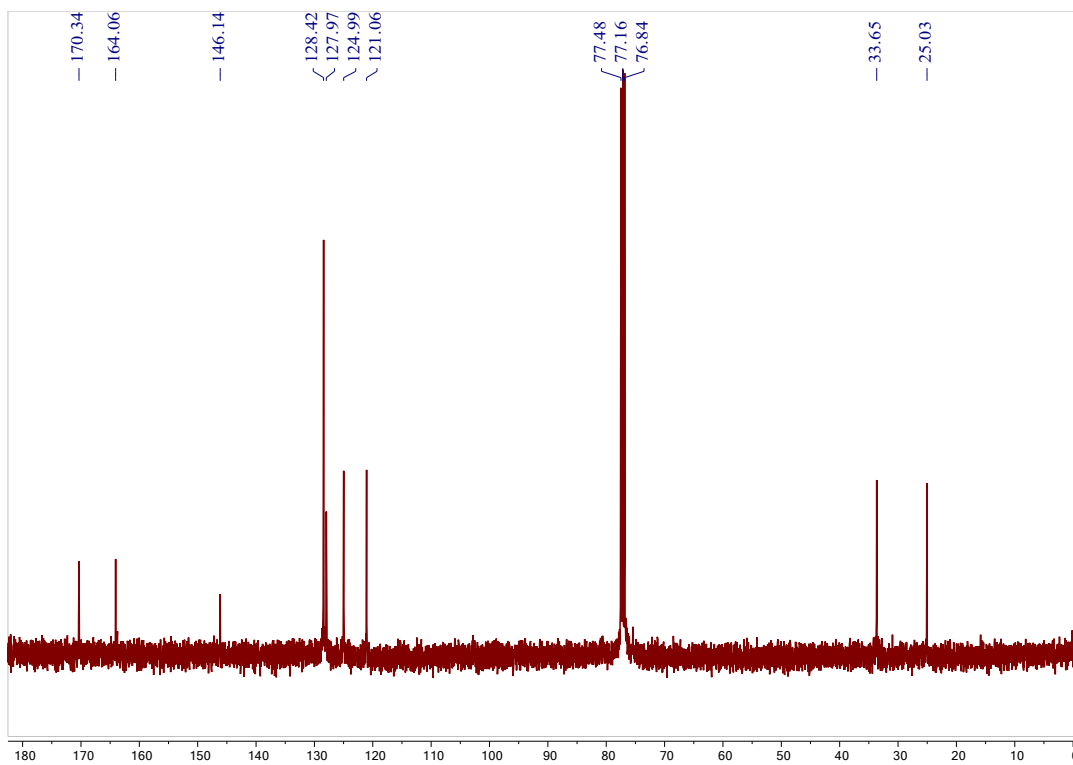
Figure S32. ^{13}C{^{1}H} NMR spectrum of [**L**^{Cl2}Cu]$_3$ in CDCl$_3$ (100 MHz, 298 K).
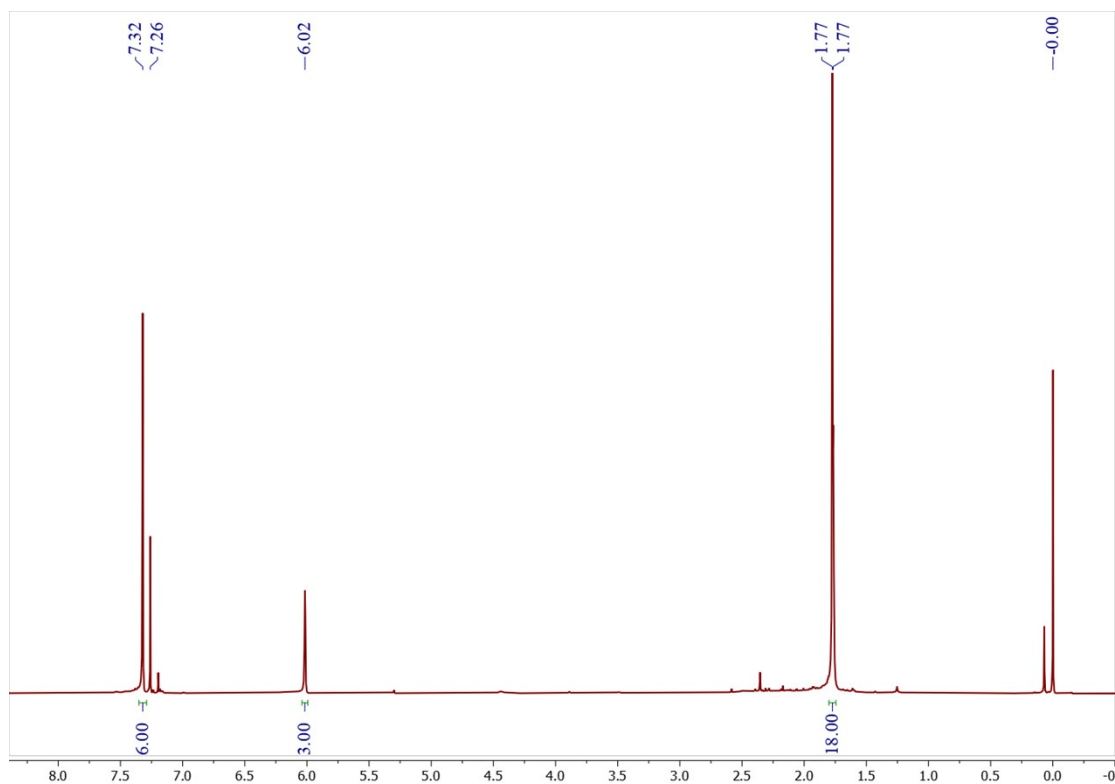
Figure S33. ^{1}H NMR spectrum of [**L**^{Cl3}Cu]$_3$ in CDCl$_3$ (400 MHz, 298 K).
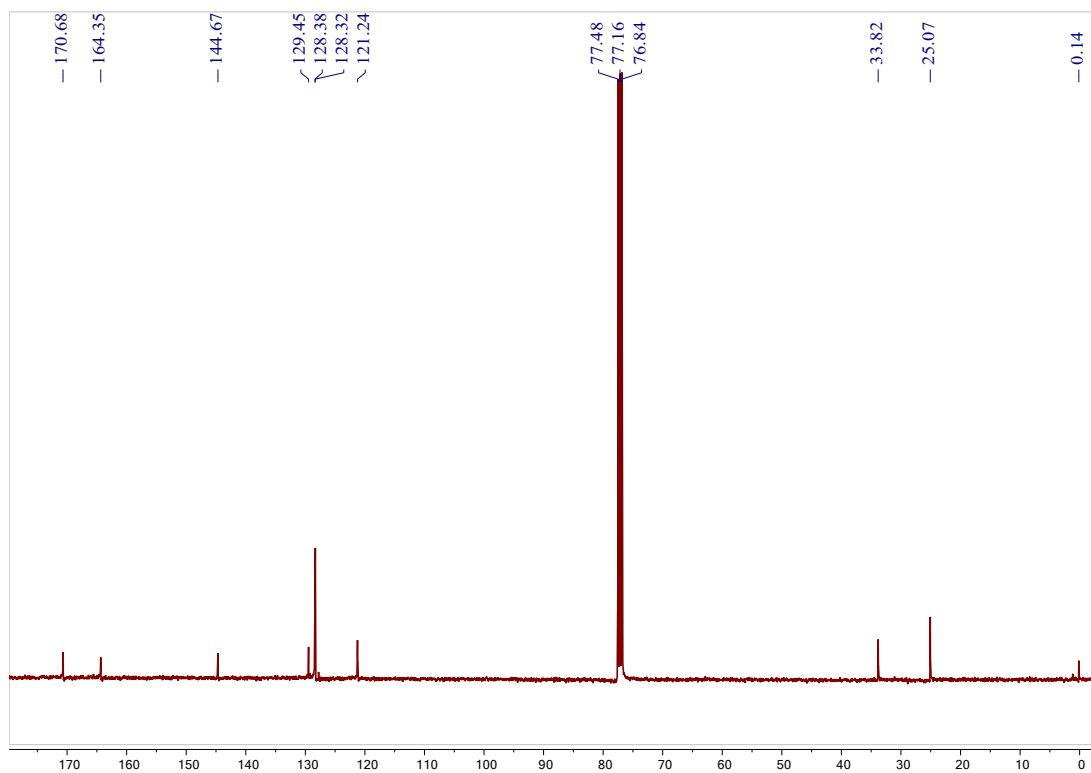
Figure S34. ^{13}C{^{1}H} NMR spectrum of [**L**^{Cl3}Cu]$_3$ in CDCl$_3$ (100 MHz, 298 K).
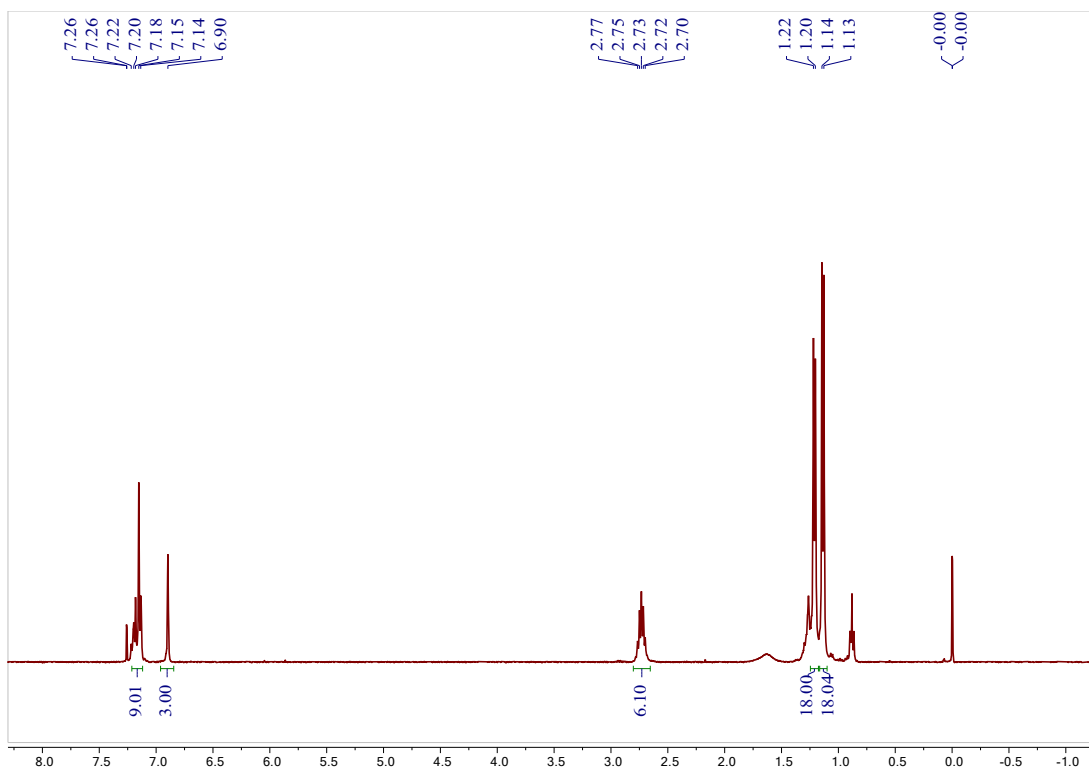
Figure S35. ^1H NMR spectrum of $[^{CF3}L_1Cu]_3$ in CDCl$_3$ (400 MHz, 298 K).
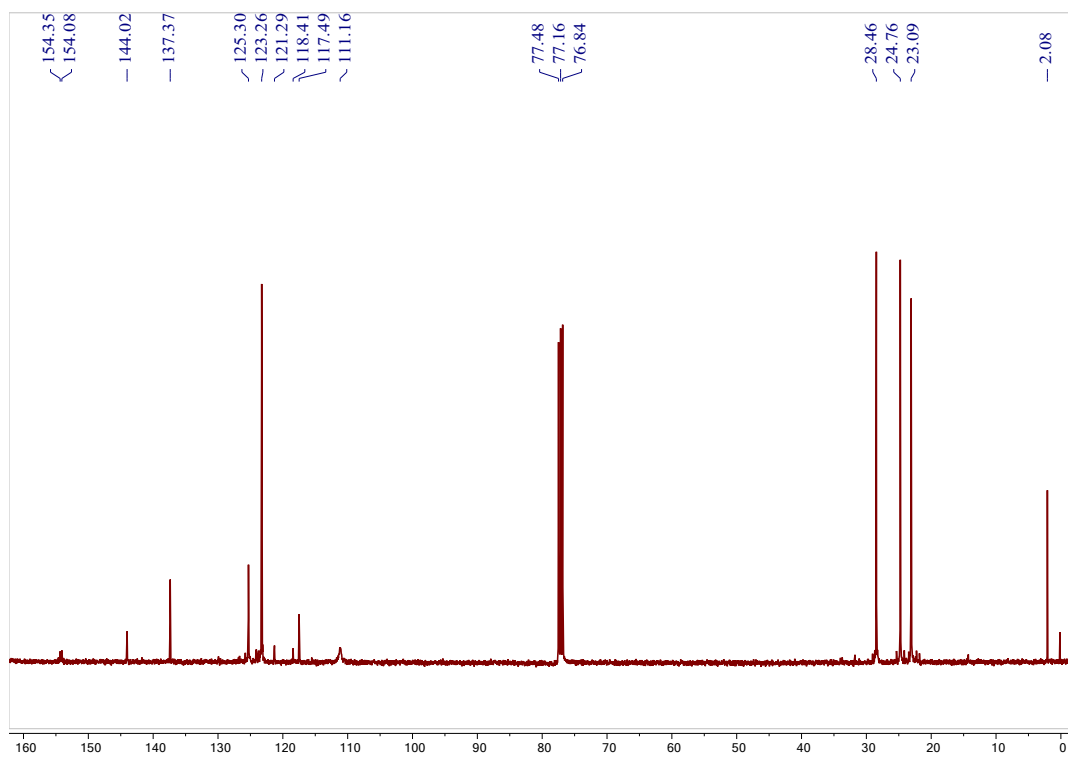
Figure S36. $^{13}C\{^1H\}$ NMR spectrum of $[^{CF3}L_1Cu]_3$ in CDCl$_3$ (100 MHz, 298 K).
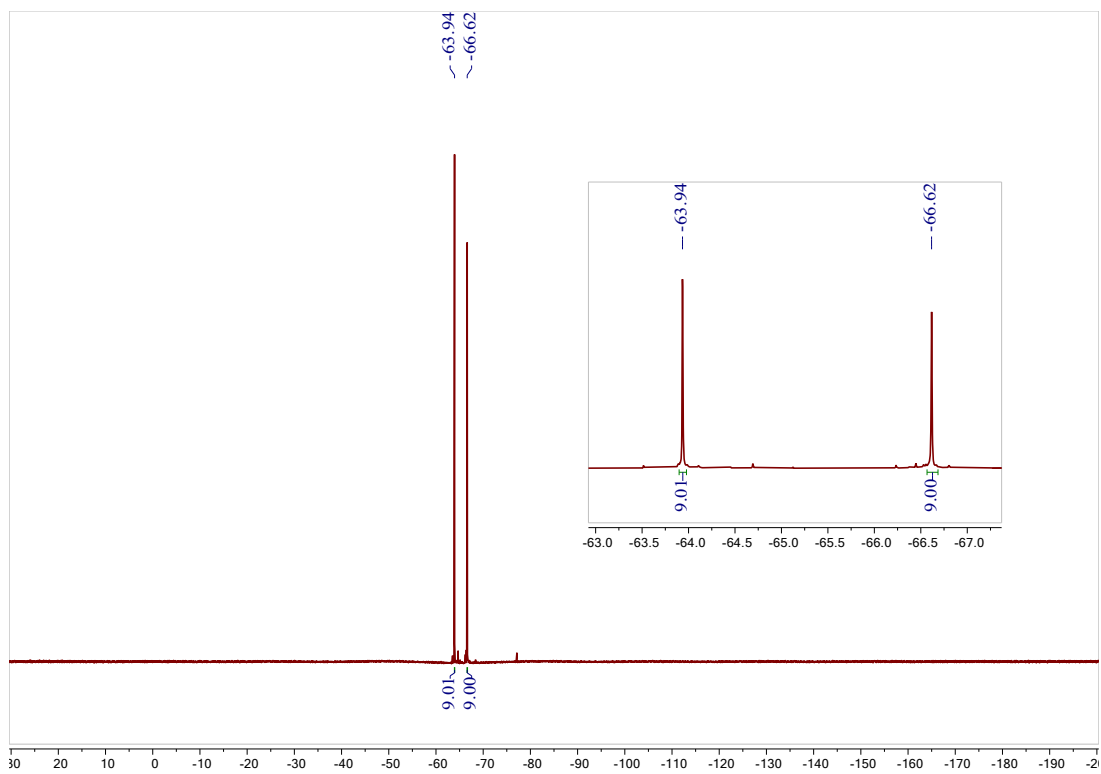
Figure S37. ^{19}F NMR spectrum of [^{CF3}**L**$_1$Cu]$_3$ in CDCl$_3$ (376 MHz, 298 K).
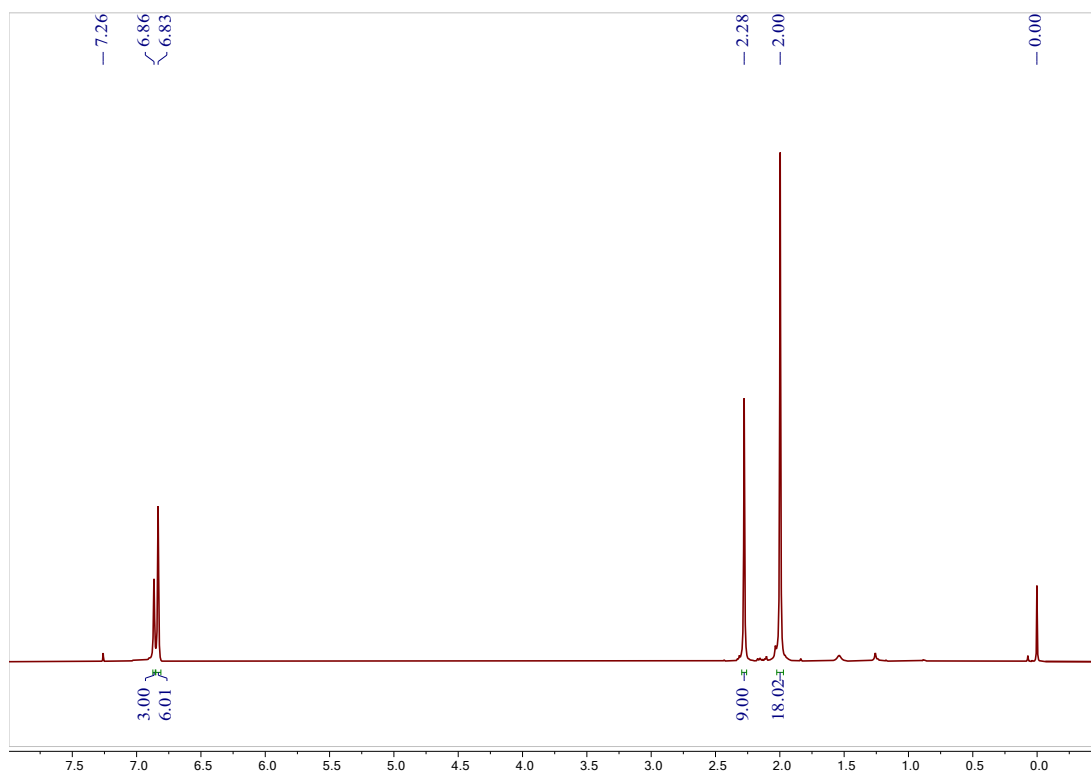
Figure S38. ^{1}H NMR spectrum of [^{CF3}**L**$_2$Cu]$_3$ in CDCl$_3$ (400 MHz, 298 K).

25
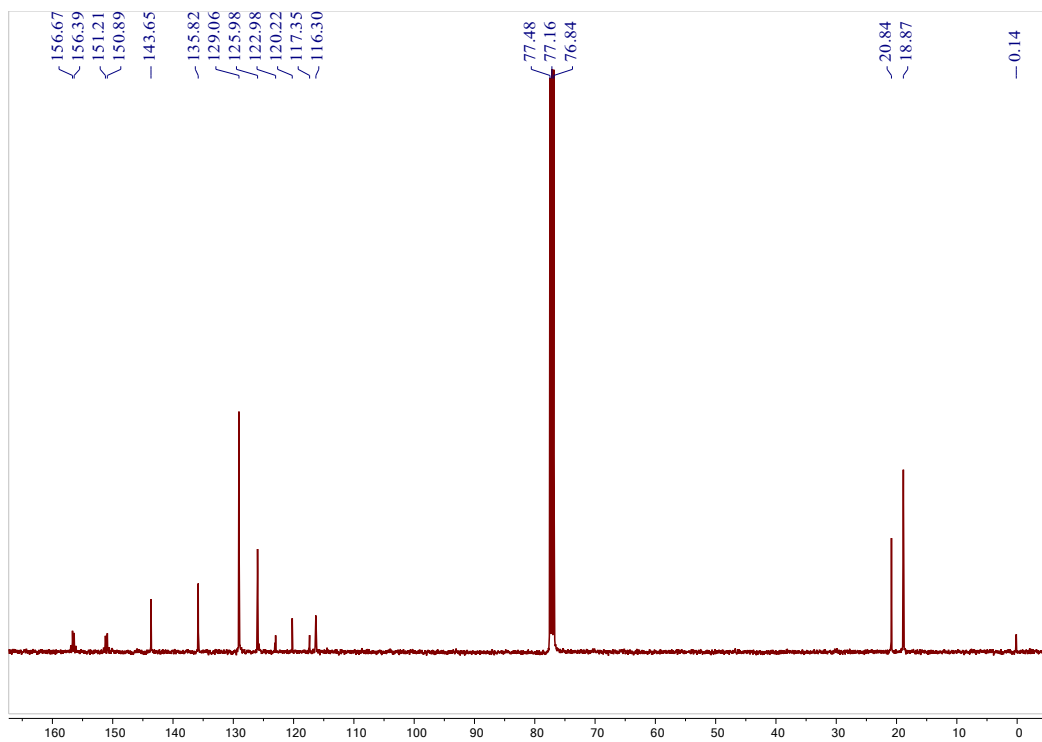
Figure S39. $^{13}C\{^1H\}$ NMR spectrum of $[^{CF3}L_2Cu]_3$ in CDCl$_3$ (100 MHz, 298 K).
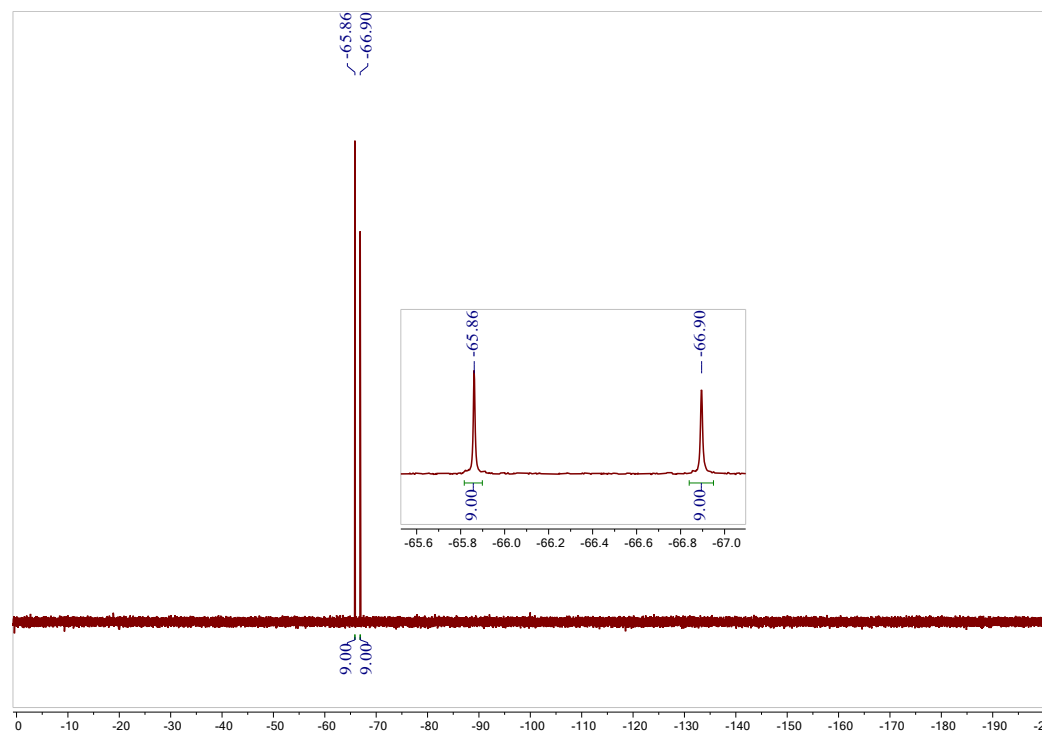
Figure S40. ^{19}F NMR spectrum of $[^{CF3}L_2Cu]_3$ in CDCl$_3$ (376 MHz, 298 K).
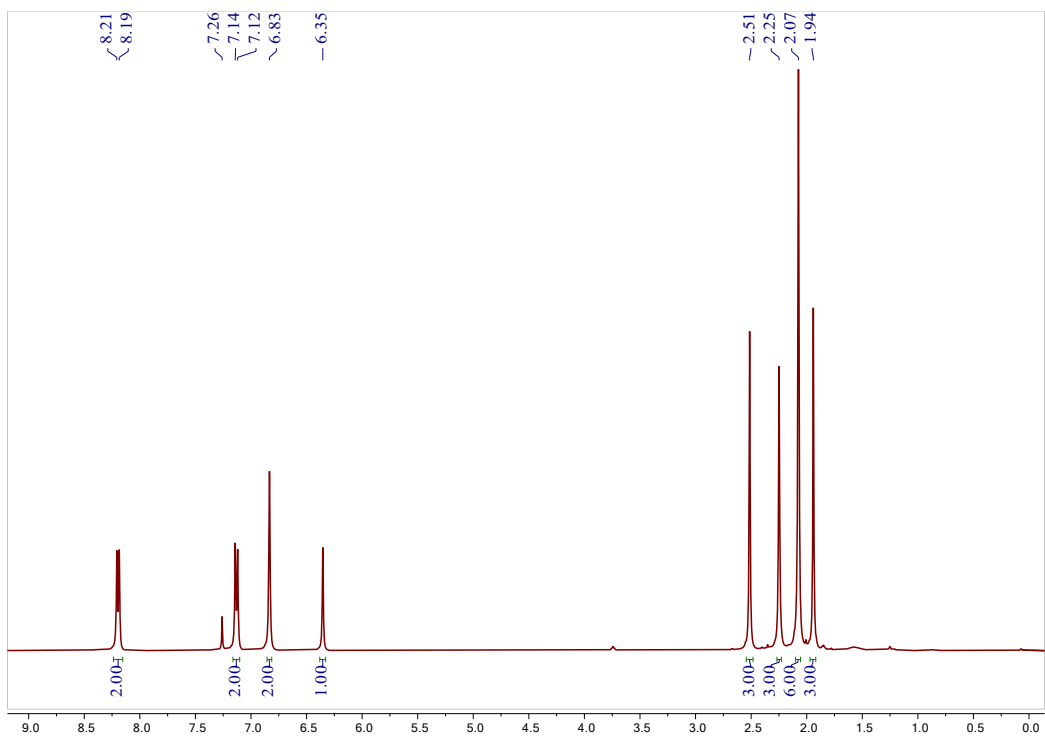
Figure S41. ^{1}H NMR spectrum of $\mathbf{L^{NO2}CuCNR}$ in CDCl$_3$ (400 MHz, 298 K).
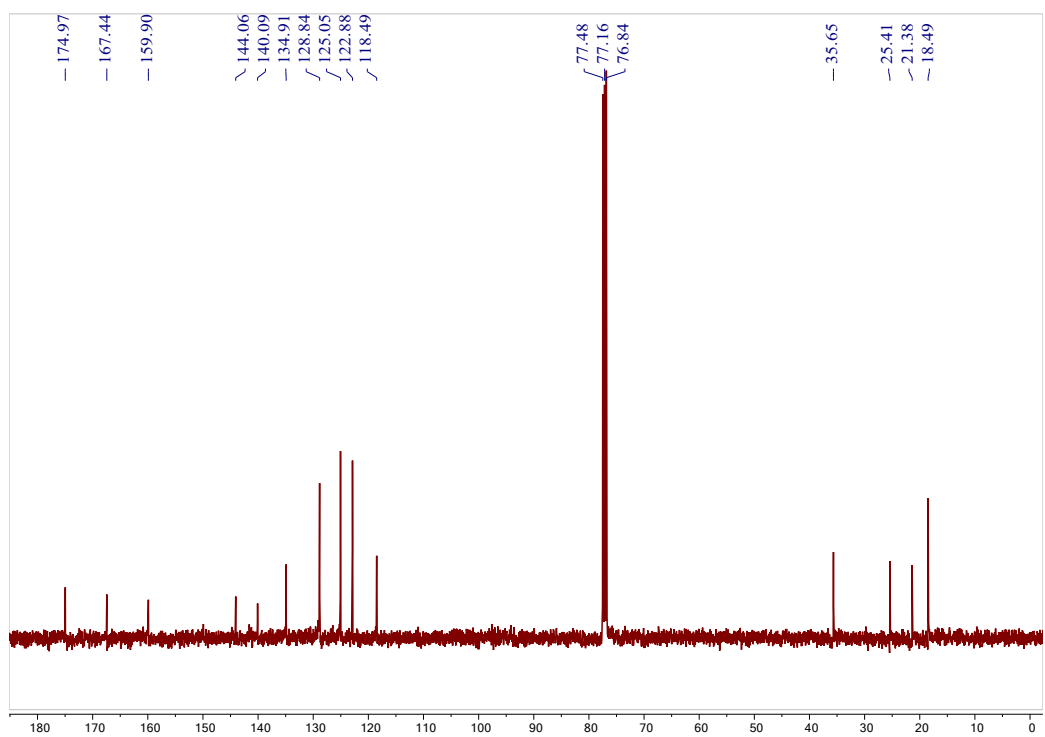
Figure S42. ^{13}C{^{1}H} NMR spectrum of $\mathbf{L^{NO2}CuCNR}$ in CDCl$_3$ (100 MHz, 298 K).
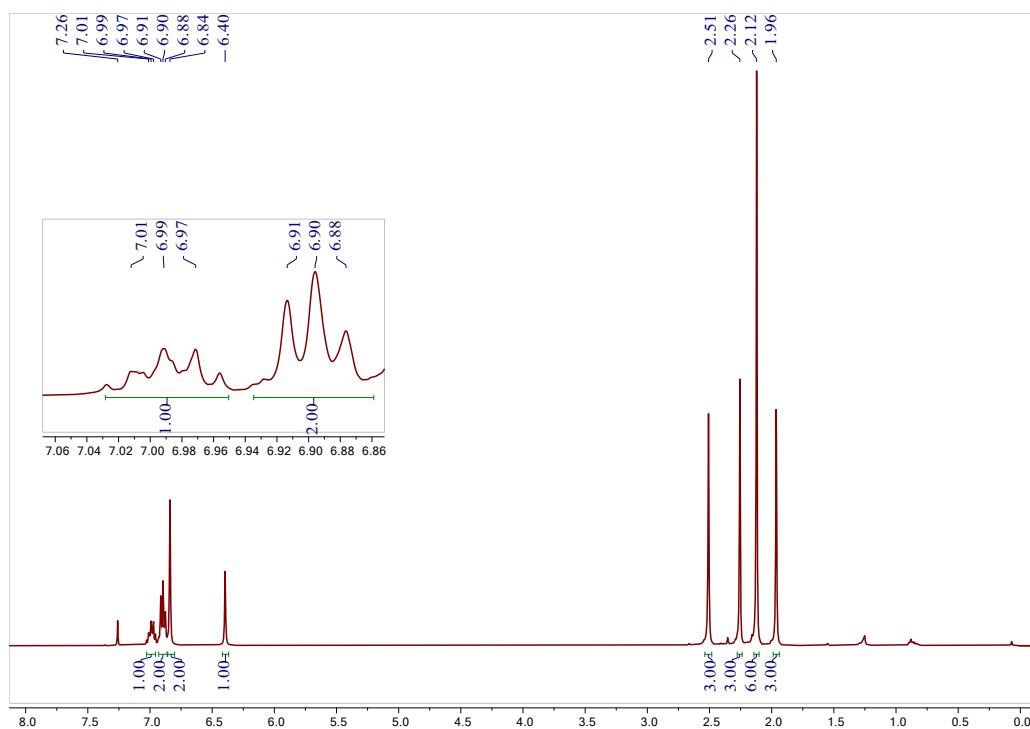
Figure S43. ^{1}H NMR spectrum of **L^{F2}CuCNR** in CDCl$_3$ (400 MHz, 298 K).
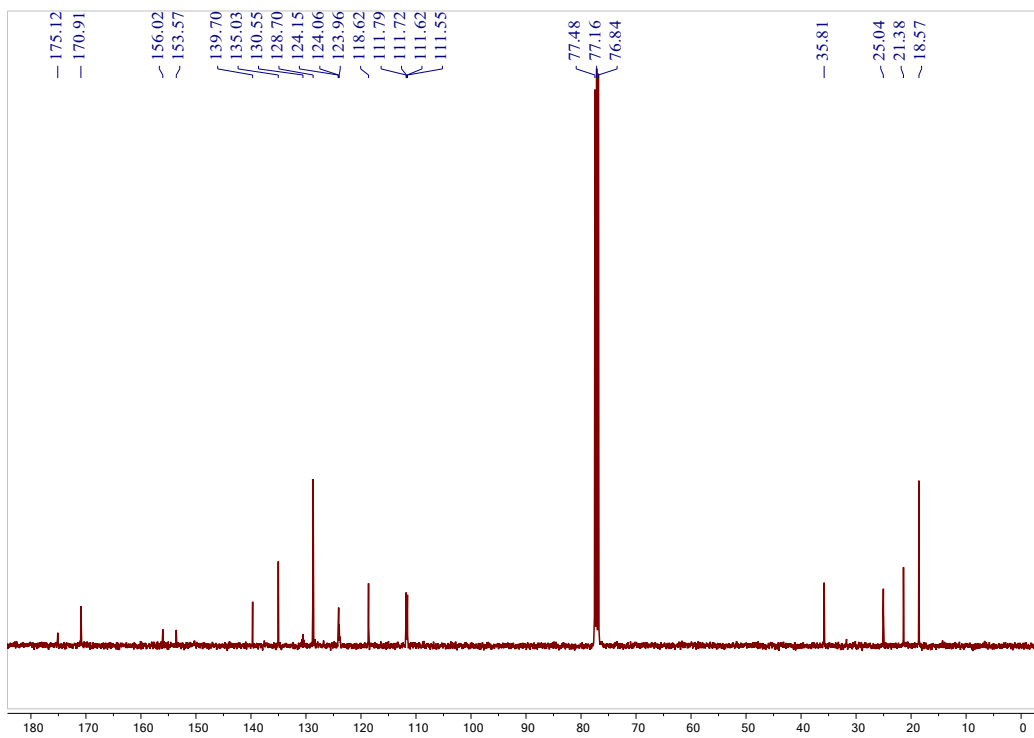
Figure S44. ^{13}C{^{1}H} NMR spectrum of **L^{F2}CuCNR** in CDCl$_3$ (100 MHz, 298 K).
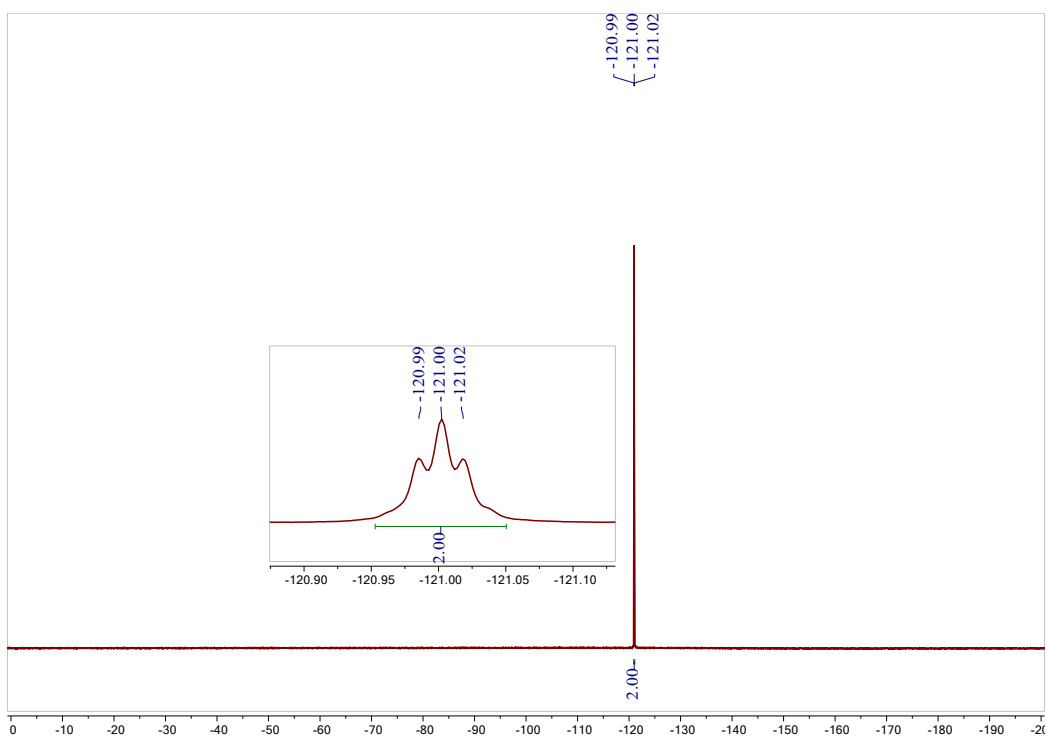
Figure S45. ^{19}F NMR spectrum of **L^{F2}CuCNR** in CDCl$_3$ (376 MHz, 298 K).
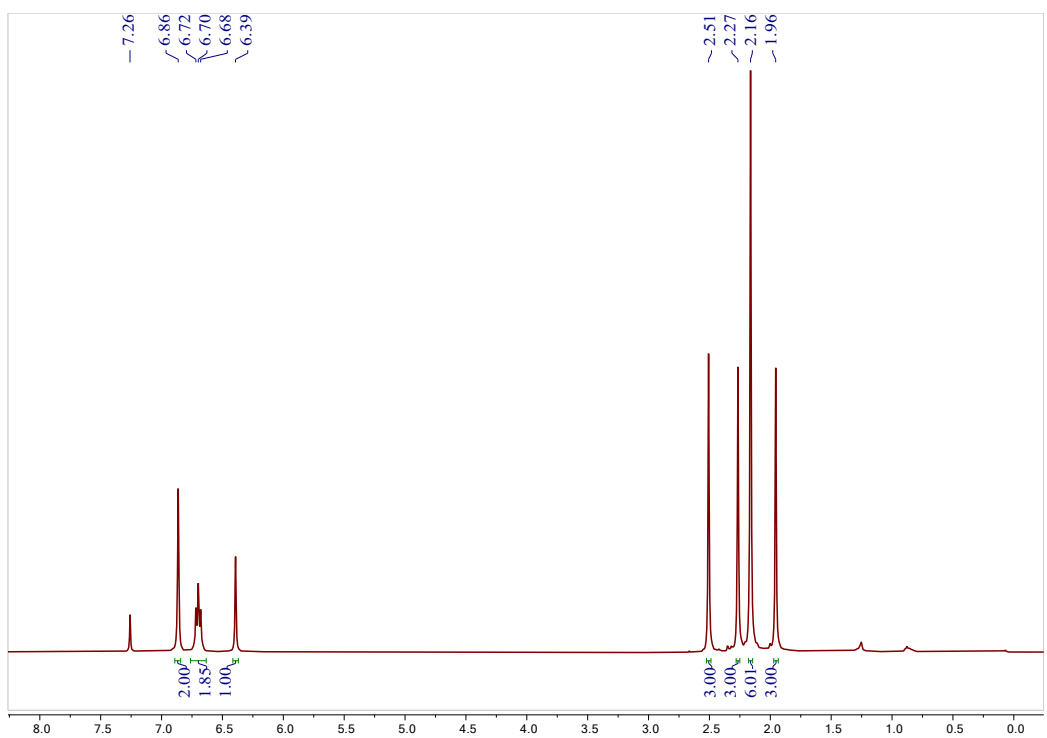
Figure S46. ^{1}H NMR spectrum of **L^{F3}CuCNR** in CDCl$_3$ (400 MHz, 298 K).
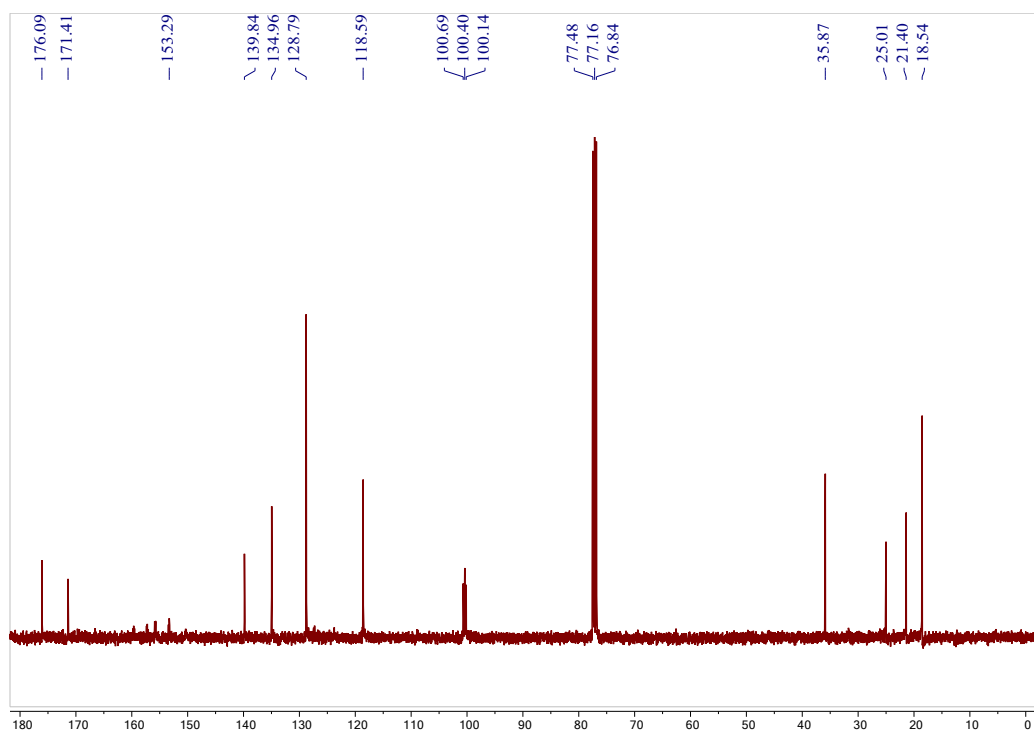
Figure S47. $^{13}C\{^1H\}$ NMR spectrum of $\mathbf{L^{F3}}$CuCNR in CDCl$_3$ (100 MHz, 298 K).
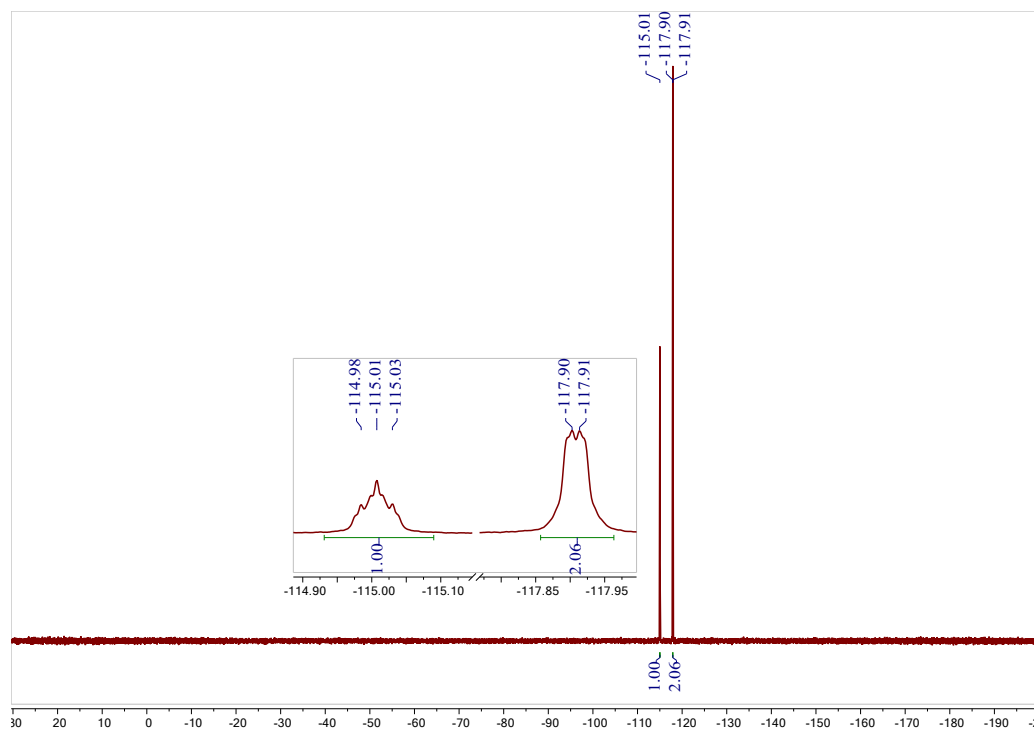
Figure S48. ^{19}F NMR spectrum of $\mathbf{L^{F3}}$CuCNR in CDCl$_3$ (376 MHz, 298 K).
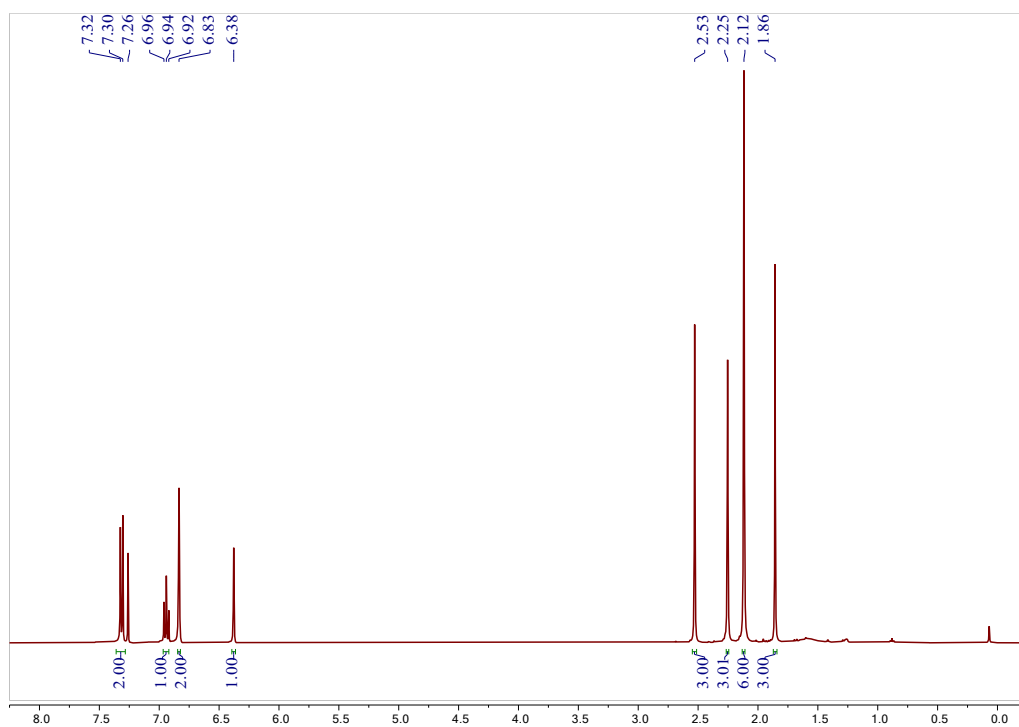
Figure S49. ^{1}H NMR spectrum of $\mathbf{L^{Cl2}CuCNR}$ in CDCl$_3$ (400 MHz, 298 K).
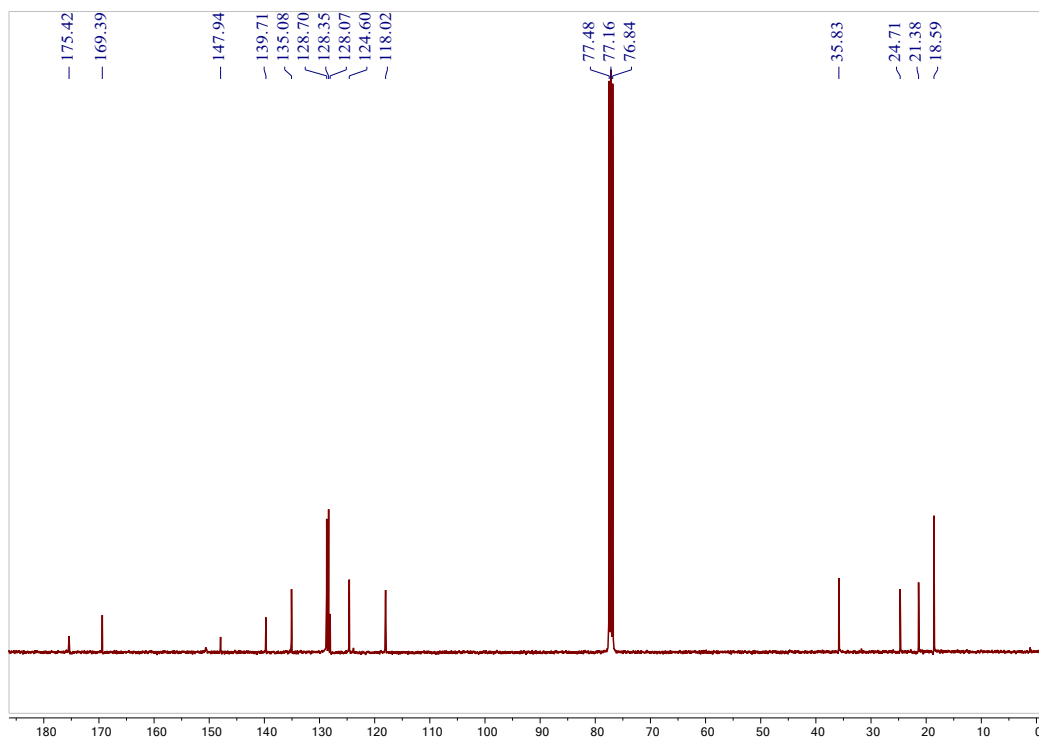
Figure S50. ^{13}C{^{1}H} NMR spectrum of $\mathbf{L^{Cl2}CuCNR}$ in CDCl$_3$ (100 MHz, 298 K).

31
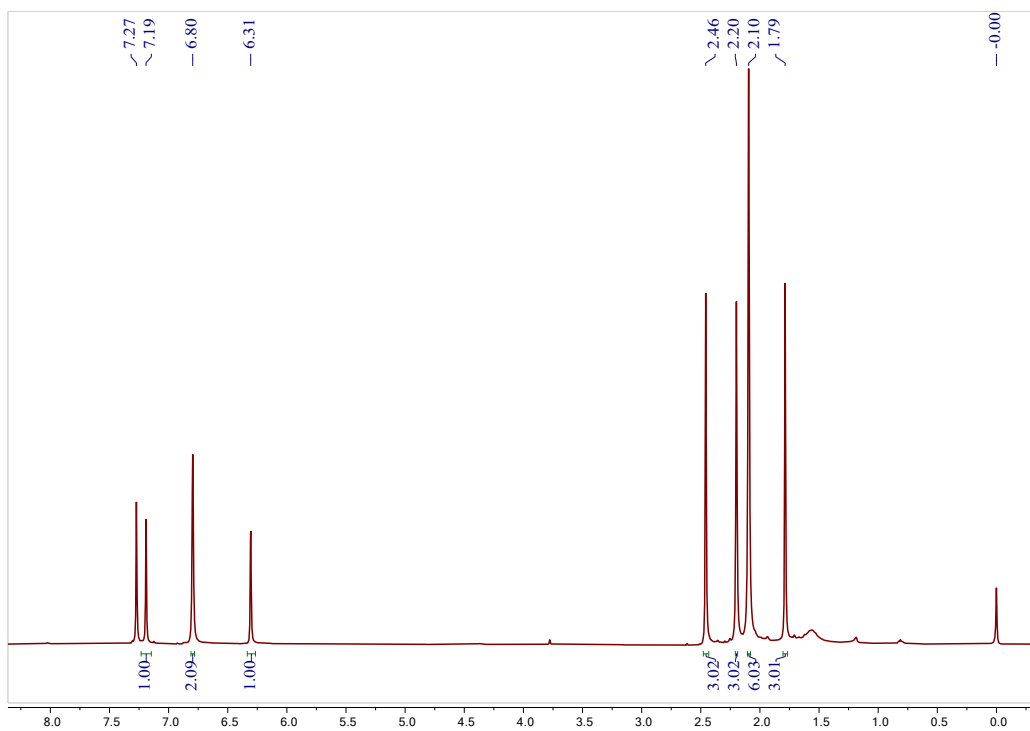
Figure S51. ^{1}H NMR spectrum of $\mathbf{L^{Cl3}CuCNR}$ in CDCl$_3$ (400 MHz, 298 K).
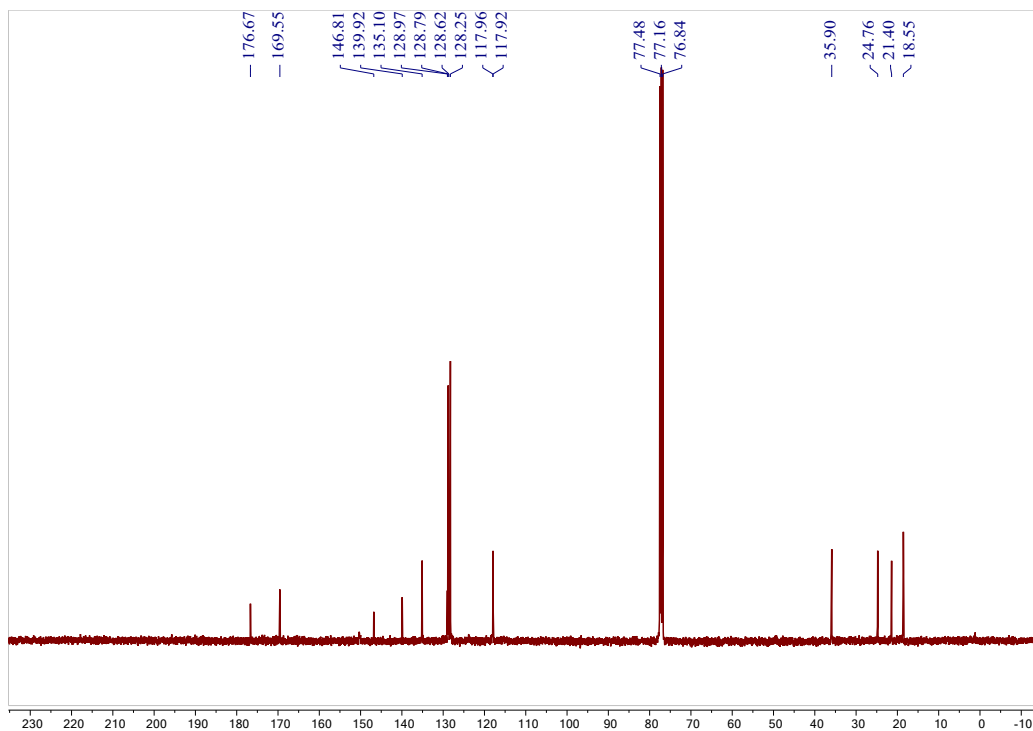
Figure S52. ^{13}C{^{1}H} NMR spectrum of $\mathbf{L^{Cl3}CuCNR}$ in CDCl$_3$ (100 MHz, 298 K).
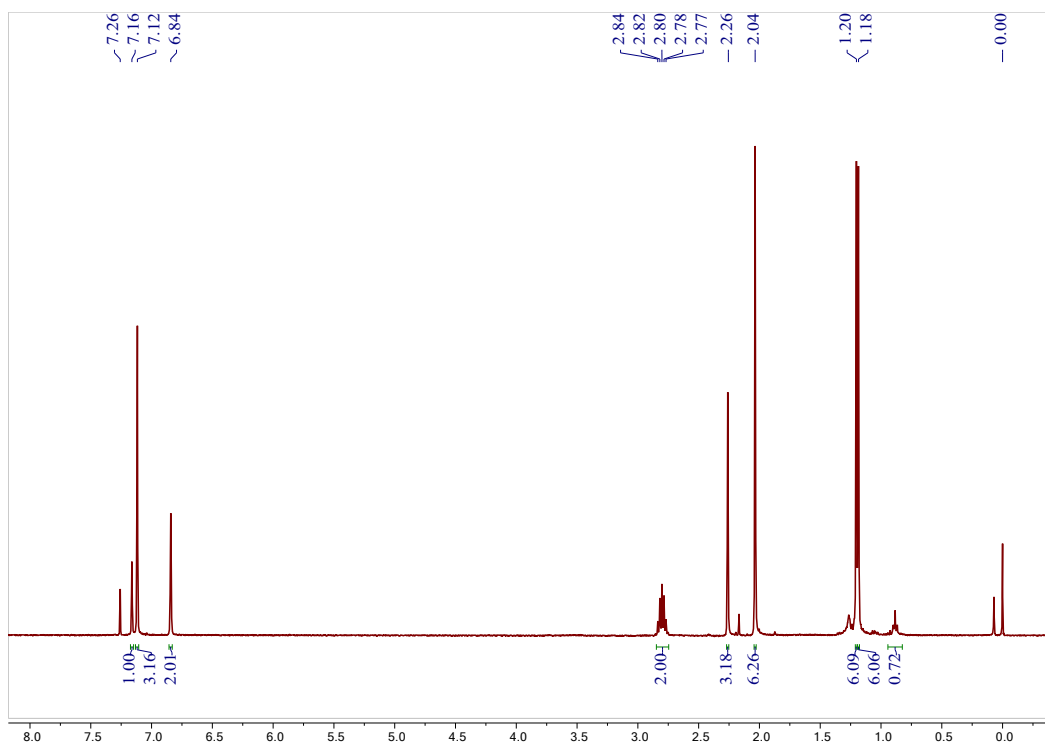
Figure S53. ^{1}H NMR spectrum of $^{CF3}L_1CuCNR$ in CDCl$_3$ (400 MHz, 298 K).
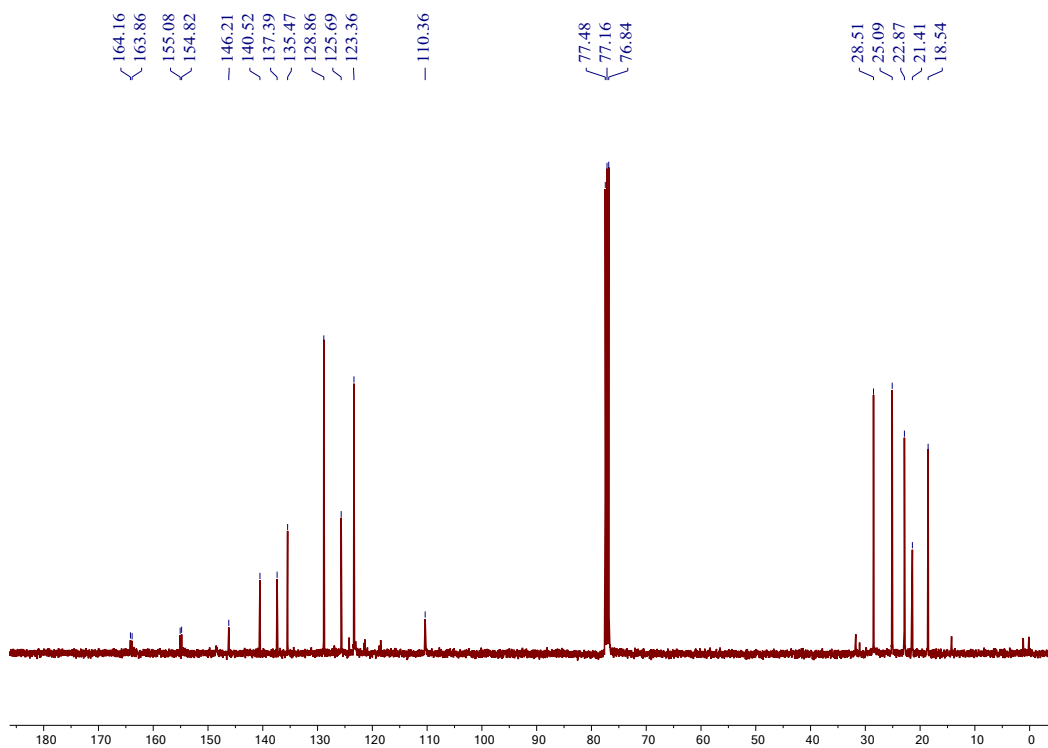
Figure S54. $^{13}C\{^1H\}$ NMR spectrum of $^{CF3}L_1CuCNR$ in CDCl$_3$ (100 MHz, 298 K).
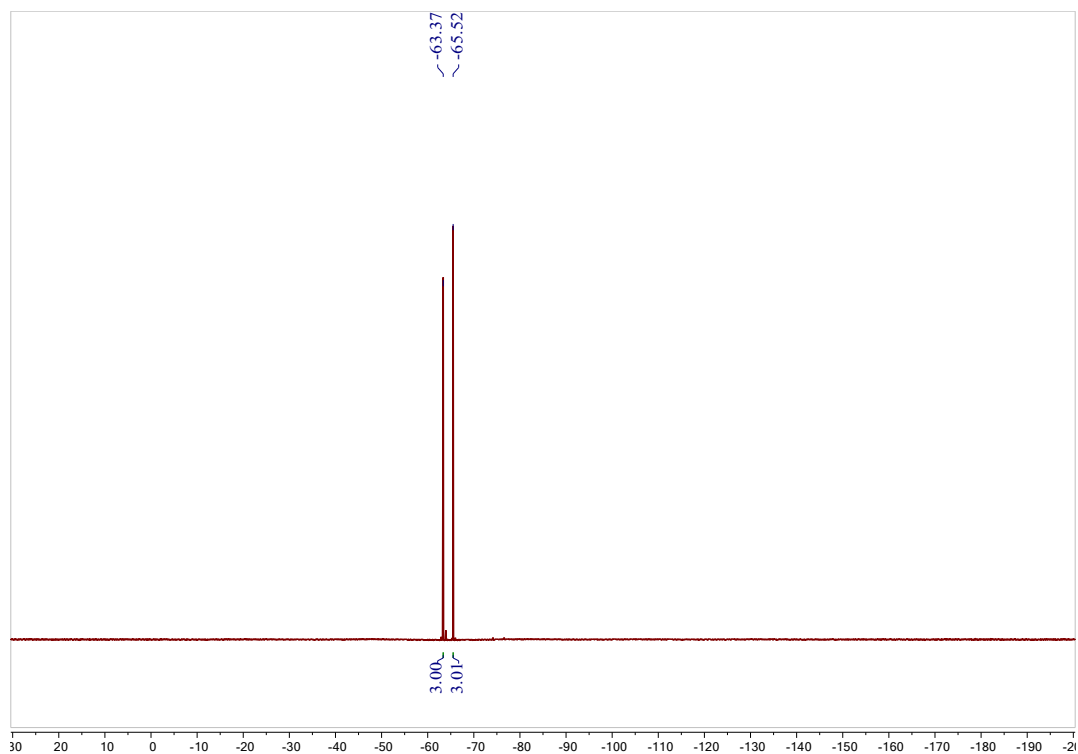
Figure S55. ^{19}F NMR spectrum of $^{CF3}L_1CuCNR$ in CDCl$_3$ (376 MHz, 298 K).
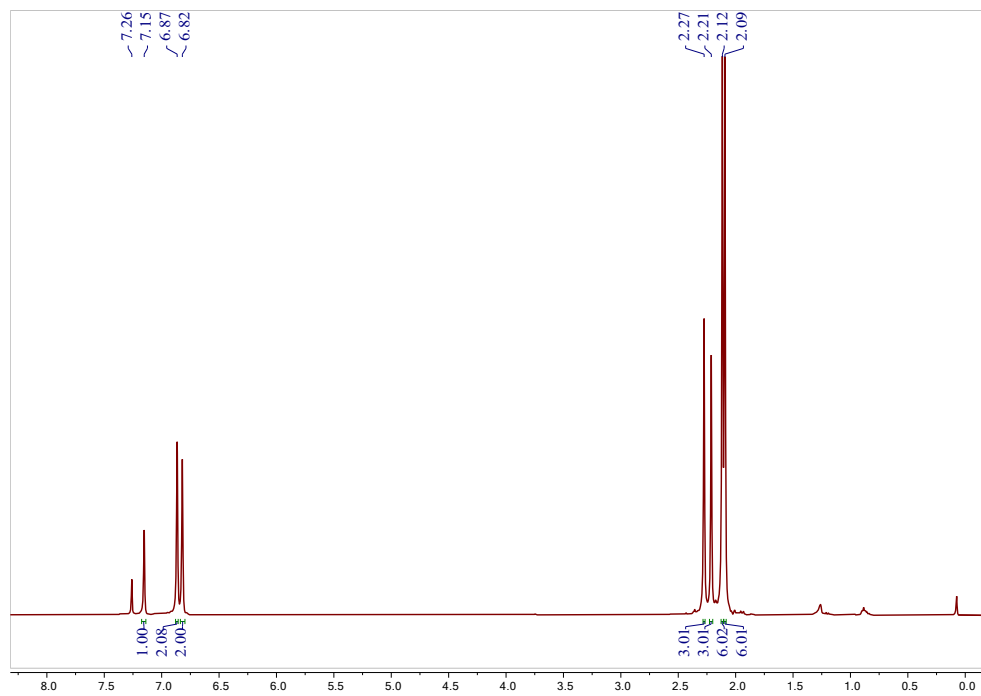
Figure S56. ^{1}H NMR spectrum of $^{CF3}L_2CuCNR$ in CDCl$_3$ (400 MHz, 298 K).
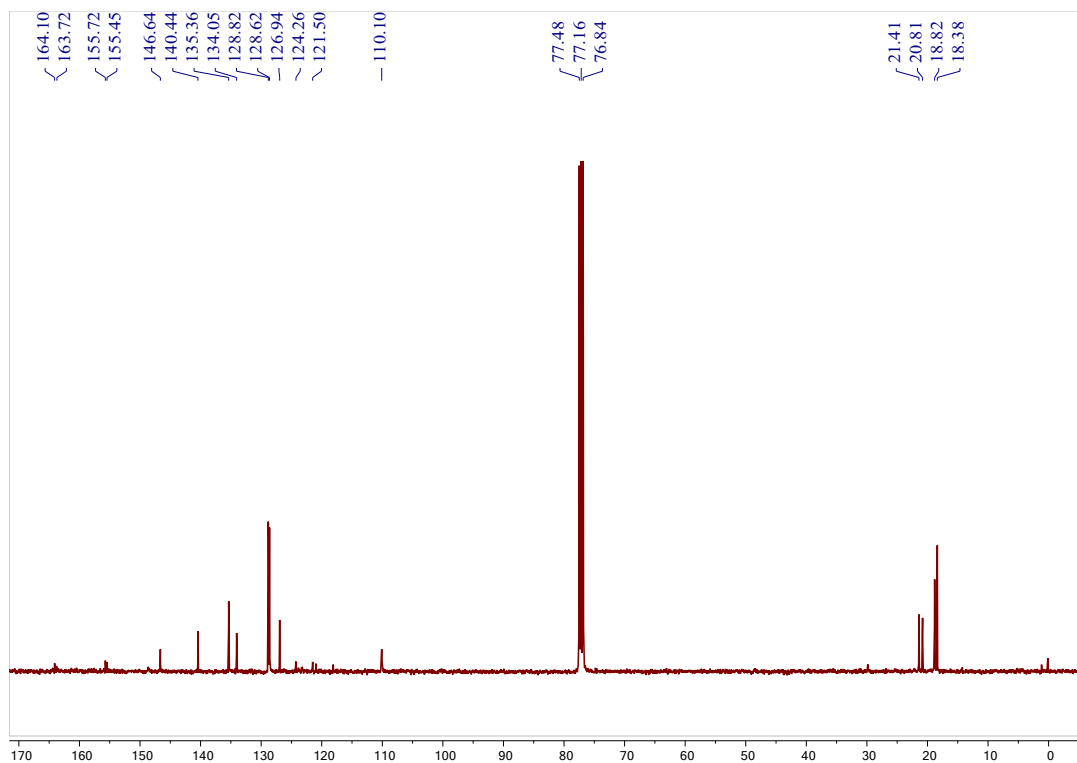
Figure S57. $^{13}C\{^1H\}$ NMR spectrum of $^{CF3}L_2$CuCNR in CDCl$_3$ (100 MHz, 298 K).
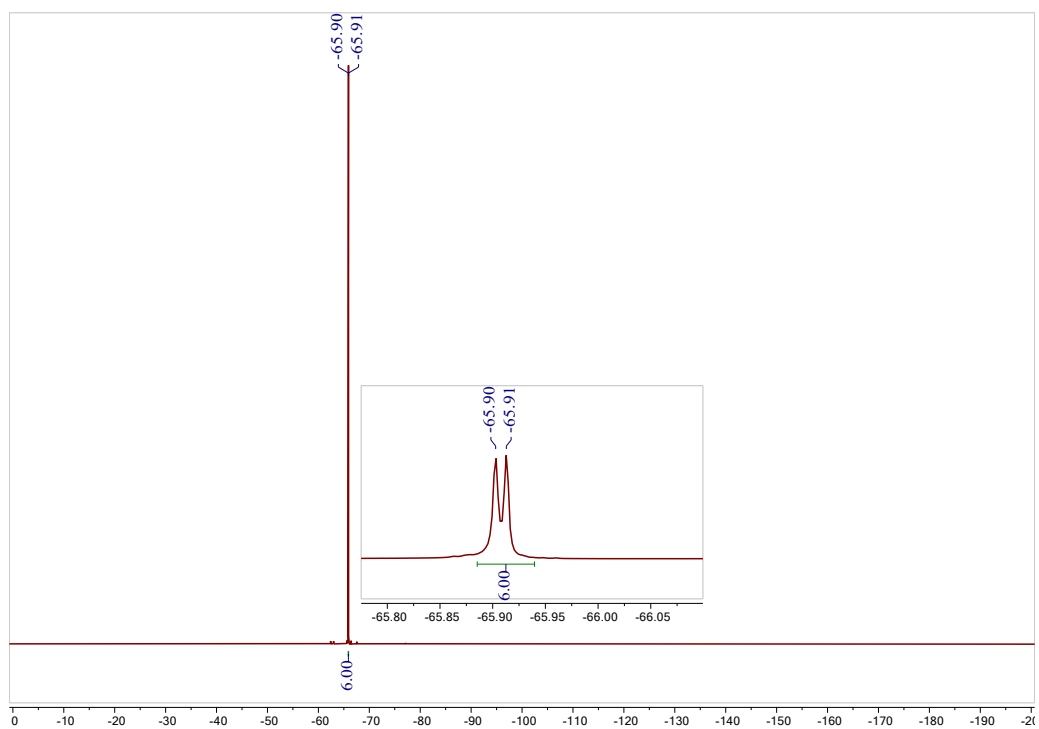
Figure S58. ^{19}F NMR spectrum of $^{CF3}L_2$CuCNR in CDCl$_3$ (376 MHz, 298 K).

Cyclic voltammetry measurements
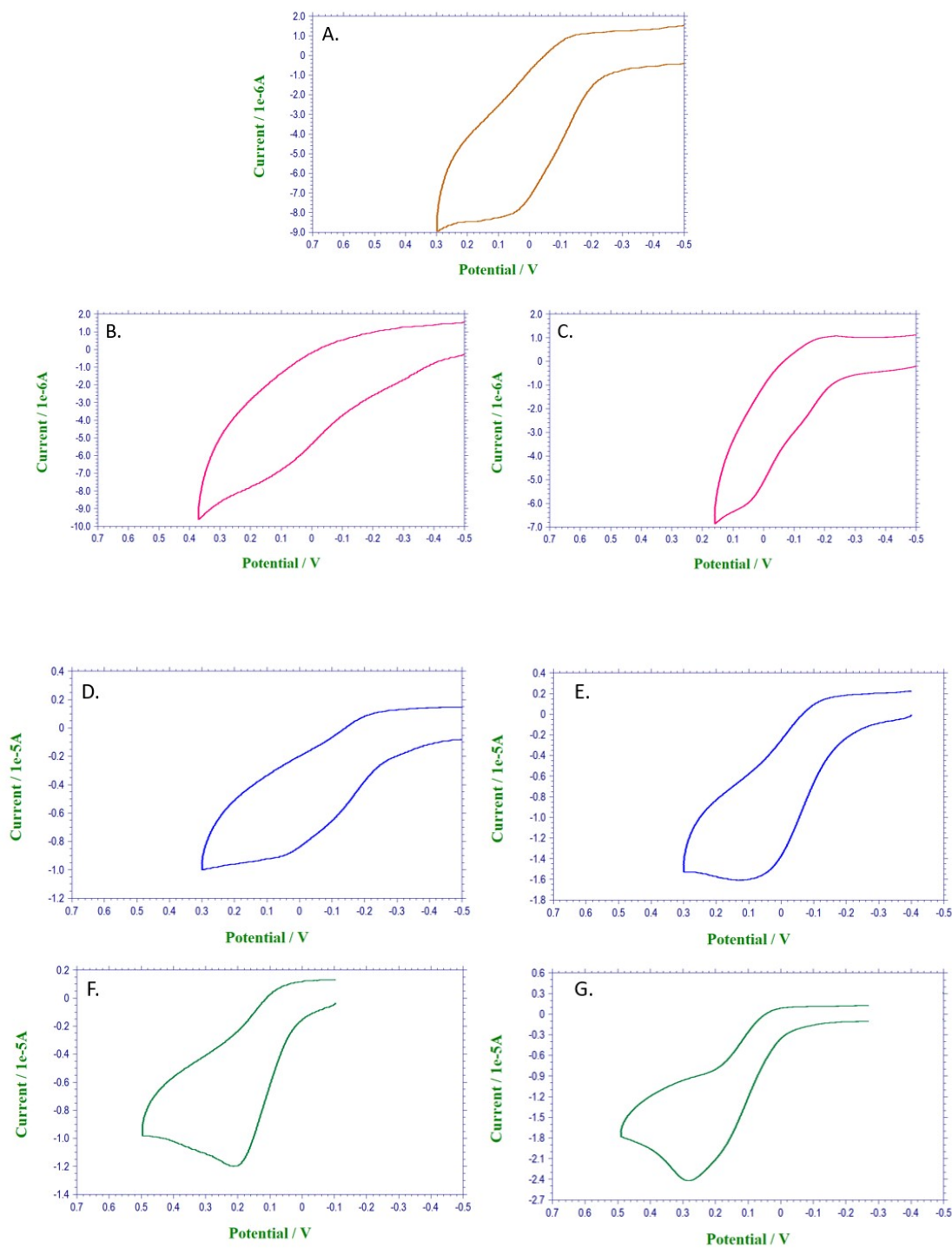
Figure S59. Cyclic voltammetry diagrams of A. [$L^{NO2}Cu$]$_3$, B. [$L^{F2}Cu$]$_3$, C. [$L^{F3}Cu$]$_3$, D. [$L^{Cl2}Cu$]$_3$, E. [$L^{Cl3}Cu$]$_3$, F. [$^{CF3}L_1Cu$]$_3$ and G. [$^{CF3}L_2Cu$]$_3$ with 10^{-4} M solutions in CH$_3$CN, respectively, using 0.1 M (Bu$_4$N)(PF$_6$) as supporting electrolyte and referenced to Fc$^{+/0}$.

FTIR measurements
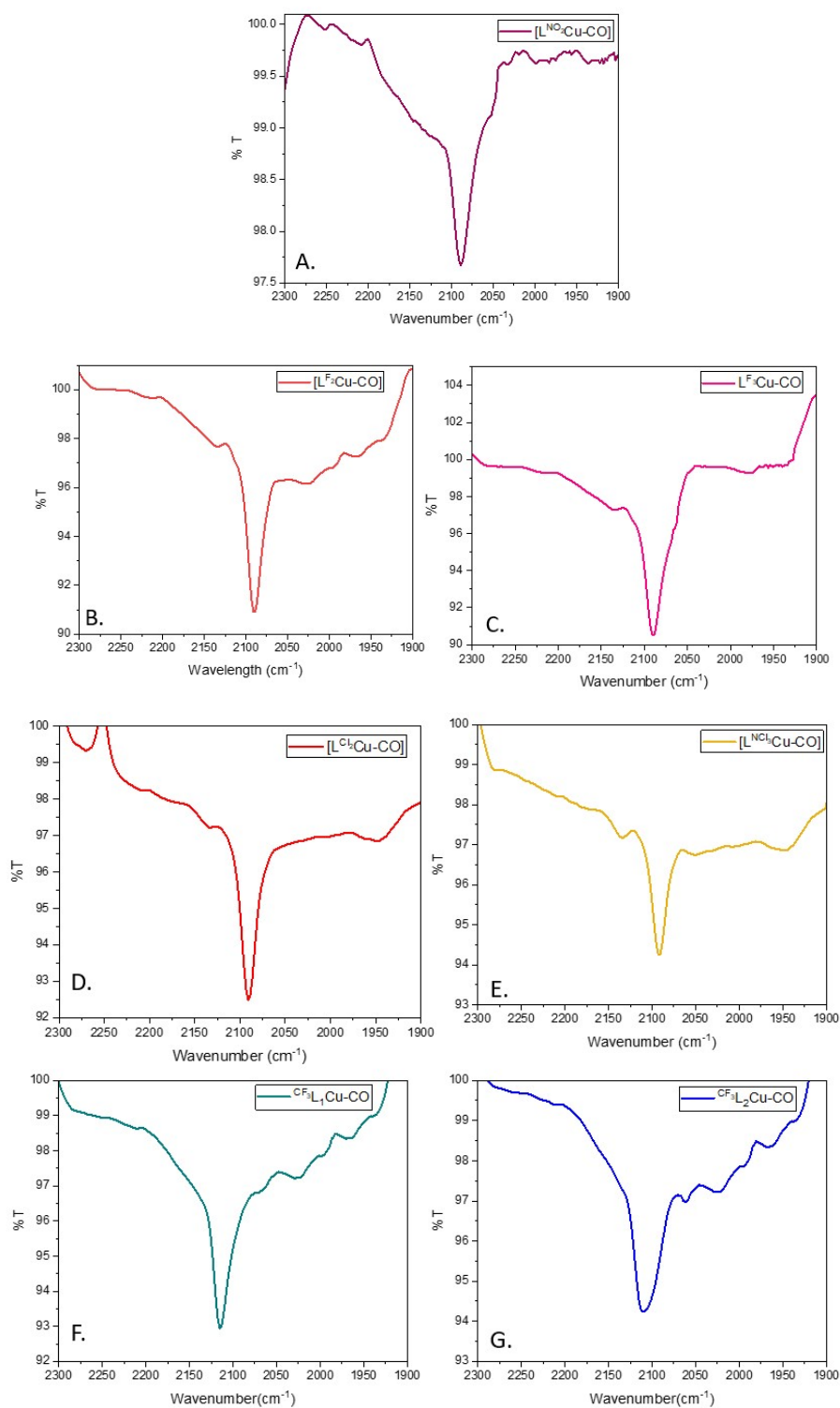
Figure S60. Solution state FTIR of LCu^I-CO adducts in THF. A. **L^{NO2}Cu-CO**, B. **L^{F2}Cu-CO**, C. **L^{F3}Cu-CO**, D. **L^{Cl2}Cu-CO**, E. **L^{Cl3}Cu-CO**, F. **^{CF3}L$_1$Cu-CO** and G. **^{CF3}L$_2$Cu-CO**.
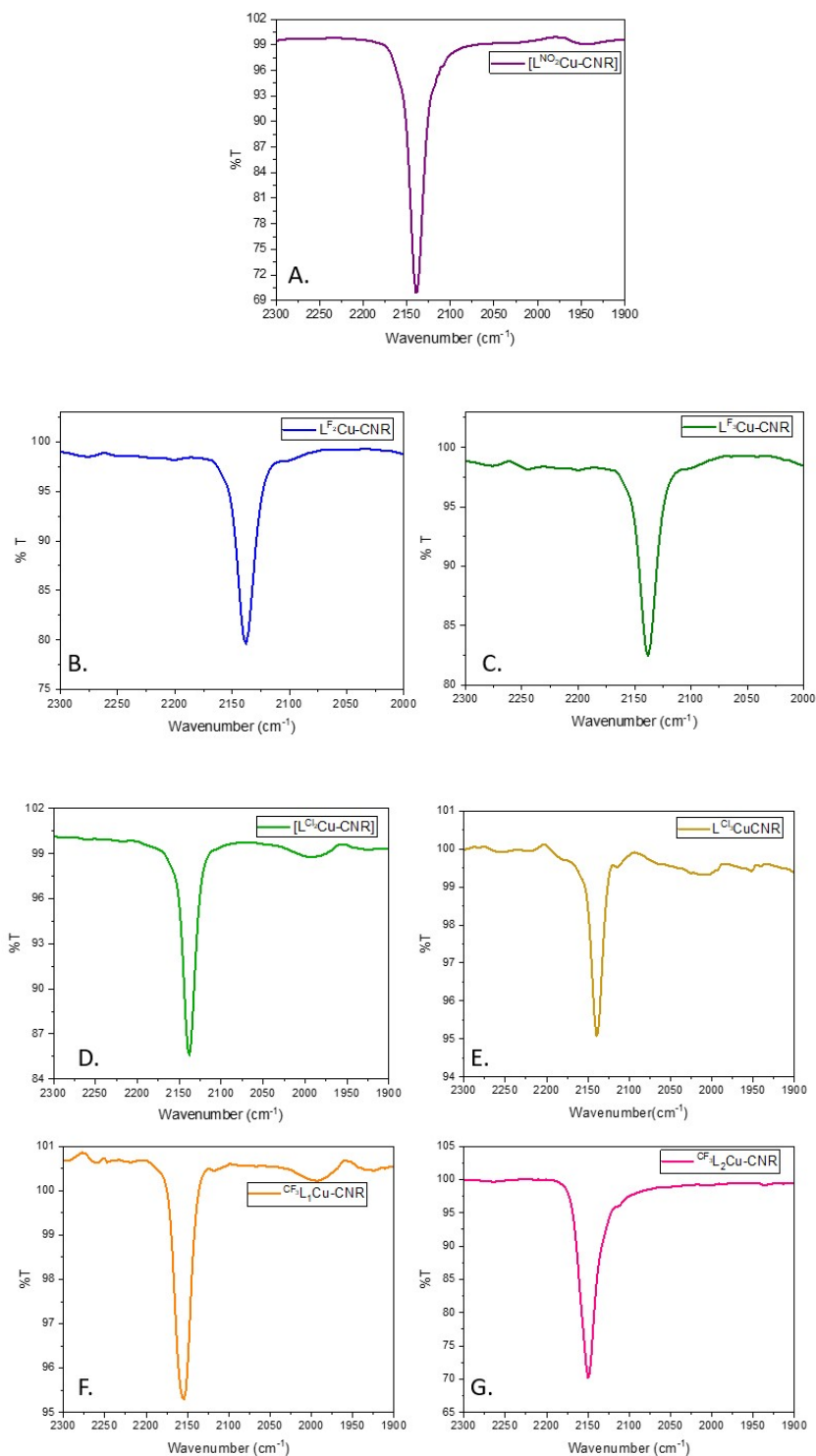
Figure S61. Solution state FTIR of LCu$^{\text{I}}$-CNR adducts in THF. A. $\mathbf{L^{NO2}}$Cu-CNR, B. $\mathbf{L^{F2}}$Cu-CNR, C. $\mathbf{L^{F3}}$Cu-CNR, D. $\mathbf{L^{Cl2}}$Cu-CNR, E. $\mathbf{L^{Cl3}}$Cu-CNR, F. $\mathbf{^{CF3}L_1}$Cu-CNR and G. $\mathbf{^{CF3}L_2}$Cu-CNR.
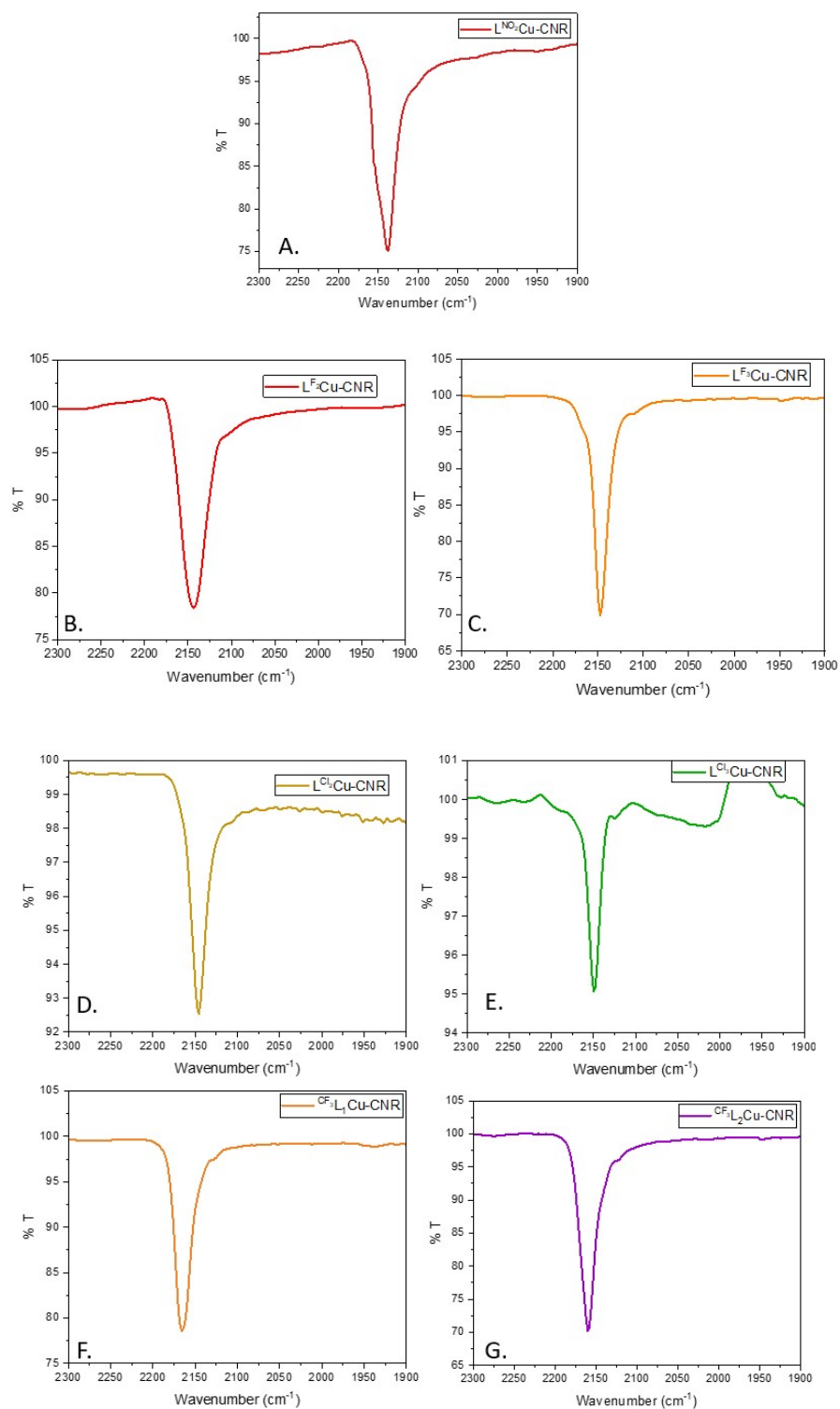
Figure S62. Solution state FTIR of LCu^I-CNR adducts in KBr. A. **L^{NO2}Cu-CNR**, B. **L^{F2}Cu-CNR**, C. **L^{F3}Cu-CNR**, D. **L^{Cl2}Cu-CNR**, E. **L^{Cl3}Cu-CNR**, F. **^{CF3}L$_1$Cu-CNR** and G. **^{CF3}L$_2$Cu-CNR**.

X-ray Crystallography
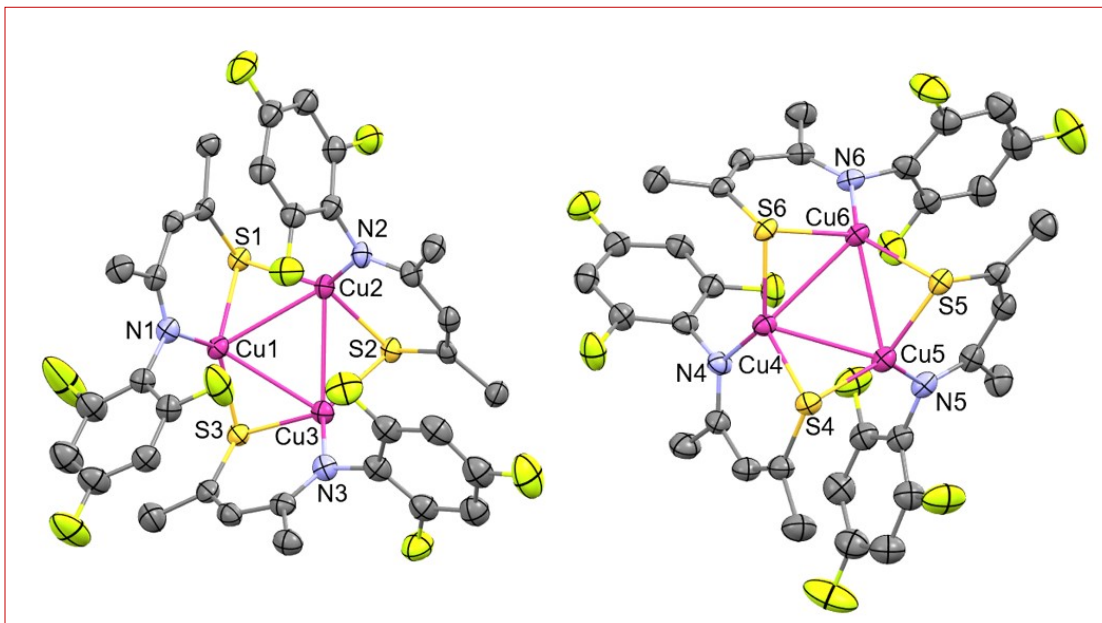
Figure S63. ORTEP X-ray structures of two independent molecules of [$\mathbf{L^{F3}Cu}$]$_3$ (a) and (b) similar to each other present in same unit cell at the 50% probability level. Hydrogen atoms are not shown for clarity.
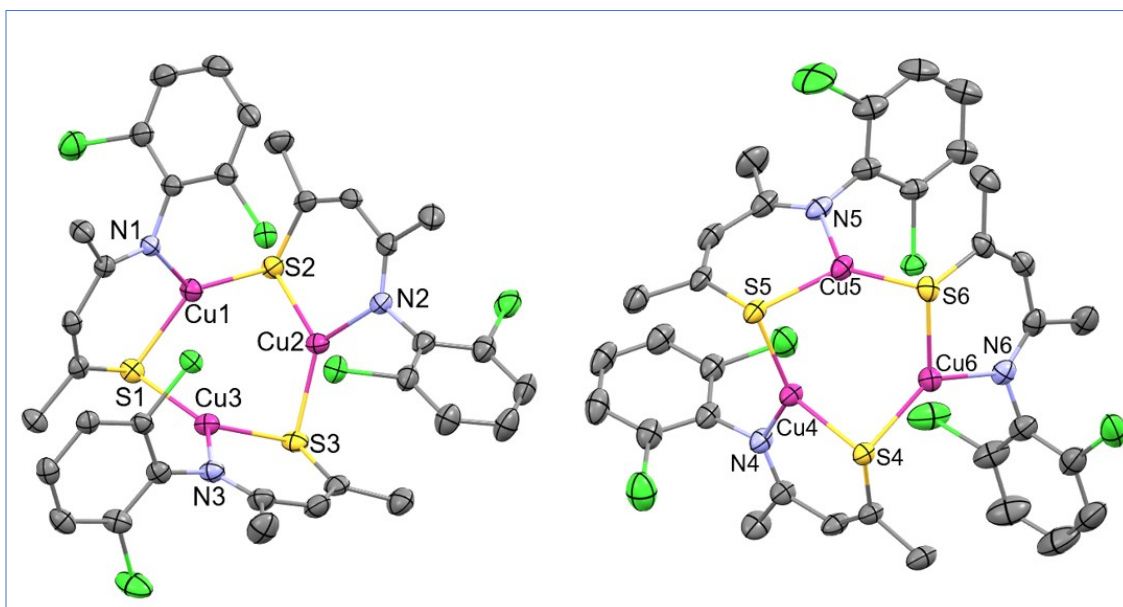
Figure S64. ORTEP X-ray structures of two independent molecules of [$\mathbf{L^{Cl2}Cu}$]$_3$ (a) and (b) similar to each other present in same unit cell at the 50% probability level. Hydrogen atoms are not shown for clarity.
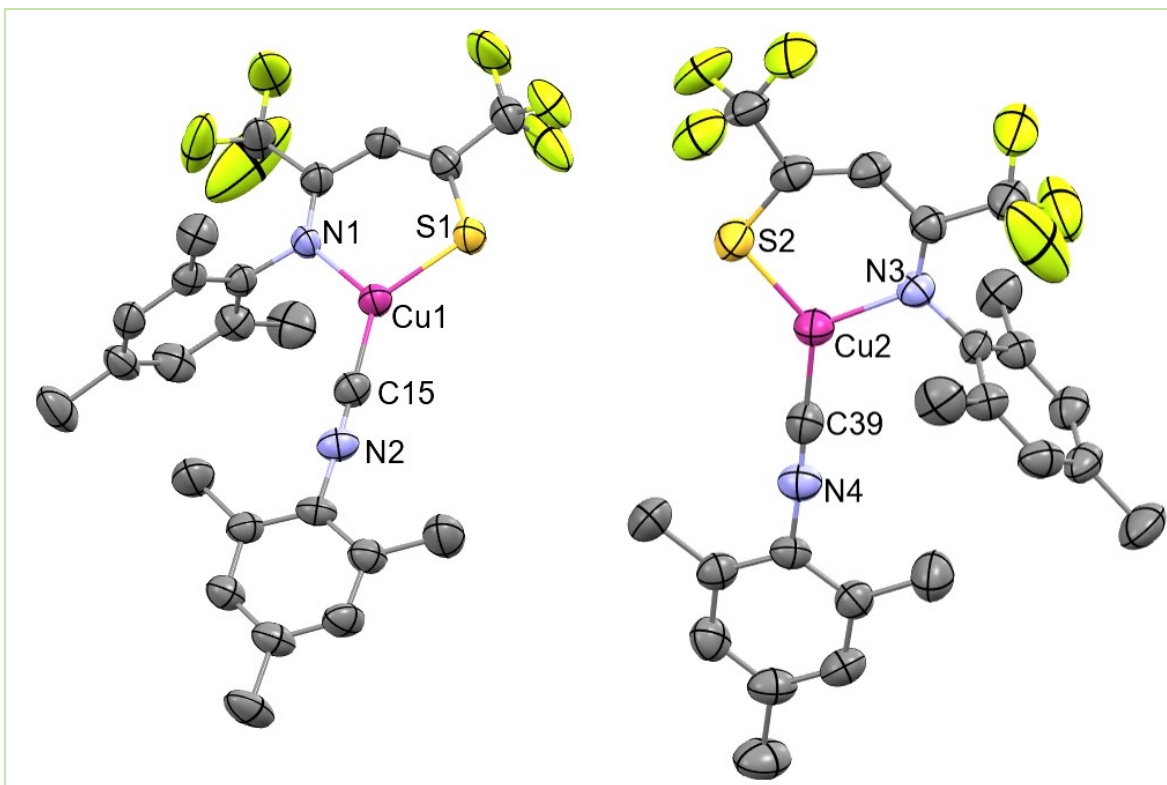
Figure S65. ORTEP diagram of identical units of ^{CF3}L$_2$Cu(2,4,6-CNC$_6$H$_2$Me$_3$) adduct Molecule A (left) and Molecule B (right) in 50% ellipsoids; all hydrogen atoms are omitted for clarity.

Linear relationship graphs
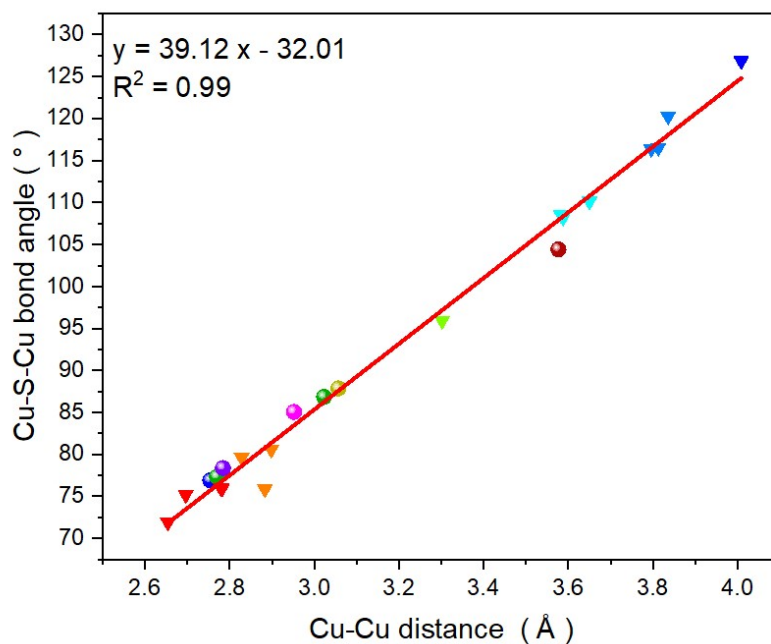
Figure S66. Determination of linear relationship between Cu···Cu bond distances and ∠Cu−S−Cu (core) angle among homoleptic [**LCu^I**]$_3$ complexes represented in **Table 2**. The [**LCu^I**]$_3$ in this work is shown as circles ● other tricopper(I) complexes were indicated as triangles ▼.
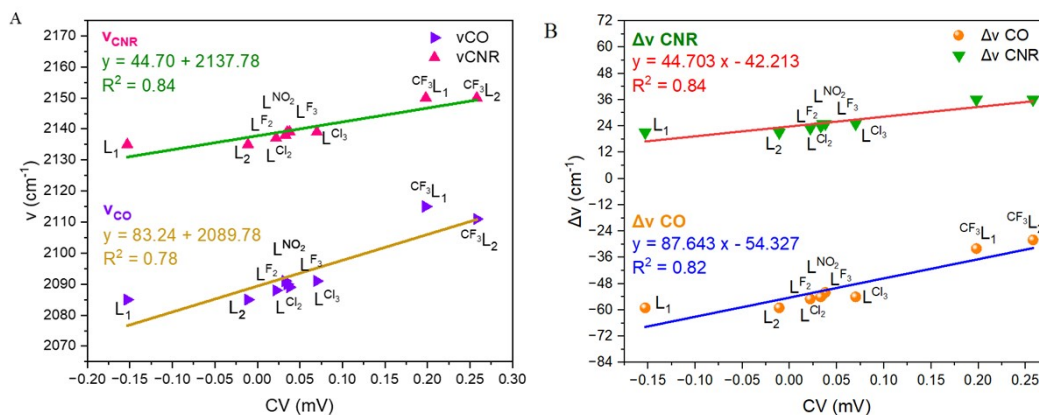
Figure S67. A. Determination of linear relationship between redox potentials (CV) versus ν_{CO} or ν_{CNR} stretching frequencies and B Redox potentials (CV) versus $\Delta\nu_{CO}$ or $\Delta\nu_{CNR}$ stretching frequencies.of corresponding β-thioketiminate **LCu^{I}CO** and **LCu^{I}CNR** adducts.
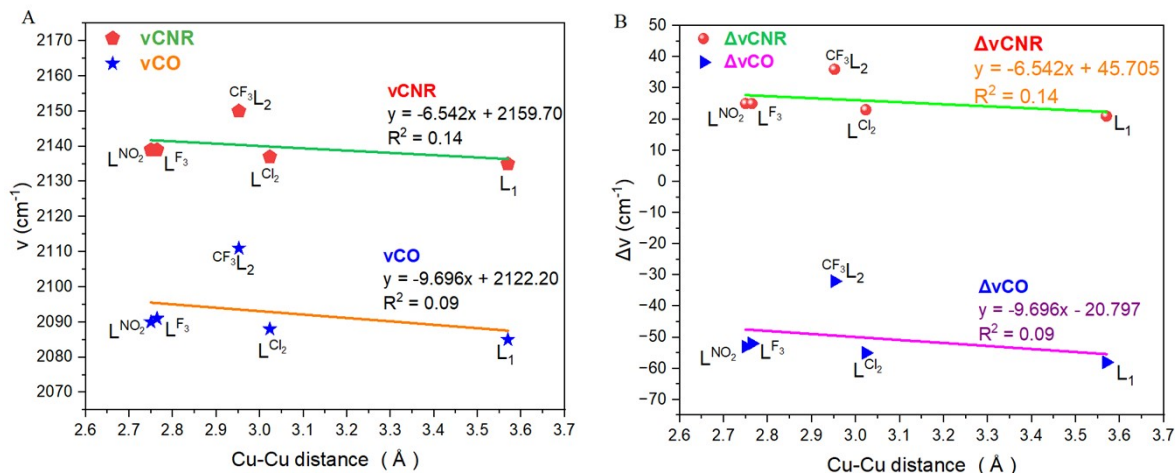
Figure S68. A. Determination of linear relationship between Cu···Cu distances versus ν_{CO} or ν_{CNR} stretching frequencies and B. Cu···Cu distances versus $\Delta\nu_{CO}$ or $\Delta\nu_{CNR}$ stretching frequencies.of corresponding β-thioketiminate **L**Cu^{I}CO and **L**Cu^{I}CNR adducts.
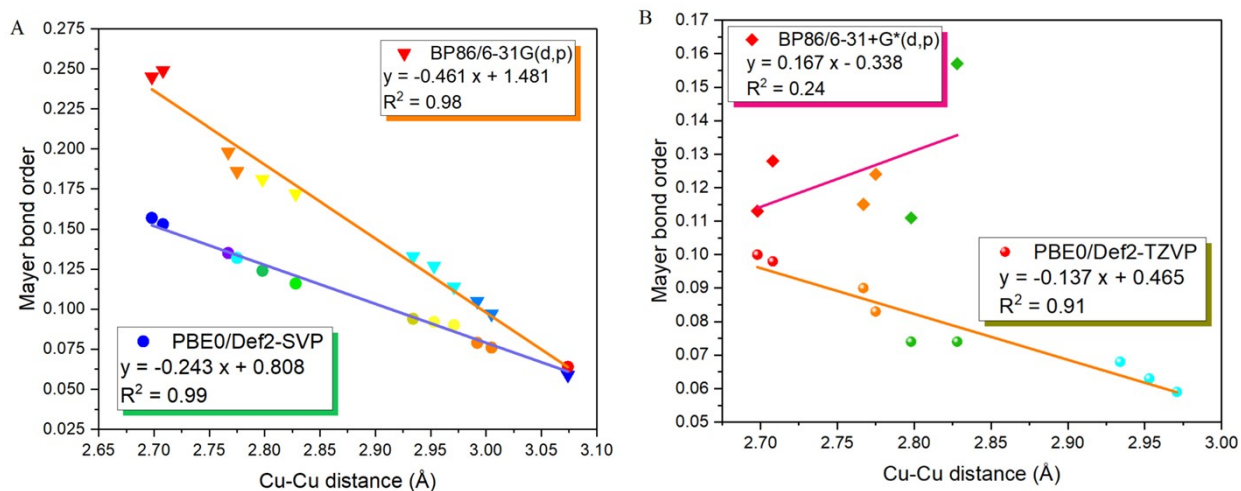
Figure S69. Determination of linear regression between Cu···Cu distance and the corresponding Mayer bond order simulated by A) BP86/6-31G(d,p) and PBE0/Def2-SVP calculations and B) BP86/6-31+G(d,p) and PBE0/Def2-TZVP calculations from crystal geometry measurements. For comprehensive information refer Table S5.
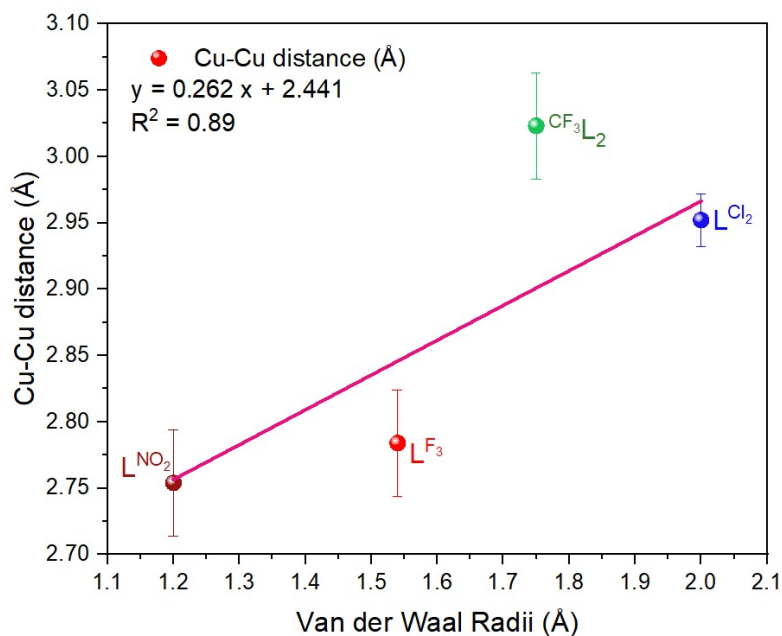
Figure S70. Determination of linear regression between Cu-Cu distance in comparison with Van Der Waals Radii of the corresponding *N*-aryl *ortho*-substituents of respective [**LCu**$^\text{I}$]$_3$ (where **L** = **L**$^\textbf{NO2}$, **L**$^\textbf{F3}$, $^\textbf{CF3}$**L**$_\textbf{2}$, and **L**$^\textbf{Cl2}$).
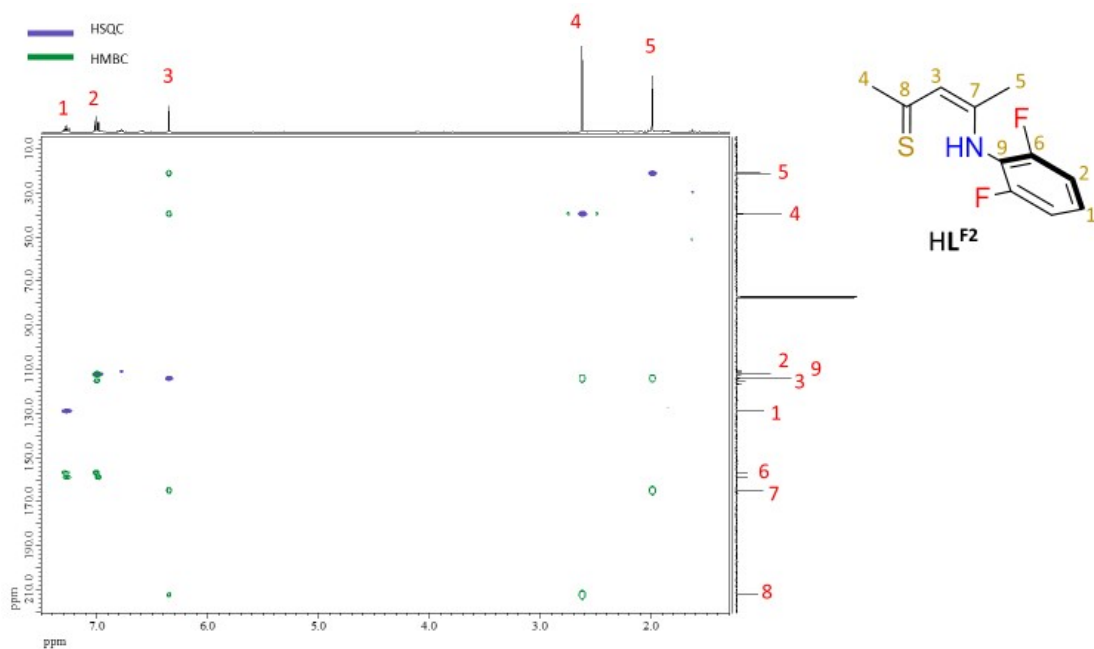
Figure S71. ^{1}H-^{13}C{^{1}H} HMBC and HSQC combined spectrum for H**L**$^\textbf{F2}$ in CDCl$_3$, 500 MHz NMR at 298 K.
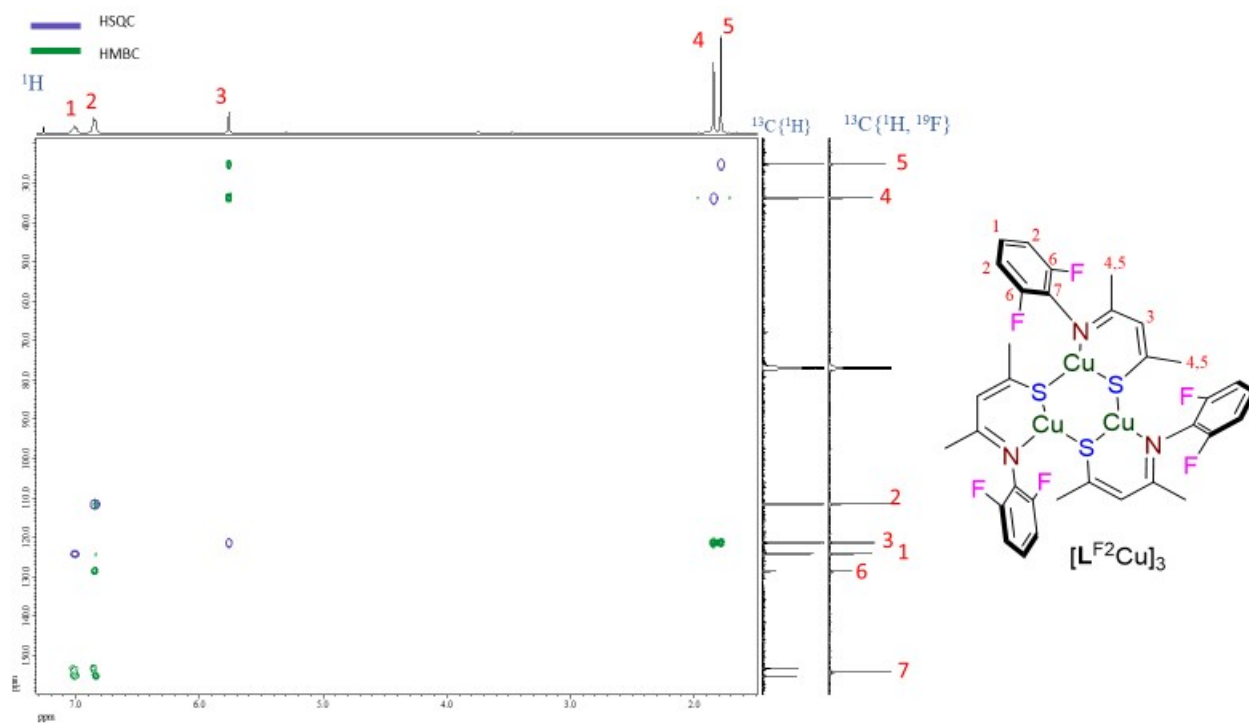
Figure S72. ^{1}H-^{13}C{^{1}H} and ^{1}H-^{13}C{^{1}H}{^{19}F} HMBC and HSQC combined spectrum for [**L**^{F2}Cu]$_3$ in CDCl$_3$, 500 MHz NMR at 298 K.

Raman Measurements and Discussion

Raman analysis for the β-thioketiminato [LCu^I]$_3$ clusters

Apart from the molecular structure analysis, the Cu···Cu short contacts can also be identified by their ν_{Cu-Cu} Raman stretching bands.[2] However, accurately defining the unambiguous ν_{Cu-Cu} Raman band poses a remarkable challenge. Notably, most Raman measurements focus on the ligand-unsupported intermolecular cuprophilic interactions,[2-4] and there are very few reports on the assignment of ν_{Cu-Cu} Raman bands for the ligand-supported intramolecular cuprophilic interactions.[5, 6] We have attempted to analyze the Raman spectrum using DFT approach. The calculations display several low-frequency modes that may be related to cuprophilic interactions. However, these vibrations involve the synchronous motion of many atoms, including S, Cu, and even ligands, making the spectrum assignment challenging. To clarify the cuprophilic interactions by experimental methods, we examined the Raman spectra for [LCu^I]$_3$ and assigned the corresponding Cu-Cu, Cu-N, and Cu-S Raman bands using their corresponding LCu^{I}CNR adducts for comparison. The Raman experiments of each [LCu^I]$_3$ complexes and their corresponding LCu^I-CNR adducts (**L = L$_1$, L^{F2}, L^{F3}, L^{NO2}, L^{Cl2}, L^{Cl3}, ^{CF3}L$_1$, and ^{CF3}L$_2$**) in the solid state by probing them on a Raman spectrometer equipped with a 633 nm diode laser. The Raman bands of [L^{NO2}Cu]$_3$ and [L$_1$Cu^I]$_3$ trimers, along with their corresponding isocyanide adducts, are shown in Figure S73. The rest of the [LCu^I]$_3$ trimers, along with LCu^I-CNR adducts (**L = L^{F2}, L^{F3}, L^{Cl2}, L^{Cl3}, ^{CF3}L$_1$, and ^{CF3}L$_2$**) were available in Figure S74.

Figure S73 illustrates the presence of the Raman band at 201 cm^{-1} for tricopper(I) complex [L^{NO2}Cu^I]$_3$, contrasting with [L$_1$Cu^I]$_3$, which lacks the Raman bands at same region. The Raman bands for the tricopper(I) complexes (**L^{F2}, L^{F3}, L^{Cl2}, and ^{CF3}L$_2$**) were observed between 200 to 210 cm^{-1} (see Figure S74), may result from the νCu-Cu vibrations of ligand-supported intramolecular cuprophilicity or the red shift of copper-ligand vibrations,[5, 6] which could be attributed to the presence of intramolecular cuprophilicity. This assignment is vividly supported by the absence of Raman bands in their corresponding LCu^I-CNR adducts, as well as a comparison with known multi-nuclear copper complexes featuring Raman bands.[2-4] Additionally, the ν_{Cu-S} and ν_{Cu-N} stretching frequencies were assigned in comparison to LCu^I-CNR Raman bands and established copper complexes with S or N coordinated.[3, 4, 7, 8] These Raman frequencies fall within the range of 230-410 cm^{-1} (see Figures S73, S74 and Table S6).
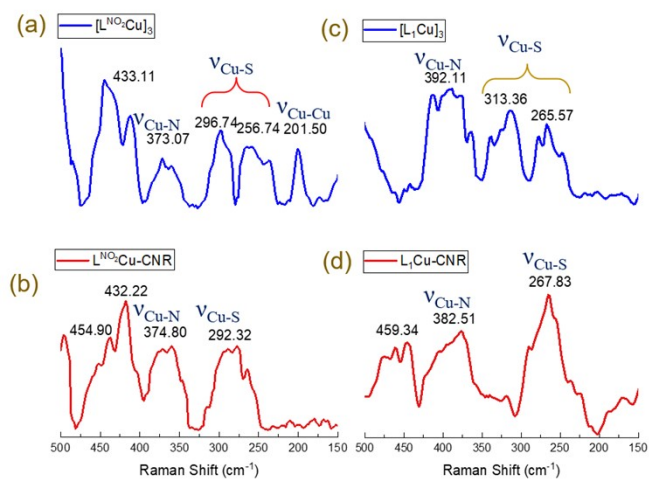
Figure S73. Illustration of Raman bands of tricopper(I) complexes [**L**Cu^I]$_3$ represented in (blue colour) and their corresponding isocyanide adducts (**L**Cu^I-CNR red colour) (a) [**L**^{NO2}Cu]$_3$, (b) **L**^{NO2}Cu-CNR, (c) [**L$_1$**Cu]$_3$, and (d) **L$_1$**Cu-CNR.
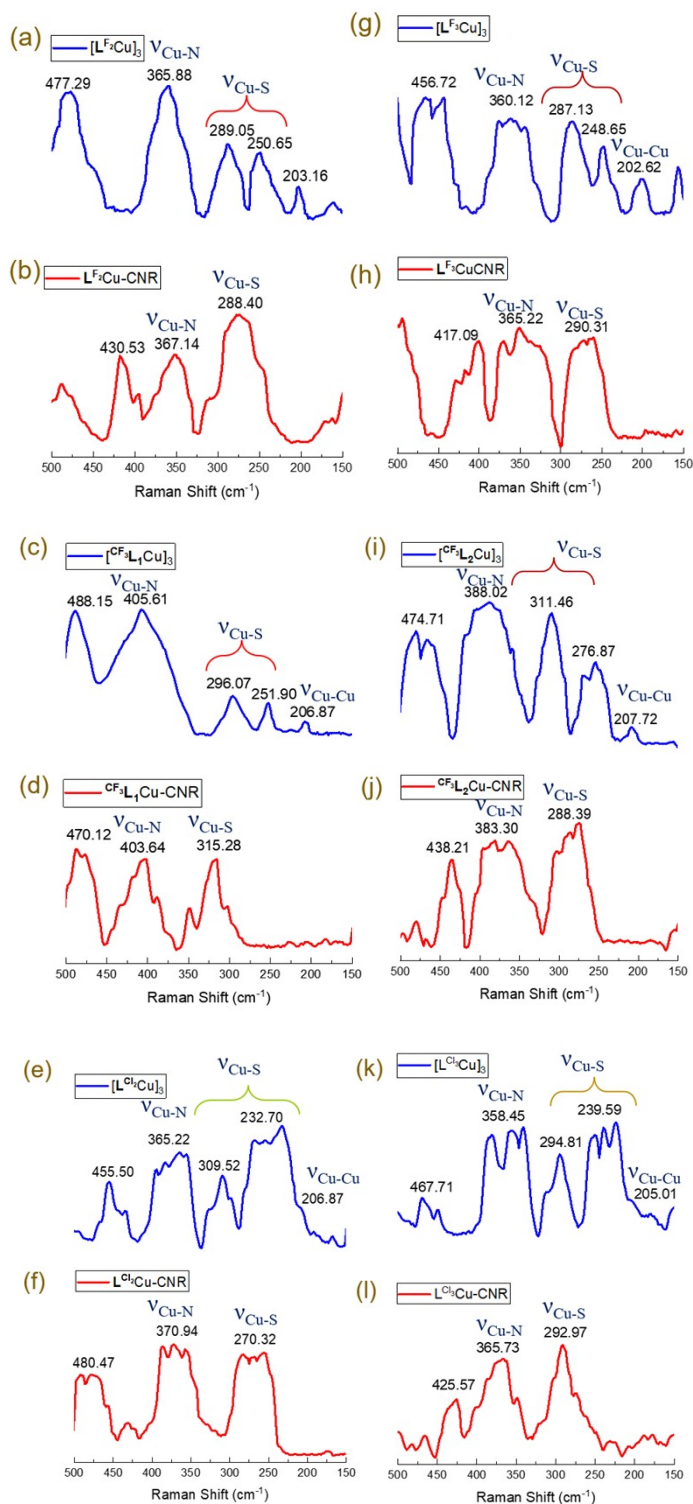
Figure S74. Illustration of Raman bands of tricopper(I) complexes [LCu^I]$_3$ represented in (blue color) and their corresponding isocyanide adducts (LCu^I-CNR red color) (a) [L^{F2}Cu]$_3$, (b) L^{F2}Cu-CNR, (c) [^{CF3}L$_1$Cu]$_3$, (d) ^{CF3}L$_1$Cu-CNR, (e) [L^{Cl2}Cu]$_3$, (f) L^{Cl2}Cu-CNR, (g) [L^{F3}Cu]$_3$, (h) L^{F3}Cu-CNR, (i) [^{CF3}L$_2$Cu]$_3$, (j) ^{CF3}L$_2$Cu-CNR, (k) [L^{Cl3}Cu]$_3$, and (l) L^{Cl3}Cu-CNR.

Tables

Table S1A. Selected Bond Distances (Å) and Bond Angles (deg) for tri-copper clusters [$L^{NO2}Cu^I$]$_3$, [$^{CF3}L_2Cu^I$]$_3$, and [L_1Cu^I]$_3$.

	[$L^{NO2}Cu^I$]$_3$	[$^{CF3}L_2Cu^I$]$_3$	[L_1Cu^I]$_3$[a]
Cu−Cu	2.768(7), 2.798(8), 2.699(7)	2.953(16), 2.934(13), 2.970(11)	3.667, 3.786, 3.313
Cu−N	1.967(3), 1.973(4) 1.970(3)	1.970(5), 1.960(5), 1.958(6)	1.964(8), 1.942(7), 1.954(7)
Cu−S$_{(chelated)}$	2.209(12), 2.214(13), 2.211(12)	2.204(18), 2.192(2), 2.199(14)	2.214(2), 2.212(2), 2.215(2)
Cu−S$_{(bridged)}$	2.238(11), 2.210(12), 2.214(13)	2.215(18), 2.216(2), 2.209(19)	2.177(2), 2.200(2), 2.196(2)
C−C$_{(NCCCS\ backbone)}$	1.461(6), 1.453(6), 1.464(6), 1.338(6), 1.342(6), 1.332(7),	1.465(9), 1.461(7), 1.450(10), 1.345(8), 1.307(9), 1.356(9)	1.461(12), 1.439(11), 1.481(13), 1.351(12) 1.356(11), 1.338(13)
C−N$_{(NCCCS\ backbone)}$	1.292(5), 1.303(5), 1.305(5)	1.285(8), 1.295(7), 1.295(8)	1.307(11), 1.305(11), 1.293(11)
C−S	1.761(5), 1.754(4), 1.749(5)	1.745(8), 1.739(7), 1.731(6)	1.736(9), 1.732(8), 1.763(9)
N−Cu−S$_{(chelated)\ (inward)}$	103.83(11), 102.32(10), 103.64(10)	105.22(19), 104.46(14), 106.23(15)	102.6(2), 102.2(2), 104.5(2)
N−Cu−S$_{(adjacent)}$	130.38(10), 126.70(10), 130.25(11)	133.70(2), 131.94(15), 134.07(13)	136.4(2), 144.4(2), 140.9(2)
S−Cu−S$_{(core)}$	124.86(5),129.70(5), 125.53(5)	120.30(8), 120.68(8), 121.18(8)	121.31(9), 112.94(9), 114.47(9)
Cu−S−Cu$_{(core)}$	78.51(4), 74.63(4), 77.52(4)	84.47(7), 83.47(6), 84.13(6)	112.46(10), 119.14(10), 97.32(8)
C$_{backbone}$−N−C$_{aryl}$	118.8(3), 118.4(4), 120.4(3)	122.8(5), 122.0(6), 121.80(5)	118.4(8), 119.02(7), 120.4(8)
∠NCCCS$_{(aryl)}$[b]	78.62, 83.37, 89.46	82.24, 87.47, 84.64	77.88, 85.49, 81.53
N-aryl Tolman cone angle	101.32, 101.76, 101.88	122.69, 122.93, 122.94	132.22, 130.10, 135.44

[a.] The [L_1Cu]$_3$ crystal data retrieved from our previous works: *Dalton Trans.* **2023**, *52* (22), 7652-7663. [b] Dihedral angle between NCCCS backbone plane and *N*-aryl ring.

Table S1B. Selected Bond Distances (Å) and Bond Angles (deg) for [**L**^{F3}Cu]₃, [**L**^{Cl2}Cu^I]₃.

	[**L**^{F3}Cu^I]$_3$^{a}		[**L**^{Cl2}Cu^I]$_3$^{a}	
	Molecule A	Molecule B	Molecule A	Molecule B
Cu−Cu	2.763(10), 2.822(10), 2.768(10)	2.828(10), 2.708(10), 2.774(10)	2.993, 3.073, 3.005	3.076, 3.093, 3.004
Cu−N	1.969(5), 1.981(5), 1.974(5)	1.971(5), 1.980(5), 1.965(5)	1.975(2), 1.972(2), 1.975(2)	1.971(2), 1.970(2), 1.978(2)
Cu−S$_{(chelated)}$	2.211(16), 2.206(16), 2.217(17)	2.205(16), 2.216(17), 2.217(16)	2.209(7), 2.211(7), 2.198(7)	2.201(7), 2.199(7), 2.210(7)
Cu−S$_{(bridged)}$	2.223(15), 2.226(16), 2.214(16)	2.210(15), 2.224(16) 2.234(16)	2.210(7), 2.207(7), 2.207(7)	2.207(7), 2.202(7), 2.203(7)
C−C$_{(NCCCS\ backbone)}$	1.353(8), 1.456(8), 1.354(8), 1.444(8), 1.351(9), 1.447(9)	1.346(8), 1.443(8), 1.341(9), 1.459(9), 1.347(8), 1.445(9)	1.352(3), 1.445(3), 1.343(4), 1.455(4), 1.353(4), 1.446(4)	1.349(4), 1.452(4), 1.351(4), 1.443(4), 1.345(4), 1.444(4)
C−N$_{(NCCCS\ backbone)}$	1.294(7), 1.308(7), 1.300(8)	1.312(8), 1.305(7), 1.308(8)	1.302(3), 1.302(3) 1.305(3)	1.300(3), 1.307(3), 1.301(3)
C−S	1.758(6), 1.759(6), 1.750(6)	1.752(6), 1.755(6), 1.752(6)	1.748(2), 1.755(3), 1.750(3)	1.751(3), 1.752(3), 1.755(3)
N$_{(amide)}$−Cu−S$_{(thioamide)(inward)}$	104.53(15), 103.61(14), 104.03(15)	104.23(14), 103.25(15), 103.98(15)	103.57(6), 104.47(6), 104.53(6)	104.12(6), 104.67(7), 102.12(6)
N$_{(amide)}$−Cu−S$_{(adjacent)}$	129.65(15), 127.93(14), 130.02(15)	130.84(15), 127.90(15), 130.63(15)	131.72(6), 131.22(6), 132.10(6)	130.39(6), 134.01(7), 133.76(7)
S−Cu−S$_{(core)}$	125.13(6), 128.29(6), 125.49(6)	124.72(6), 128.54(6), 124.49(6)	124.59(3), 124.19(3), 123.22(3)	124.06(3), 124.93(3), 121.05(3)
Cu−S−Cu $_{(core)}$	77.09(5), 79.36(5), 77.09(5)	74.96(5), 77.34(5), 79.66(5)	85.75(2), 85.22(2), 88.48(2)	88.99(2), 86.07(3), 88.47(2)
C$_{amide}$−N−C$_{aryl}$	118.2(5), 116.4(5), 118.5(5)	117.3(5), 117.6(5), 118.0(5)	118.2(2), 118.1(7), 118.7(2)	119.0(2), 119.2(2), 118.5(2)
∠NCCCS$_{(aryl)}$^{b}	85.12, 79.90, 85.11	74.88, 75.92, 85.19	74.54, 80.52, 81.42	77.83, 75.55, 85.02
N-aryl Tolman cone angle	114.14, 114.40, 114.98	114.50, 114.50, 114.53	128.19, 127.38, 127.90	128.98, 128.59, 127.59

[a]There are two independent molecules of [**L**^{NF3}Cu^I]$_3$ and [**L**^{NCl2}Cu^I]$_3$ in their unit cell. [b]Dihedral angle between NCCCS backbone plane and *N*-aryl ring.

Table S2. Selected bond distances (Å) and bond angles (deg) for ^{CF3}**L**CuCNR and **L**Cu^{I}CNR adducts

	^{CF3}**L$_1$**Cu(2,4,6-CNC$_6$H$_2$Me$_3$)	^{CF3}**L$_2$**Cu(2,4,6-CNC$_6$H$_2$Me$_3$)		**L$_1$**Cu(2,4,6-CNC$_6$H$_2$Me$_3$)[a]	**L$_2$**Cu(2,4,6-CNC$_6$H$_2$Me$_3$)[a,b]		
		Molecule A	Molecule B		Molecule A	Molecule B	Molecule C
Cu−N(amide(aryl))	1.979(3)	1.981(5)	1.972(5)	1.967(4)	1.970(4)	1.977(4)	1.950(4)
Cu−S	2.168(13)	2.174(19)	2.169(2)	2.174(15)	2.175(13)	2.161(13)	2.175(15)
C−C(NCCCS backbone)	1.499(7)	1.512(10)	1.442(9)	1.424(8)	1.433(7)	1.440(7)	1.441(7)
	1.386(6)	1.390(4)	1.355(9)	1.360(8)	1.358(7)	1.361(6)	1.360(7)
C−N	1.409(5)	1.477(3)	1.304(7)	1.302(7)	1.308(6)	1.297(6)	1.307(6)
C−S	1.692(4)	1.697(7)	1.698(7)	1.730(5)	1.730(5)	1.729(5)	1.706(5)
Cu−C(isocyanide)	1.856(5)	1.853(7)	1.859(7)	1.847(6)	1.844(5)	1.837(5)	1.835(5)
C≡N(isocyanide)	1.144(3)	1.156(8)	1.147(8)	1.154(8)	1.157(6)	1.161(6)	1.155(6)
N(amide(aryl))−Cu−S	104.73(10)	102.71(15)	103.98(16)	103.19(14)	102.79(11)	103.87(11)	104.89(12)
C(isocyanide)−Cu−S	132.24(15)	135.7(2)	135.5(2)	136.25(18)	136.35(15)	142.51(16)	132.79(17)
C(isocyanide)−Cu−N(amide(aryl))	123.03(17)	121.50(3)	120.4(3)	120.5(2)	120.44(19)	113.53(19)	122.0(2)
C(amide)-N-C(aryl)	124.48	122.50	122.57	119.54	119.85	121.04	118.86
∠NCCCS(aryl)[c]	88.58	88.30	89.54	86.50	88.79	88.54	89.92

[a.] The **L$_1$**Cu(2,4,6-CNC$_6$H$_2$Me$_3$) crystal data retrieved from our previous works: *Dalton Trans.* **2023**, *52* (22), 7652-7663. [b]There are three independent crystal structures of **L$_2$**Cu(2,4,6-CNC$_6$H$_2$Me$_3$) similar to each other in same unit cell. [c]Dihedral angle between NCCCS plane and the *N*-aryl ring.

Table S3. Cyclic voltammetry data for obtained tricopper(I) complexes in MeCN solutions

Complex	E_{pa}
$[\mathbf{L^{NO2}Cu}]_3$	0.035
$[\mathbf{L^{F2}Cu}]_3$	0.038
$[\mathbf{L^{F3}Cu}]_3$	0.070
$[\mathbf{L^{Cl2}Cu}]_3$	0.022
$[\mathbf{L^{Cl3}Cu}]_3$	0.033
$[\mathbf{^{CF3}L_1Cu}]_3$	0.198
$[\mathbf{^{CF3}L_2Cu}]_3$	0.258

[a]All values reported vs NHE, by adding 0.64V to the value measured vs the ferrocene/ferrocenium couple in CH_3CN with Bu_4NPF_6 as electrolyte and potentials (in V vs. $Fc^{+/0}$) were measured at a glassy carbon electrode at a scan rate of 100 mVs^{-1}.

Table S4. Crystallographic data for synthesized β-thioketiminate tricopper(I) complexes and isocyanide adducts

	[$L^{NO2}Cu$]$_3$	[$L^{F3}Cu$]$_3$	[$^{CF3}L_2Cu$]$_3$	[$L^{Cl2}Cu$]$_3$	$^{CF3}L_1Cu$-CNR	$^{CF3}L_2Cu$-CNR
Empirical formula	$C_{34}H_{35}Cl_2Cu_3N_6O_6S_3$	$C_{74}H_{70}Cu_6F_{18}N_6O_2S_6$	$C_{42}H_{36}Cu_3F_{18}N_3S_3$	$C_{40}H_{38}Cl_6Cu_3N_3S_3$	$C_{27}H_{29}CuF_6N_2S$	$C_{24}H_{23}CuF_6N_2S$
Formula weight	981.38	1990.96	1211.54	1060.23	591.12	549.04
T° K	200(2)	130(2)	200(2)	113(2)	200(2) K	200(2) K
Crystal size mm^3	0.14 × 0.05 × 0.01	0.4 × 0.3 × 0.1	0.39 ×0.18 × 0.03	0.4 × 0.4 × 0.2	0.46 × 0.32 × 0.09	0.25 × 0.16 × 0.05
Crystal system	Triclinic	Monoclinic	Monoclinic	Monoclinic	Triclinic	Triclinic
Space group	P$_{-1}$	P2$_1$/c	P2$_1$/c	P2$_1$/c	P$_{-1}$	P$_{-1}$
a(Å)	12.8659(8)	18.8952(5)	21.3849(10)	13.1496(2)	10.3295(5)	11.8903(8)
b(Å)	14.5520(10)	15.8452(3)	9.3117(4)	15.5846(2)	11.7668(6)	13.8732(10)
c(Å)	14.7553(8)	27.6238(8)	25.5615(12)	43.1275(5)	13.5546(7)	15.8152(12)
α(deg)	102.293(2)	90	90	90	105.523(2)	90.204(10)
β(deg)	107.274(2)	99.566(3)	108.784(2)	98.1340(10)	104.4380(10)	90.424(10)
γ(deg)	114.886(2)	90	90	90	108.1630(10)	107.321(2)
V (Å^3)	2203.5(2)	8155.5(4)	4819.0(4)	8749.3(2)	1405.15(12)	2490.4(3)
Z	2	4	4	8	2	4
D$_{calcd}$ (g cm^{-3})	1.479	1.622	1.670	1.610	1.397	1.464
μ(mm^{-1})	1.744	1.779	3.702	1.988	0.909	1.020
Reflns mcasd/indep	65088	105899	24019	190634	20172	22546
Data/restrains/params	8130/0/493	14310/1861/1021	8410 / 83 / 607	15434/3942/1135	4989 / 0 / 347	8581 / 0 / 619
GOF	0.997	1.055	1.105	1.036	1.060	1.060
R$_{int}$	0.0946	0.0614	0.0510	0.0416	0.0553	0.0570
R$_l$[I>2σ] (all data)	0.0473, (0.1242)	0.0622, (0.1299)	0.0774, (0.2105)	0.0291, (0.0647)	0.0644, (0.1515)	0.0806, (0.1394)
R$_w$[I>2σ] (all data)	0.0702, (0.1370)	0.0793, (0.1356)	0.1023, (0.2369)	0.0336, (0.0664)	0.0804, (0.1636)	0.1352, (0.1657)
Max. peak/hole (e$^-$/ Å^3)	0.513/-0.481	1.59/-0.89	0.643/-0.798	0.94/-0.66	1.196/-1.091	0.949/-0.571

Table S5. Mayer bond order analysis to measure Cu···Cu short contacts by using crystallographic parameters.

Complex	Cu···Cu distance	Mayer Bond order		
		BP86/6-31G(d,p)	PBE0/Def2-SVP	PBE0/Def2-TZVP
$[L^{NO2}Cu]_3$	2.698	0.245	0.157	0.100
	2.767	0.198	0.135	0.090
	2.798	0.181	0.124	0.074
$[L^{NF3}Cu]_3$	2.708	0.249	0.153	0.098
	2.775	0.186	0.132	0.083
	2.828	0.172	0.16	0.074
$[^{CF3}L_2Cu]_3$	2.934	0.133	0.094	0.068
	2.953	0.127	0.092	0.063
	2.971	0.114	0.090	0.059
$[L^{NCl2}Cu]_3$	2.992	0.105	0.079	<0.05
	3.005	0.097	0.076	<0.05
	3.074	0.059	0.064	<0.05

Table S6. List of $\nu_{Cu\text{-}Cu}$, $\nu_{Cu\text{-}S}$, and $\nu_{Cu\text{-}N}$, Raman stretching frequencies for β-thioketiminate tricopper(I) clusters $[LCu^I]_3$ and their corresponding isocyanide adducts LCu^I-CNR.

	$[L^{NO2}Cu^I]_3$	$[L^{F2}Cu^I]_3$	$[L^{F3}Cu^I]_3$	$[L^{Cl2}Cu^I]_3$	$[L^{Cl3}Cu^I]_3$	$[^{CF3}L_1Cu^I]_3$	$[^{CF3}L_2Cu^I]_3$	$[L_1Cu^I]_3$
$\nu_{Cu–Cu}$	201.50 [s]	204.13 [s]	200.91 [br]	206.87 [sh]	205.01 [sh]	206.87 [vw]	207.72 [w]	-
$\nu_{Cu\text{-}S}$	256.74	250.65	248.65	232.70	239.59	251.90	276.87	265.57
	296.74	289.05	287.13	309.52	294.81	296.07	311.46	313.36
$\nu_{Cu–N}$	373.07	365.88	360.12	365.22	358.45	405.61	388.02	390.55

	$L^{NO2}Cu^I$-CNR	$L^{F2}Cu^I$-CNR	$L^{F3}Cu^I$-CNR	$L^{Cl2}Cu^I$-CNR	$L^{Cl3}Cu^I$-CNR	$^{CF3}L_1Cu^I$-CNR	$^{CF3}L_2Cu^I$-CNR	L_1Cu^I-CNR
$\nu_{Cu\text{-}S}$	292.32	288.40	290.31	270.32	292.97	315.28	288.39	267.83
$\nu_{Cu–N}$	374.80	367.14	365.22	370.94	365.73	403.64	383.30	382.51

Note: s = strong, br = broad, sh = shoulder, w = weak, vw = very weak

1. V. S. S. Penki, Y.-L. Chang, H.-Y. Chen, Y.-T. Chu, Y.-T. Kuo, D. P. Dorairaj, S. Sudewi, S.-W. Ding and S. C. N. Hsu, *Dalton Trans.*, 2023, **52**, 7652-7663.
2. G. M. Chiarella, D. Y. Melgarejo, A. Rozanski, P. Hempte, L. M. Perez, C. Reber and J. P. Fackler Jr, *Chem. Commun.*, 2010, **46**, 136-138.
3. N. V. S. Harisomayajula, S. Makovetskyi and Y. C. Tsai, *Eur. J. Chem.*, 2019, **25**, 8936-8954.
4. N. V. S. Harisomayajula, B.-H. Wu, D.-Y. Lu, T.-S. Kuo, I.-C. Chen and Y.-C. Tsai, *Angew. Chem. Int. Ed.*, 2018, **57**, 9925-9929.
5. C. A. López, Fackler, J.P.Jr, Staples, R.J., Wang, S. I Winpenny, R.E.P., *Croat. Chem. Acta*, 1995, **68**, 793-823.
6. C.-M. Che, Z. Mao, V. M. Miskowski, M.-C. Tse, C.-K. Chan, K.-K. Cheung, D. L. Phillips and K.-H. Leung, *Angew. Chem. Int. Ed.*, 2000, **39**, 4084-4088.
7. D. W. Randall, S. D. George, P. L. Holland, B. Hedman, K. O. Hodgson, W. B. Tolman and E. I. Solomon, *J. Am. Chem. Soc.*, 2000, **122**, 11632-11648.
8. M. E. Helton, P. Chen, P. P. Paul, Z. Tyeklár, R. D. Sommer, L. N. Zakharov, A. L. Rheingold, E. I. Solomon and K. D. Karlin, *J. Am. Chem. Soc.*, 2003, **125**, 1160-1161.

References